Spectroscopic Studies of Deoxyribonucleic Acid at the Au(110)/Electrolyte Interface

Thesis submitted in accordance with the requirements of the University of Liverpool for the degree of Doctor in Philosophy by

Christopher Peter Mansley

Department of Physics

2010

To Libby, an angel that inspired me to never give up.

Abstract

The data reported in this thesis describes the behaviour of the nucleic acid cytosine and single stranded and double stranded calf thymus deoxyribonucleic acid (DNA) at the Au(110)/electrolyte interface.

The adsorption of the biological molecule cytosine at the Au(110)/electrolyte interface was studied using the surface probing technique of Reflection Anisotropy Spectroscopy (RAS). 0.1 mM of cytosine in NaH_2PO_4/K_2HPO_4 was injected into an electrochemical cell and adsorbed onto the Au(110) substrate. The adsorption kinetics were studied as a function of solution concentration, applied electrode potential and pH. It was shown that the cytosine molecule adsorbs along the top rows of the Au(110) substrate along the $[1\,\bar{1}0]$ principle axis. Simulations were used to suggest that the cytosine molecules "freeze" the (1×1) surface structure of the Au(110) substrate.

Single and double stranded calf thymus DNA were shown to self adsorb at the Au(110)/electrolyte interface and that they have preferential ordering. The idea of the DNA strands exhibiting preferential ordering with the absence of an electrode potential on the Au(110) sample lead to the investigation of the DNA adsorbed on a polycrystalline Au sample to determine whether the self assembly was due to DNA-substrate or DNA-DNA interactions.

The biological molecules cytosine, cytidine 5′-monophosphate (CMP), an oligonucleotide consisting only of ten cytosine bases (poly-C (10 nucleotides)), single stranded DNA and double stranded DNA were used in a series of experiments. Each experiment used RAS to study the effect on the optical response of the molecules adsorbed at the Au(110) surface before and after the removal of any liquid from the system. The study shows that the absence of a liquid from the system affects the optical response of the cytosine, CMP, poly-C and the single and double stranded DNA on Au(110). These results are used to suggest that the liquid environment helps protect these biological molecules from harmful ultra violet (UV) radiation.

Acknowledgements

The past four years have been difficult to say the least, but the journey that has been my Ph.D. has given me the belief and knowledge that I can achieve great things with my life. However, this new found self belief could not have been achieved without the support and encouragement from many people.

Firstly I would like to thank Peter Weightman for providing me with an opportunity to excel. His constant support, wisdom and laughter have made working with him an absolute honour and a joy. Secondly, I must thank Caroline "Tea" Smith. Without Caroline the whole research group would collapse. She has been a rock to me and I will never forget her and the help she has consistently given me. Never again will I drink a cup of tea without thinking of her.

The rest of the research group have also made working at the university an unforgettable experience. I thank Trevor Farrell and Paul Harrison for their endless dedication to fixing everything that breaks in the lab. I also thank my fellow students, Gareth Holder (the man with the most infectious giggle), James Convery, Liz Barritt, Nick Almond and Gerard Dolan who over the years have provided a brilliant atmosphere to work in. A special thanks is extended to Clive Edwards from the School of Biological Sciences at the University of Liverpool for his advice on the biological aspects of the work reported in this thesis.

I thank my friends at university, Peter Nugent who has been there with me since day one, Andrew Bowfield and Joseph Croft for the endless banter, in depth discussions and the highs and lows we went through at the Penny Lane quiz. To Patrick Staunton, Nick Jenkinson, Ceri Davies, Pete Armitage, Alex Brownrigg, Abdi Noor and Paul Gardner, thank you for the laughs, and the countless hours of football.

Back in Scunthorpe I have two of the most amazing friends a guy could ever wish for, Andrew Brown and Robin McNally. I thank you for the continuous laughs and experiences we share as friends. I hope we never grow up. I also thank my Auntie Tina and my Nan, as well as my extended family of Marion, Hannah and Brendon.

I must not forget Joseph and Anna, otherwise known as my parents. The past four years have been long and emotional but never has your support for me wavered. I thank you for nurturing me into the young man that I have become and I hope that I make you proud.

Finally, I thank the two most important people in my life; the one that has always been there for me and the one I hope will always be there with me.

My brother Paul has never stopped believing in me; from the moment I was born he has reassured me and spurred me on to become the best of my ability. I owe so much of my success to him. He will forever be my hero.

To my sensational woman. Without Claire I would never have completed this journey. Her belief in me raised my spirits when I thought that everything in life was going against me. The love and laughter that we share is a way of life that I hope will never end. Claire, to me you are perfect and I love you.

Acronyms

ADRAS	Azimuth Dependent Reflection Anisotropy Spectroscopy
AFM	Atomic Force Microscopy
CASSCF	Complete Active Space Self-Contained Field
CD	Circular Dichroism
CMP	Cytidine 5′-Monophosphate
CV	Cyclic Voltammetry
DFT-GGA	Density-Functional Theory
DNA	Deoxyribonucleic Acid
ds-DNA	Double Stranded Deoxyribonucleic Acid
DVM	Digital Voltmeter
EC-STM	Electrochemical Scanning Tunnelling Microscopy
ERS	Electroreflectance Spectroscopy
ESCA	Electron Spectroscopy for Chemical Analysis
FCC	Face Centred Cubic
FWHM	Full Width at Half Maximum
IHP	Inner Helmholtz Plane
IR	Infra-Red
IRRAS	Infra-Red Reflection Anisotropy Spectroscopy
LEED	Low Energy Electron Diffraction
MCU	11-Mercapto-1-Undecanol
MEG	Malemide Ethyl Glycol
MUAM	11-Mercaptoundecylamine
OCP	Open Circuit Potential
OHP	Outer Helmholtz Plane
PDC	1,4-Phenylene Diisothiocyanate
PEM	Photoelastic Modulator
PMT	Photomultiplier Tube
PZC	Potential of Zero Charge
QCM	Quartz Crystal Microbalance

RAS	Reflection Anisotropy Spectroscopy
RDS	Reflection Difference Spectroscopy
RNA	Ribonucleic Acid
SBZ	Surface Brillouin Zone
SCE	Standard Calomel Electrode
SDA	Surface Dielectric Anisotropy
SE	Spectroscopic Ellipsometry
SERS	Surface Enhanced Raman Spectroscopy
SLFE	Surface Local Field Effect
SPR	Surface Plasmon Resonance
ss-DNA	Single Stranded Deoxyribonucleic Acid
STM	Scanning Tunnelling Microscopy
UHV	Ultra High Vacuum
UPD	Underpotential Deposition
UV	Ultra Violet
UV-VIS	Ultra Violet - Visible
XPS	X-Ray Photoelectron Spectroscopy
XRD	X-Ray Diffraction

Contents

Chapter 1

Introduction

This chapter describes the aims of this thesis and explains the importance of the work presented. This chapter also gives an outline of the content of the thesis.

1.1 Surface Science and the Solid/Liquid Interface

Surface science has been embraced throughout the scientific world since its genesis almost half a century ago. The development of Ultra High Vacuum (UHV) environments has enabled a plethora of experimental techniques such as Low Energy Electron Diffraction (LEED), X-Ray Photoelectron Spectroscopy (XPS) and Scanning Tunnelling Spectroscopy (STM), to prosper and yield exciting results which have gone on to benefit the entire world. Despite this large influx of results, the focus of the subject is now being directed away from the UHV techniques towards studies of surfaces in ambient conditions.

In particular, studies of solid/liquid interfaces have arisen from the desire to increase knowledge of the behaviour of biological molecules and systems, which require a liquid environment in order to exhibit their functional activity. There is a need to develop techniques that can be used to study solid/liquid interfaces. One such technique is RAS. RAS enables the study of the behaviour and functionality of biological molecules *in situ*, in three dimensions and can successfully investigate systems under ambient and electrochemical conditions as well as UHV environments.

By bringing together biology, chemistry and physics, RAS has the capacity to provide a major contribution to the world of biological and medical research.

1.2 Electrochemistry

The importance of electrochemistry combined with the increasing development of optical probing techniques is reaping benefits for both industrial and scientific research sectors. The interface between the electrolyte and the surface of an electrode facilitates studies of importance for scientific and industrial applications as this is the region where a large proportion of important interactions occur. Such applications include the exploitation of DNA labelled nanoparticles, bioarray technologies and the development of Surface Plasmon Resonance (SPR) and heterogeneous catalysis.

1.3 Thesis Aims

This thesis reports RAS investigations into the adsorption and behaviour of biological molecules on the Au(110) surface. The thesis also reports the preferential ordering of biological molecules onto the Au(110) crystal under a variety of conditions. All the experiments in this thesis use an Au(110) substrate and a section of this thesis reports the behaviour of the Au(110) surface under several conditions.

The biological molecules investigated became increasingly complex as the research progressed in terms of both electronic and physical structure.

1.4 Thesis Structure

Chapter 2: Experimental Apparatus and Theory

The experimental technique of RAS is introduced with each of the instrument components described in detail. The spectrometer layout is described alongside the theoretical analysis of the passage of light through the system. A schematic of the electrochemical cell used in the research is also given together with a description of the solid/liquid interface.

A new RAS instrument which can be used in the UV range of light is described and its differences from the standard RAS instrument in terms of components and capabilities are discussed.

Chapter 3: The Au(110) Surface

As most of the experiments described in the research were performed on the Au(110) surface, this chapter provides a summary of previous work on this surface. It has been established that the Au(110) surface adopts the (1×2) 'missing row' surface reconstruction when under UHV conditions in order to minimise its surface energy. However, the Au(110) has a tendency to change its ordering between the (1×1) structure and the (1×2) and (1×3) surface reconstructions depending on its environment. This chapter explores the behaviour of the Au(110) surface under an

electrochemical environment. Previous work which lead to a determination of the RAS spectral profiles of all three reconstructions of the Au(110) surface is described.

This chapter also describes theoretical simulations which use an empirical model to simulate the experimental RA spectra produced by the Au(110) sample.

The chapter concludes with an introduction to the results obtained from an Au(110) sample under liquid using RAS in the UV range of the electromagnetic spectrum.

Chapter 4: The Determination of the Structure of Cytosine Monolayers Adsorbed at the Au(110)/Electrolyte Interface

RAS is used to investigate the behaviour of biological molecules at the Au(110)/electrolyte interface. The characteristics and functionality of these interfaces are of great interest for the evolution of bio-electronics. Cytosine is one of the nucleic acids found in DNA and this chapter investigates its behaviour and alignment on an Au(110) crystal as a function of concentration, pH and electrode potential.

Chapter 5: The Detection of DNA Adsorbed at the Au(110)/Electrolyte Interface

The natural progression from studying the RAS of nucleic acid bases found in DNA is to study the RAS of DNA itself. This chapter introduces the DNA structure and previous studies of this important molecule. Results are then presented of the RAS of both single stranded DNA (ss-DNA) and double stranded DNA (ds-DNA) adsorbed on the Au(110) surface. A follow up investigation into the RAS of DNA adsorbed on polycrystalline gold is used to explore if the preferential ordering of DNA at the gold interface is a result of DNA-DNA interactions or is dominated by the effect of the substrate.

Chapter 6: The Effect of a Phosphate Buffer on the RAS of DNA on Au(110)

The results obtained from the previous chapter lead to interesting investigations into how the presence of a buffer solution effects the coupling of the DNA to the dielectric function of the Au(110) substrate. Experiments using both the RA spectrometers to provide extended range RA spectra are conducted to show the change in the optical response of the samples when the buffer solution is removed from the cell. The results of these experiments are presented and provide a possible insight into how these biological molecules survived early Earth and the abundance of damaging UV radiation prior to the growth of the ozone layer.

Chapter 2

Experimental Apparatus and Theory

The objective of this chapter is to describe the theory behind Reflection Anisotropy Spectroscopy and the function of each of the experimental components within the spectrometer. The chapter also includes a description of the make up and function of the electrochemical cell used in the research. In addition the mathematical formalism of light describing the passage through the spectrometer is explained.

2.1 Reflection Anisotropy Spectroscopy

RAS evolved from a similar technique known as Spectroscopic Ellipsometry (SE) [1,2]. RAS is a non-destructive optical probe which can provide surface sensitive information about some cubic crystals by means of exploiting their optical surface anisotropy. The information gained from RAS experiments is obtained by measuring the difference in the reflectance (Δr) of normal incidence plane-polarised light between two orthogonal directions in the surface plane (x,y) normalised to the mean reflectance (r):

$$\frac{\Delta r}{r} = \frac{2(r_x - r_y)}{(r_x + r_y)} \tag{2.1}$$

where the reflectances r_x and r_y are the complex Fresnel reflection amplitudes corresponding to the two orthogonal surface directions, x and y, respectively.

UHV techniques that are used to obtain surface sensitivity have predominantly exploited the short mean free path of electrons. However, light is able to penetrate deeper into a sample and is less sensitive to the surface, but if the sample is a cubic crystal then any anisotropic reflectance in normal incidence and reflection will occur exclusively from the sample's surface and not from the bulk, since the optical response of the bulk to normal incidence light is isotropic. In these conditions RAS of a surface is observed and is highly sensitive to surface structure and processes. The nature of this technique allows RAS to be used under a variety of environments provided that those environments are optically transparent. The addition of RAS to surface probing techniques allows some limitations of UHV experiments to be overcome, sanctioning the investigations of solid/liquid interfaces, particularly those of electrodes within an electrochemical environment.

2.1.1 The RA Spectrometer

RAS can be considered to be a special form of SE, since the experimental set-up is very similar albeit with some important differences. SE illuminates a sample with linearly polarised light close to that of the Brewster angle [3]. Conversely, RAS works with linearly polarised light which illuminates the sample at near normal incidence (≤5°). RAS was initially known as Reflection Difference Spectroscopy (RDS) and was developed in the 1980's by Aspnes and his co-workers [4]. The purpose of its development was to monitor the growth of III-IV semiconductors in near atmospheric pressures [5]. RAS has since been successfully utilised to study metal surfaces in both UHV and air [6], the metal/liquid interface within an electrochemical environment [7] and lead to the study of the adsorption of biological molecules at metal/liquid interfaces [8-12]. Figure 2.1 shows the components of the RA spectrometer [6], which are described in the order that the light travels through the system. It should be noted that mirrors, not displayed in the schematic of figure 2.1, are positioned before and after both the polariser and the analyser in order to facilitate and enhance control over the direction and focal length of the light.

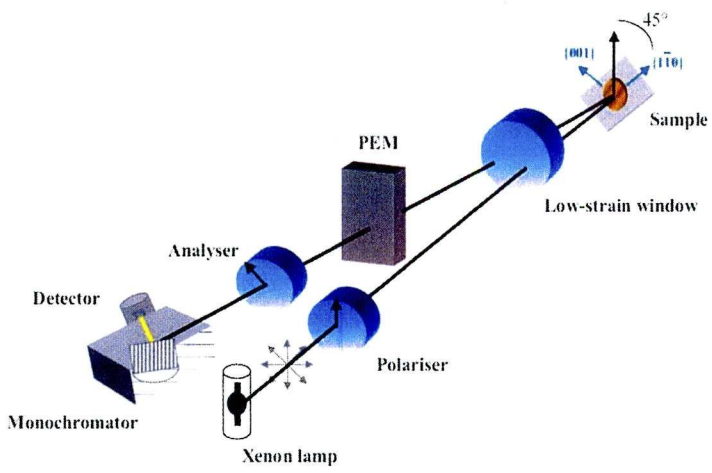

Figure 2.1: A schematic of the fundamental components of an RA spectrometer. Taken from [6].

Xenon Lamp

The Xenon lamp that is used to provide the necessary high intensity source of light is a Hamamatsu 75 Watt Super-Quiet 9 Xenon arc discharge lamp, used in combination with a stabilised power supply (Hamamatsu C4621-02) in order to minimise any fluctuations from the mains supply. The light radiated from the lamp is generated from an arc discharge when high voltages are applied across the anode to a high performance cathode situated in a Xenon gas environment. This form of light source is used for RAS experiments due to its sustainable output of a continuous spectrum of light between the infrared (IR) and UV range (1.5 eV - 5.5 eV) of the electromagnetic spectrum. The Xenon gas pressure in the lamp can vary for up to one hour after it is turned on. Only after waiting an hour after powering up can experiments be carried out with a confidence that a new thermal equilibrium has been successfully achieved and, more importantly, a maximal and unchanging photon flux.

Mirrors

The mirrors used in a RA spectrometer are concave front coated UV enhanced aluminium on glass, with a thin silica coating to inhibit mechanical abrasion. Initially their purpose is to convert the diverging light produced by the Xenon lamp into a parallel beam of focused light which is incident on the sample. Towards the latter part of the optical path of the RA spectrometer the intrinsic astigmatism of the mirrors allows the reflected light from the sample; which has now passed through the photoelastic modulator (PEM) and analyser, to be re-focused onto the narrow 1 mm vertical input slit of the monochromator.

Polariser

The difference in the reflections r_x and r_y in the x and y directions respectively are, frequently very small, to the point where the polariser and analyser require an extinction ratio larger than 10^5. Taking this into account, there are two classes of prism type polarisers which can be used to provide the desired results for RAS. The first are beam splitting polarisers which include Rochon and Wollaston polarisers.

These consist of two adjacent quartz prisms that separate the ordinary and extraordinary polarised beams which have polarisations that are perpendicular to one and other. Conversely, there are Glan prism polarisers that separate the two polarised beams by total internal reflection resulting in the emergence of a single beam of light. Glan prism polarisers are often preferred for UHV apparatus as they pose no restrictions on the location of components in the optical layout, which in turn permits a more compact experimental layout.

Rochon type prism polarisers are used in the research due to their greater efficiency at transmitting light in the UV region. The decision not to use Glan prism polarisers in the research reported in this thesis is acceptable as there are no UHV RAS measurements to present. Nonetheless, attention must be paid to ensure that the two beams exiting the Rochon polariser do not overlap.

Low-Strain Window

Once the polarised light exits the Rochon prism, it passes through a low-strain window prior to entering the electrochemical cell and interacting with the sample. The window contributes a small amount to the RAS signal as it has minor inhomogeneous birefringence. The contribution of the window can subsequently be removed by subtracting a corresponding spectrum from all raw experimental data.

Photoelastic Modulator

The model of PEM used in this thesis is a Hinds Instruments Inc., PEM Quartz 90. A PEM is essentially a waveplate which modulates the polarisation ellipse of the light reflected from the sample by means of manipulating the property of stress induced birefringence. This guarantees the collection of both the real and imaginary parts of the waveform. This effect is attained by the application of an electric field to a piezoelectric crystal that is coupled to an appropriate transparent material such as fused silica. The crystal is driven at its resonant frequency of 50 kHz which allows sequential resolution at the microsecond timescale to be reached.

The PEM induces an oscillating birefringence to the optical element which only affects the light linearly polarised parallel to the modulation axis and the light

linearly polarised perpendicular to the modulation axis remains unchanged. The light parallel to the modulation axis travels faster than the perpendicular component when the fused silica is compressed. Conversely, when the silica is stretched, the parallel component travels slower than the perpendicular component. This phase difference is known as the retardation, (Γ). Therefore the elliptically polarised light from the surface will be phase modulated depending on the polarisation when passing through the PEM, but the light from the bulk will remain linearly polarised and thus pass through unaffected due to the intensity of the reflected light being equal in all phases.

Analyser

The analyser converts the phase-modulated signal from the PEM into an amplitude modulated signal that can be detected. The analyser uses Rochon type prisms of the same design as the polariser, although it is orientated 45° with respect to the polariser in order to produce a modulated signal that switches between two linearly polarised states.

Monochromator

A monochromator is required in this system so that the light from the analyser can be divided into discrete wavelengths for detection. A Jobin Yvon monochromator is used with a holographic grating with 1200 grooves per mm, capable of dealing with an energy range of 1.5 eV – 6.2 eV. In conjunction with this, a computer controlled stepping motor is used to position the grating and thus determine the wavelength of the light entering the detector.

Detector

A Hamamatsu (PMT Hamamatsu R955) multi-alkali cathode photomultiplier tube (PMT) is positioned directly behind the exit slit of the monochromator. Here the intensity of the light exiting the monochromator can be measured. The PMT converts the intensity modulated waveform into a small current, typically in the order of nanoamps and is then amplified. This amplified signal is then converted

into a voltage relative to that of the initial intensity of the light. This signal is made up of two components, a DC offset which is related to the reflectivity and an AC component which is superimposed onto the DC offset and relates to the anisotropy of the surface. A lock-in amplifier is required to separate the two components for analysis.

Silicon photodiodes can also be used for RAS but are most efficient at longer wavelengths and perform poorly in the UV range of the spectrum. An appropriately chosen coating can be applied to convert UV photons for detection in the visible range but to the detriment of sensitivity. Due to this loss of sensitivity in the visible range, the PMT was the preferred choice of detector.

Lock-In Amplifier

A lock-in amplifier is used to analyse the AC and DC voltage signals coming from the PMT. The model used was an EG&G 5210 (dual phase) lock-in amplifier manufactured by Perkin Elmer Instruments running at a frequency range of 0 Hz - 120 kHz. It measures the Fourier coefficients of the first and second harmonics of the signal which carry the real and imaginary parts of the RA signal. A blocking capacitor is applied to separate the AC and DC voltage signals. Lock-in amplifiers of this description can be used to detect signals of very specific frequencies that would otherwise be obscured by noise. This function is imperative for the detection of the RA signal.

To produce accurate measurements and correct identification of the signal a reference voltage of the same frequency and phase relationship is supplied to the lock-in. The difference in frequencies of the signal of interest, with regard to this locked in signal, can then be tracked. To achieve this the locked in reference signal is taken from the PEM.

2.2 The Propagation of Light Through the System

To interpret an RA signal accurately, a full and well defined method of determining the state of polarisation of the light reflected from the surface of the sample is required. It is applicable to start with the definition of the electric field vector, E, of a light wave that can be represented as the superposition of two orthogonal states.

$$E(z,t) = E_x(z,t) + E_y(z,t) \tag{2.2}$$

where

$$E_x(z,t) = E_{0x}\cos(kz - \omega t + \phi_x) \tag{2.3}$$

and

$$E_y(z,t) = E_{0y}\cos(kz - \omega t + \phi_y) \tag{2.4}$$

The resulting wave, **E**, is therefore the vector sum of components,

$$E(z,t) = \hat{x}E_{0x}\cos(kz - \omega t) + \hat{y}E_{0y}\cos(kz - \omega t + \delta) \tag{2.5}$$

where E_{0x} and E_{0y} are the amplitudes of the waves in the x and y directions respectively, k is the wavenumber, z is the position in space, ω is the angular frequency, t is time, ϕ_x and ϕ_y are the phases of the wave x and y waves respectively and δ in equation 2.5 is the relative phase between the two components. Figure 2.2 shows the states of polarisation and their corresponding normalised Jones vector representations, where α is 45°. The Jones vector notation was devised by R. Clark Jones in 1941 and it describes the state of polarisation of light in terms of the electric field vector.

The Jones vector notation will now be used to describe the propagation of the light through the RAS apparatus. The notation is only valid for polarised light and is very succinct. The Xenon lamp emits light which is unpolarised, but the light emerging from the polariser is observed in a definable polarisation state for the remainder of its passage throughout the experimental system and thus the

application of the Jones vector formalism is viable. The resulting wave E, written as a Jones vector is:

$$E(z,t) = \begin{bmatrix} E_{0x}e^{i\delta x} \\ E_{0y}e^{i\delta y} \end{bmatrix} \tag{2.6}$$

where δ_x and δ_y are the appropriate phases. The magnitudes of E_{0x} and E_{0y} determine the directions of polarisation, but if the magnitudes are equal ($E_{0x} = E_{0y}$) and out of phase by $\pm\pi/2$ the result becomes a state of circular polarisation. Figure 2.3 shows that the magnitude remains constant but the direction of E alters over time and follows a circular path with angular frequency ω.

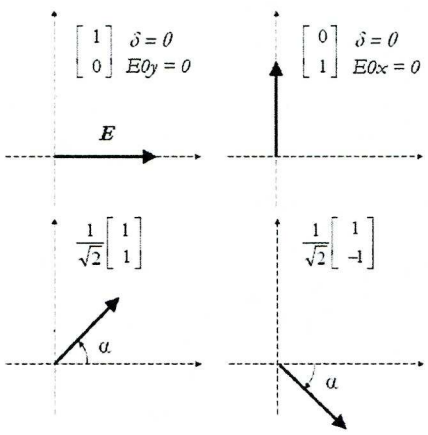

Figure 2.2: The common linear polarisation states.

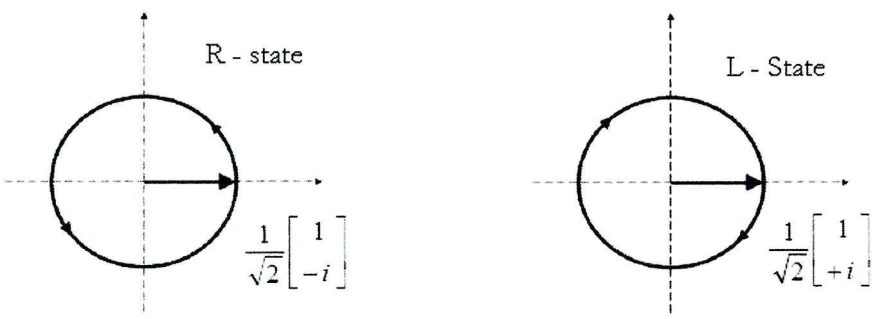

Figure 2.3: Circular polarisation states.

If the resultant vector continues to rotate in this manner but, also experiences changes in magnitude, the resulting state is of elliptical polarisation. This occurs when $E_{0x} \neq E_{0y}$ and the phase difference, δ, is a multiple of $\pm\pi/2$ or when $E_{0x} = E_{0y}$ but the phase difference, δ, is not a multiple of $\pm\pi/2$. The elliptical polarisation state is illustrated in figure 2.4.

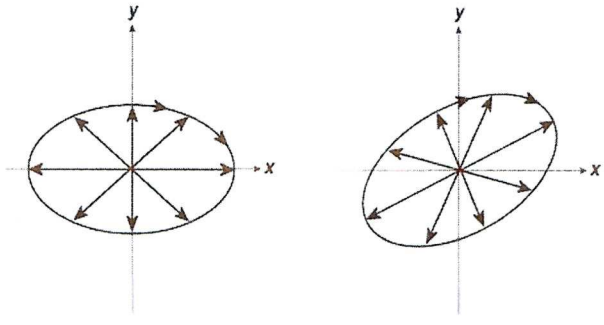

Figure 2.4: Elliptically polarised states.

Within RAS the light that is reflected from the sample will either be of a circular polarisation state or an elliptically polarised state. The light reflected from the bulk of the sample will be of a circular polarisation state, but more significantly to RAS, the surface anisotropy will induce an elliptical polarisation state. The PEM then induces retardation into the elliptically polarised light in different directions. The circularly polarised light, which arises from the bulk of the sample, will propagate through the PEM without modification due to the intensity of its resultant vector being the same in all phases. As the retardation only occurs to the elliptically polarised light, it is possible to extract harmonics from the amplitude modulation giving information which only derives from the surface anisotropy.

With the use of Jones vector, M, which describes the effect of all the optical components, the polarisation state of the light as it propagates through the system can be tracked from the state of polarisation state incident to the system, E_i , to the state of polarisation of the light emerging from the system, E_f, and arriving at the detector.

$$E_f = ME_i \tag{2.7}$$

The effect of each component on the polarisation state of the light can be described by a (2×2) matrix, which can then be combined to give the Jones matrix, M. For notation purposes it is useful to describe the optical axes of each component. The polariser and analyser have a transmission axis, *t*, and an extinction axes, *e*. The PEM has a fast, *f*, and a slow, *s*, axis. The sample axes (*x,y*) are taken to be in the [1 $\bar{1}$0] and [001] surface directions. These axes define the reference frame for each component. A rotation matrix, *R*, is used to convert the Jones vector representing the polarisation state of the light to those of the optical component with which it is interacting.

$$R(\theta) = \begin{bmatrix} \cos(\theta) & -\sin(\theta) \\ \sin(\theta) & \cos(\theta) \end{bmatrix} \tag{2.8}$$

The orientations of the reference frames of the polariser, modulator and analyser are specified by the azimuth angles *P*, *M* and *A* respectively. This correlates to the transmission axes for the polariser and analyser and the fast axis of the modulator. The azimuths are measured from the *x* direction of the sample and are defined as positive for an anti-clockwise rotation. The first component the light is incident upon, is the polariser. Once the light has passed through this component it can be assigned the Jones matrix TP^{te}, since it is in the *te* reference frame of the polariser.

$$T_P^{te} = \begin{bmatrix} 1 & 0 \\ 0 & 0 \end{bmatrix} \tag{2.9}$$

This must then be multiplied by the rotation matrix *R(P)* so that it is in the *xy* plane of the sample:

$$R(P)T_P^{te} = \begin{bmatrix} \cos P & \sin P \\ -\sin P & \cos P \end{bmatrix} \begin{bmatrix} 1 & 0 \\ 0 & 0 \end{bmatrix} = \begin{bmatrix} \cos P & 0 \\ -\sin P & 0 \end{bmatrix} \tag{2.10}$$

Prior to reflecting from the surface the light will enter the electrochemical cell via a strain-free window. The orientation of the window axes are not known, and are therefore assumed to coincide with that of the xy frame of the sample. As the window will have some birefringence, it will have an associated fast and slow axis resulting in some retardation of the incident light beam between the two directions. This can be represented by:

$$T_{WI}^{xy} = \begin{bmatrix} 1 & 0 \\ 0 & e^{i\delta WI} \end{bmatrix} \tag{2.11}$$

where, δ_{WI} is the retardation of the incident beam by the window. δ is defined by:

$$\delta = \frac{4\pi d}{\lambda}\left(n_e - n_o\right) \tag{2.12}$$

where, d is the thickness of the material, λ is the wavelength of the light, and n_e, n_o, are the refractive indices of the extraordinary and ordinary directions of the material respectively. Once reflection from the surface has taken place, the light will once again exit the cell via passage through the window. This time the light will pass via a different part of the window with an associated retardation δ_{WO}. The Jones matrix for the surface is:

$$T_S^{xy} = \begin{bmatrix} r_x & 0 \\ 0 & r_y \end{bmatrix} \tag{2.13}$$

Once reflection from the surface has taken place the light will pass through the PEM. The rotation matrix must once again be applied for the change from the xy to the reference frame of the PEM.

$$T_M^{fs} = \begin{bmatrix} 1 & 0 \\ 0 & e^{i\delta_M} \end{bmatrix}\begin{bmatrix} \cos M & -\sin M \\ \sin M & \cos M \end{bmatrix} = \begin{bmatrix} \cos M & -\sin M \\ \left(e^{i\delta_M}\sin M\right) & \left(e^{i\delta_M}\cos M\right) \end{bmatrix} \tag{2.14}$$

The conversion to an amplitude modulated signal then occurs at the analyser requiring the same matrix as applied for the polariser and once again the rotation matrix.

$$T_A^{te} R(A-M) = \begin{bmatrix} 1 & 0 \\ 0 & 0 \end{bmatrix} \begin{bmatrix} \cos(A-M) & -\sin(A-M) \\ \sin(A-M) & \cos(A-M) \end{bmatrix} = \begin{bmatrix} \cos(A-M) & -\sin(A-M) \\ 0 & 0 \end{bmatrix} \tag{2.15}$$

The matrix for the polarisation state for the fully propagated light, M, is obtained by combining the matrices of each element. This must be done in the order which the light interacts, since the matrices are non-commutative. Combining equations 2.10, 2.11, 2.13, 2.14 and 2.15 as follows:

$$M = T_A^{te} R(A-M) T_M^{fs} R(M) T_{WO}^{xy} T_S^{xy} T_{WI}^{xy} R(P) T_P^{te} \tag{2.16}$$

Evaluating 2.16 gives:

$$M = \begin{bmatrix} a_{11} & 0 \\ 0 & 0 \end{bmatrix} \tag{2.17}$$

where:

$$\begin{aligned} a_{11} = {} & (\cos(A-M)\cos M - \sin(A-M)(e^{i\delta_M} \sin M))(r_x \cos P) - \\ & (-\cos(A-M)\sin M - \sin(A-M)(A-M)(e^{i\delta_M} \cos M))(r_y e^{i\delta_{WO}} e^{i\delta_{WI}} \sin P) \end{aligned} \tag{2.18}$$

The values of the angles P, A and M used are -45°, 0° and 45° respectively. Thus:

$$\sin(\pm 45°) = \pm\frac{1}{\sqrt{2}}, \cos(\pm 45°) = \frac{1}{\sqrt{2}}, \sin(0°) = 0, \cos(0°) = 1,$$

Inserting the above values into equation 2.18, gives:

$$a_{11} = \frac{r_x}{2\sqrt{2}}(1 + e^{i\delta_M}) + \frac{r_y e^{i\delta_{WO}} e^{i\delta_{WI}}}{2\sqrt{2}}(e^{i\delta_M} - 1) \tag{2.19}$$

Since a_{11} is the only non-zero term in the system matrix, M, the initial equation 2.7

$$E_f = \begin{bmatrix} a_{11} & 0 \\ 0 & 0 \end{bmatrix} \begin{bmatrix} 1 \\ 0 \end{bmatrix} = \begin{pmatrix} a_{11} \\ 0 \end{pmatrix} \tag{2.20}$$

The window terms can be simplified too:

$$e^{i\delta_{WO}} e^{i\delta_{WI}} = e^{i(\delta_{WO} + \delta_{WI})} = e^{i\delta_W} \tag{2.21}$$

The total retardation induced by the window strain, although finite, is small. Thus it is possible to expand the exponential in terms of a power series:

$$e^{i\delta_W} = 1 + i\delta_W + \frac{(i\delta_W)^2}{2!} + \frac{(i\delta_W)^3}{3!} + ... \approx 1 + i\delta_W \tag{2.22}$$

Equation 2.19 becomes:

$$a_{11} = \frac{1}{2\sqrt{2}}\left[\left(r_x - r_y\right) + \left(r_x - r_y\right)e^{i\delta_M} - i\delta_W r_y\left(1 - e^{i\delta_M}\right)\right] \tag{2.23}$$

The Fresnel coefficients r_x and r_y present in equation 2.23 are complex quantities and can therefore be written in terms of their real and imaginary components:

$$r_x = a + ib \qquad r_y = c + id \tag{2.24}$$

The term relating to the retardation of the modulator can be written in a similar manner using De Moivre's theorem:

$$e^{i\delta_M} = \cos(\delta_M) + i\sin(\delta_M) \tag{2.25}$$

After some manipulation a_{11} becomes:

$$\left(2\sqrt{2}\right)a_{11} = \alpha + i\beta \tag{2.26}$$

where α and β are the real and imaginary parts of a_{11}. Assuming that the detector and monochromator are polarisation independent, then the polarisation of the light beyond the analyser is no longer altered and only the time dependent intensity, at each wavelength, is measured by the detector. The measured time dependent intensity, I, is proportional to the square of E_i, which depends on a_{11}, thus:

$$I \propto \left|\left(2\sqrt{2}\right)a_{11}\right|^2 = \alpha^2 + \beta^2 \tag{2.27}$$

Following some extensive algebraic manipulation, equation 2.27 becomes:

$$\begin{aligned} I \propto |a_{11}|^2 = {} & \frac{1}{4}\left[\left(a^2+b^2\right)+\left(c^2+d^2\right)+\left(c^2+d^2\right)\delta_W^2\right] \\ & +\frac{1}{4}\left[\left(a^2+b^2\right)-\left(c^2-d^2\right)-\left(c^2+d^2\right)\delta_W^2\right]\cos(\delta_M) \\ & +\frac{1}{2}\left[(ad-dc)-(ac+bd)\delta_W\right]\sin(\delta_M) \end{aligned} \tag{2.28}$$

This may be written in the form:

$$I = I_{dc} + I_{\omega}\sin(\delta_M) + I_{2\omega}\cos(\delta_M) \tag{2.29}$$

The PEM varies the retardation (δ_M) sinusoidally:

$$\delta_M = \alpha(\lambda)\sin(\omega t) \tag{2.30}$$

where ω is the resonant angular frequency of the modulator and $\alpha(\lambda)$ is the modulation amplitude. δ_M is proportional to the applied excitation voltage and it is a function of the wavelength of light. The frequency components of the signal are determined by the Fourier expansions of the $\cos(\delta_M)$ and $\sin(\delta_M)$ terms:

$$\cos\left(\alpha\sin(\omega t)\right) = J_0(\alpha) + 2\sum_{n=1}^{\infty} J_{2n}(\alpha)\cos(2n\omega t) \tag{2.31}$$

$$\sin\left(\alpha\sin(\omega t)\right) = 2\sum_{n=1}^{\infty} J_{2n-1}\alpha\sin\left((2n-1)\omega t\right) \tag{2.32}$$

where $J_n(\alpha)$ is the Bessel function of argument α and of order n. For the case of $J_0(\alpha) = 0$, achieved by adjusting the voltage applied to the PEM, equation 2.29 becomes:

$$I = I_{dc} + I_{\omega} 2J_1\alpha\sin(\omega t) + I_{2\omega} 2J_2\alpha\cos(2\omega t) + ... \tag{2.33}$$

The first term of equation 2.28 is time-independent, and this can be thought of as a DC term. By comparing the terms in equation 2.28 and equation 2.33 the intensity coefficients are determined. It is assumed that for small surface anisotropies $r_x \sim r_y$ for additive terms. By considering only the first order window strain terms, the normalised frequency terms are found to be:

$$I_{dc} \sim \frac{\left(|r_x|^2 + |r_y|^2\right)}{2} = R \tag{2.34}$$

$$\frac{I_{\omega}}{I_{dc}} \sim \mathrm{Im}\left(\frac{\Delta r}{r}\right) - \delta_W \tag{2.35}$$

$$\frac{I_{2\omega}}{I_{dc}} \sim \mathrm{Re}\left(\frac{\Delta r}{r}\right) \tag{2.36}$$

Hence I_{dc} is a measure of the reflectivity. The imaginary part of ($\Delta r/r$) is measured at frequency, ω, and is found to be dependent on the first-order window strain term, whereas the signal at 2ω measures the real part of ($\Delta r/r$) and is only sensitive to the second order window strain term. As a result of this the majority of the RAS measurements reported are of the real part of the RAS signal, since for imaginary measurements window strain effects are substantial and make conclusions on the probed system more complicated. Experimentally real and imaginary parts of the signal are separated by their frequency dependence.

Errors

Error is introduced into the formulism by the possible misalignment of the optical components and the sample. Any misalignment of the polarisation dependent components will result in an offset of the measured Re ($\Delta r/r$). This offset does not introduce new features but creates problems when quoting the absolute values of Re($\Delta r/r$). Changes in the measured spectra can be treated with more certainty. The effects of misalignment have been studied in detail [13]. It was found that the relationship between the polariser and modulator is very sensitive to misalignment, but an analyser misalignment has less of an impact. The RA spectra are also found to be sensitive to the anisotropy introduced by the low-strain window. Therefore a window correction is required to be subtracted from the RA spectra to remove the influence of the window.

2.3 Electrochemistry

Electrochemistry is the study of chemical reactions which involve the transfer of electric charge between a chemical species and an electrode. Electron transfer at an electrode is a molecular scale event that involves the movement of a negatively charged species between the electrode and species in the solution. The potential gradient at the surface instigates this process but, due to this occurring at such small distances between the electrode and the solution, the potential gradient can be in the order of 10^{10} Vm^{-1} [14]. Understanding the interfacial region of electrodes needs a

comprehension of the influence of the potential field and the electrostatic consequences, which are the movement of charged ions in solution being attracted to the surface, the structure of the adsorbed species and the effects that the potential field has in that region. This region is the core of electrochemistry and a thorough knowledge of it is essential to the understanding of the kinetics of electron transfer.

In 1853, Hermann von Helmholtz created the term "electric double layer" to portray the solid/liquid interface. He suggested a model formed under the assumption that no electrons are able to traverse the interface between the electrode and the solution, in other words that the interface contains no Faradic processes. The resulting electrode surface preserves electrical neutrality across the surface due to an induced charge density of the electrode surface that is balanced by an equal yet opposite charge density of the electrolyte. The opposing charge of the solution arises from the redistribution of the electrolyte ions to the surface of the electrode. The attracted anion approaches the electrode at a distance that is defined by the solvation shell of the ion. The model is analogous to the one used to describe a parallel plate capacitor of molecular dimensions consisting of two plates of equal yet opposite charge with a linear potential drop between them. One of the plates is the metal electrode that has its own surface excess charge, whereas the other plate is accredited to the plane which passes through the centre of the solvated ions at their closest approach. This is known as the Outer Helmholtz Plane (OHP).

Successive modifications to the model by Gouy [15,16], Chapman [17] and Stern [18] and lastly by Grahame in 1947 [19], generates the current acknowledged model as depicted in figure 2.5. It takes into account the electrostatic attraction/repulsion of the ions to the electrode is opposed by the Brownian motion in the solution. As Brownian motion results in the dispersion of excess charge, the charge in the solution is spread over the diffuse layer as opposed to being concentrated at the OHP. However, the distribution of this charge is not homogeneous across the diffuse layer, and the greater part of the charge is situated near to the electrode surface with a minority extending past the OHP.

For a complete picture of the interface, it is necessary to take into consideration that there are two forms of adsorption onto the surface: non-specific adsorption and specific adsorption. The ions that undergo non-specific adsorption

are only held in position by electrostatic forces. Conversely, the solvated ions that are specifically adsorbed are bound by weak solvation shells, e.g. anions such as Cl^- and Br^-, and they give away part of those solvation shells to form a chemical bond with the surface of the electrode. The plane through the centre of the ions is defined as the Inner Helmholtz Plane (IHP).

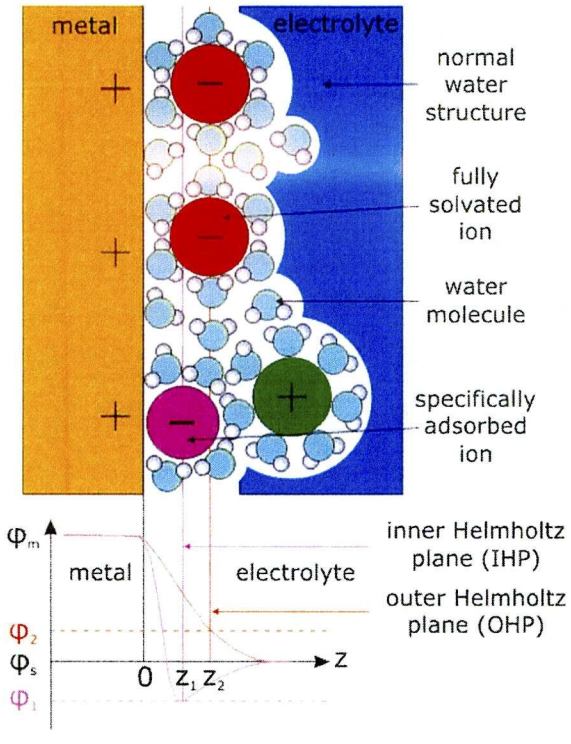

Figure 2.5: A schematic illustration of a metal/electrolyte interface and a graph of the potential drop across the electrochemical interface. Adapted from [20].

For the non-specific adsorption of ions, a linear drop in potential across the interface is assumed (red line in figure 2.5), whereas for specific adsorption there is a steeper potential drop at the surface (purple line in figure 2.5) and an over-shooting of the potential with respect to the bulk electrolyte value occurs. The potentials φ_m, φ_s, φ_1 and φ_2 correspond to potentials inside the metal, the electrolyte, the IHP at Z_1 and the OHP at Z_2 respectively.

When a potential is applied to the electrode in electrolyte its surface will become more charged and the value of the surface charge will depend on the electrode material, the electrolyte used and the potential applied. If the potential is

made more negative, electrons will flow into the surface resulting in a negatively shifting surface charge. Conversely, if the potential is made more positive, electrons will move out of the surface and its charge will become less negative and eventually positive. This leads to the concept of the potential of zero charge (PZC), which is the potential for a particular electrode/electrolyte combination where the surface has neither positive nor negative charge. The model described previously describes the surface in this state.

2.3.1 Measuring Electrode Potential

The reactions of interest in electrochemical systems occur at the working electrode. It is, therefore, essential to be able to accurately control the potential drop across the working-electrode/solution interface (Φ_W-$\Phi_{solution}$). However, direct measurement of the absolute potential-difference across this interface is not possible. In a one-electrode cell, for example, measurement of the potential drop attempted with a standard digital voltmeter (DVM) is not possible since free-electrons will not pass from the DVM probe to the solution and therefore it does not make electrical contact. By introducing a second electrode the potential difference can be measured between the two electrodes. However, this is an indirect measurement and is in fact a difference of two metal/solution potential drops.

$$\begin{aligned} \Delta\Phi &= (\Phi_{metal(A)} - \Phi_{solution}) - (\Phi_{metal(B)} - \Delta\Phi_{solution}) \\ \Delta\Phi &= \Phi_{metal(A)} - \Phi_{metal(B)} \end{aligned} \tag{2.37}$$

In a two-electrode set-up, if one of the electrodes represents a test system and the other a reference system (reference electrode), then the potential difference is written as:

$$\Delta\Phi = (\Delta\Phi_{test} - \Delta\Phi_{solution}) - (\Delta\Phi_{reference} - \Delta\Phi_{solution}) \tag{2.38}$$

The potential drop across a reference electrode/solution interface remains constant, and the potential drop can now be written as:

$$\Delta\Phi = (\Phi_{test} - \Phi_{solution}) - k \tag{2.39}$$

where k is a constant.

It is still not possible to directly probe the value of $\Phi_{test} - \Phi_{solution}$, but the changes in this value can be determined. The use of a reference electrode is thus an important part of electrochemistry laboratory experiments. The experiments reported in this thesis involve the application of an external potential difference across the working electrode/solution interface. Set-ups using two electrodes are not applicable here, since the current will be large. Large currents can alter the ionic concentration in the solution and therefore the difference between the reference electrode and the measured potential will no longer be constant. This problem is overcome by the addition of a third "counter electrode" which allows the passage of current between it and the working electrode, as opposed to the passage of current between the working electrode and the reference electrode. For measurements in this thesis the counter electrode is a piece of platinum gauze given its inert nature and large surface area.

2.3.2 The Electrochemical Cell

A purpose built three electrode spectro-electrochemical cell (figure 2.6) is used for the RAS experiments described in this thesis. A standard calomel electrode (SCE), consisting of Hg/Hg_2SO_4 in saturated aqueous KCl is used as the reference electrode. The reference electrode is separated from the electrochemical cell by a closed Teflon tap to prevent chloride contamination with a luggin capillary to minimise the distance between the working electrode and the reference electrode to avoid the potential drop. Voltages throughout this thesis are quoted versus SCE. The light from the RAS instrument enters the cell through the low-strain silica window at the front of the cell. Argon gas is bubbled into the electrochemical cell to de-gas the

cell and prevent oxygen contamination of the electrolyte. The luggin capillary used to reduce the effective distance between the reference and working electrodes is not shown in figure 2.6.

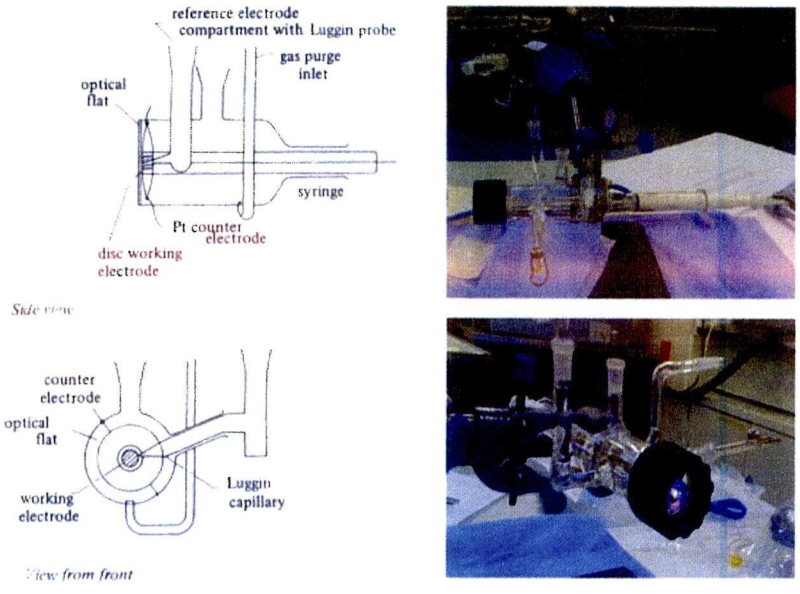

Figure 2.6: A schematic [21] and pictures of the electrochemical cell.

2.4 Crystal Preparation

The Au(110) crystals used throughout the research reported in this thesis are single crystals of 99.999% purity in the form of discs of diameter 10 mm, thickness 2 mm, with an exposed area of 0.5 cm^2 and are oriented to an accuracy of 0.1°. Prior to the experiments, the crystals were mechanically polished to 0.25 μm using cycles of diamond paste of 6 μm, 1 μm, and 0.25 μm and cleaned in an ultrasonic bath. A butane micro-torch was then used to flame anneal the crystals. This involved heating the crystals in the flame until it glowed orange, and then allowing it to cool before repeating the process 15 times [7,22]. This is the case for all experiments presented in this thesis. Following the flame anneal the crystal was cooled in air before putting in ultra-pure water (Millipore Q System, 18 MΩ cm) and then transferred to the electrochemical cell.

2.5 Ultra-Violet Reflection Anisotropy Spectrometer

The majority of RAS studies are undertaken using the photo-elastic modulated spectrometer based on the Aspnes design [6,23,24] and are carried out over the spectral range 1.5 eV to 5.5 eV. The reason for the above range seems to be partly historical, as the RAS technique was originally developed for, and applied to, the study of semiconductor surfaces [6,23-25], and partly on the ability of readily available optical components to cover a wide spectral range with a single instrument.

With RAS established as a highly sensitive and reproducible method for identifying molecular interactions at surfaces [8,9,26-32] in addition to monitoring semiconductor surfaces usually in a gaseous ambient, it has now been used to probe the interactions of nucleic acid bases [11,33] and amino acids [10] at Au(110)/electrolyte interfaces and to monitor the adsorption of ss-DNA and ds-DNA at Au(110)/electrolyte interfaces [34,35]. The latter work showed that both ss-DNA and ds-DNA bind to the gold surface and that RAS could detect the bound molecules. However in order to study the more intense optical transitions that occur in DNA requires an instrument that will go up to 7.0 eV [32,36,37] and circular dichroism (CD) studies confirm that the most sensitive region of the spectrum for distinguishing between DNA sequences is around 180 nm (~ 7.0 eV) [38]. However the present RA spectrometers generally cover the range 1.5 eV to 5.5 eV.

Recent advances in the technique of SE have allowed measurements up to 10.0 eV; this is obtained using synchrotron radiation as its source [39,40]. Research on nucleic acids adsorbed on diamond [32] and Si(111) surfaces [36,37] has also been carried out using synchrotron based ellipsometric techniques. While these studies have revealed useful information on the far UV optical spectra of biological molecules the synchrotron studies require a UHV environment. This is a considerable limitation since biological molecules require a liquid environment in order to exhibit their functional behaviour which is one of the main motivations for studying them. This subsection describes the development of a RAS instrument in close collaboration with Dr. Trevor Farrell. The new UV RAS instrument in combination with a low energy instrument, provides RA spectra from 1.5 eV to

7.0 eV. The overall aim is to enable RAS studies of bio-molecules on Au/electrolyte interfaces where the optical transitions are most intense and in preparation for such studies the new instrument was used to obtain an extended range RA spectrum of the commonly used Au(110)/electrolyte interface [7,10,11,33-35].

In seeking to extend the range of RAS measurements the following factors need to be considered. Of the prism polarisers in common use for wide range spectral studies the Glan type are restricted to calcite, imposing an upper limit of about 5.5 eV. Quartz enables the range to be extended to about 6.0 eV but beam-splitting polarisers such as Rochon, Woolaston or Sernamont prisms must be used. The range can be extended to beyond 7.0 eV if magnesium fluoride beam splitting polariser prisms are used.

The usual light source for RAS studies is the short arc Xenon lamp which when encapsulated in a fused silica tube provides a constant intensity light output up to about 4.0 eV and then falling steadily to about 6.2 eV. Light is absorbed in air at energies above 6.5 eV and thus overlap of orders experienced with extended range gratings does not occur at energies above 3.3 eV. The falling characteristics of the lamp output together with the lower intensity of the higher orders mitigate against order overlap being a problem for lower energies. Beyond 5.5 eV it is preferable to use a deuterium lamp and if energies greater than 6.2 eV are to be studied then a magnesium fluoride window is required. However such a lamp is not suitable for energies lower than 3.0 eV. Since the light output of the deuterium lamp increases with increasing energy from 3.0 eV this can result in problems due to the overlap of orders.

For these reasons it appears that for optimal results over an extended range two instruments are required and a UV instrument based on the Aspnes design [23,24] and situated in an argon filled glove box was developed for this purpose. The lamp and detector combination placed an effective lower limit to the energy range of 4.0 eV whilst residual air in the glove box coupled with the long optical path imposed an effective upper limit of 7.2 eV. Thus order overlap was not a problem. When the sample was immersed in aqueous electrolyte the upper limit was reduced by absorption in the liquid depending on the depth of immersion; typically the limit was 6.9 eV. A list of the components that are used for the two spectrometers is given

in table 2.1. All mirrors in both spectrometers were front-faced coated UV enhanced aluminium.

Optical Item	**UV-VIS Spectrometer**	**Far UV Spectrometer**
Light Source	Hamamatsau Short Arc Xenon Discharge Lamp	Hamamatsu Deuterium Lamp
Polariser/Analyser	Quartz Rochon Prisms Halbo Optics & Carl Lambrecht	MgF_2 Sernamont Prisms Halbo Optics
PEM	Hinds PEM90 Quartz Optical Head	Hinds PEM 90 CaF_2 Optical Head
Monochromator	Jobin Yvon H10	Jobin Yvon H20
Detector	Hamamatsu R955	Hamamatsu R8486

Table 2.1: A list of components and manufactures used in the RA spectrometers.

The use of two spectrometers to provide a single continuous spectrum over an extended range requires an overlap of each spectrometer's individual range so that matching may be accomplished. This is important since different light sources, detectors and amplifiers and polarisers are used in the two instruments. Matching is facilitated if there is a strong feature in the overlap region. The ranges of the two spectrometers used are:

UV-VIS	1.5 eV – 5.5 eV
Far UV	4.0 eV – 7.2 eV

The overlap range is 4.2 eV to 5.0 eV.

The 4.3 eV peak in the Si(110) spectrum sits comfortably in this range and spectra of Si(110) in the two spectrometers enables the scaling factor which is a correction for the difference in sensitivity of the two instruments, to be obtained. However the determination of the scaling factor alone is insufficient to obtain the best match. A translation along the intensity axis is also required. This arises because of the difficulty in defining the true zero base line of $Re(\Delta r/r)$ which is compounded

when two different instruments are used. The polariser angle P is predetermined by the Jones vector analysis [41] but changes in P of minutes of arc can shift the baseline significantly. Whilst using a micrometer adjustment in the polariser mounts it is unlikely that the two polarisers will be set at precisely the same angle. With the UV-VIS spectrometer, P is set so that $\mathrm{Re}(\Delta r/r)$ is near zero at 2.4 eV since there are no spectral features in Si at this energy and when the sample is rotated through 90° the two spectra are, as expected [42] mirror images of each other with the line of reflection being very close to $\mathrm{Re}(\Delta r/r) = 0$ over the whole range. Since 2.4 eV is outside the range of the far UV spectrometer, the $\mathrm{Re}(\Delta r/r)$ of this instrument is set to near zero (before the scaling factor was applied) at 6.0 eV as in preliminary experiments where no features in the Si(110) spectrum were observed near this energy. Since 6.0 eV is outside the range of the UV-VIS spectrometer, it is likely therefore that there will be a small error in these zero settings which will be manifest as a displacement of one spectrum with respect to the other. A translation of $\mathrm{Re}(\Delta r/r) = 0.7\times10^{-3}$ applied to the spectrum from the far UV instrument gave an extremely good match, as shown in figure 2.7.

It should be recognised that in the above matching procedure the scaling factor is constant irrespective of the materials being studied but the translation factor may differ, depending on the polariser angles.

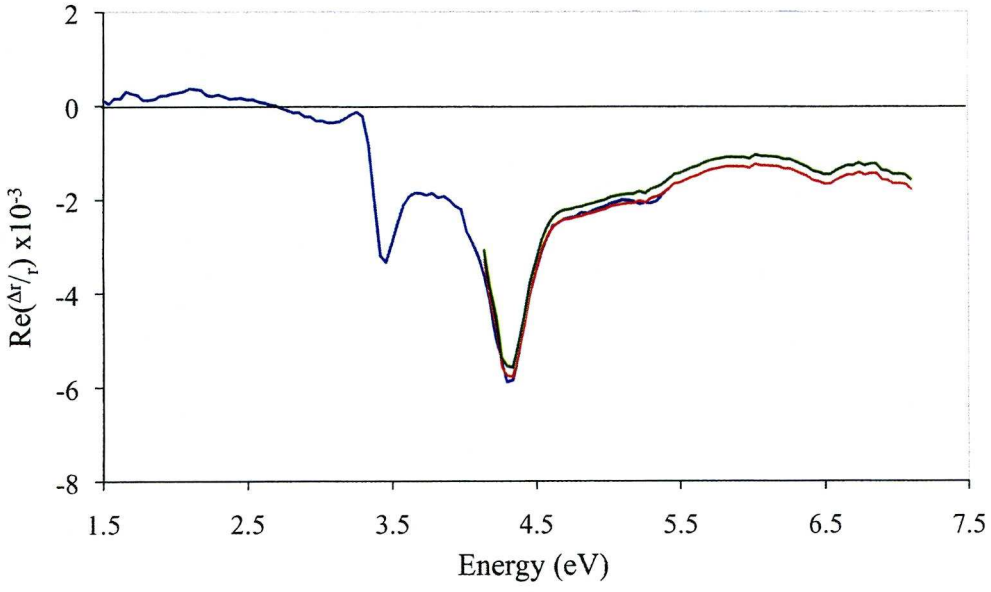

Figure 2.7 Matching the two spectrometers using Si(110) in the UV-VIS (blue line), the UV (green line) and the translated UV (red line).

2.6 References

[1] T. E. Jenkins, *J. Phys. D: Appl. Phys.* **32**, R45 (1999)

[2] K. Vedam, *Thin Solid Films* **313**, 1 (1998)

[3] *Ellipsometery and Polarised Light*, R. M. Azzam and N. M. Bashara (Amsterdam: Elsevier, 1997)

[4] D. E. Aspnes, E. Colas, A. A. Studna, R. Bhat, M. A. Koza and V. G. Kermidas, *Phys. Rev. Lett.* **61**, 2782 (1988)

[5] J. F. McGilp, *Prog. Surf. Sci.* **49**, 1 (1995)

[6] P. Weightman, D. S. Martin, R. J. Cole and T. Farrell, *Rep. Prog. Sci.* **68**, 1251 (2005)

[7] B. Sheridan, D. S. Martin, J. R. Power, S. D. Barrett, C. I. Smith, C. A. Lucas, R. J. Nichols and P. Weightman, *Phys. Rev. Lett.* **85**, 04618 (2000)

[8] C. I. Smith, A. J. Maunder, C. A. Lucas, R. J. Nichols and P. Weightman, *J. Electromchem. Soc.* **150**, E233 (2003)

[9] C. I. Smith, G. J. Dolan, T. Farrell, A. J. Maunder, D. G. Fernig, C. Edwards, D. S. Martin and P. Weightman, *J. Phys.: Condens. Matter* **16**, S4385 (2004)

[10] R. LeParc, C. I. Smith, M. C. Cuquerella, R. L. Williams, D. G. Fernig, C. Edwards, D. S. Martin and P. Weightman, *Langmuir* **22**, 3413 (2006)

[11] C. I. Smith, A. Bowfield, G. J. Dolan, M. C. Cuquerella, C. P. Mansley, D.G. Fernig, C. Edwards and P. Weightman, *J. Chem. Phys.* **130**, 044702 (2009)

[12] A. Bowfield, C. I. Smith, G. J. Dolan, M. C. Cuquerella, C. P. Mansley and P. Weightman, *e-J. Surf. Sci. Nanotech.* **7**, 225 (2009)

[13] A. Maunder, *Ph. D. Thesis*, The University of Liverpool (2001)

[14] *A First Course in Electrode Processes*, D. Pletcher (The electrochemistry consultancy, 1991)

[15] G. Gouy. *Compt. Rend.* **149**, 654 (1909)

[16] G. Gouy. *J. Phys.* **9**, 457 (1910)

[17] D. L. Chapman. *Phil. Mag.* **25**, 475 (1913)

[18] O. Stern. *Z. Electrochem.* **30**, 508 (1924)

[19] D. C. Grahame, *Chem. Rev.* **41**, 441 (1947)

[20] D. M. Kolb, *Surf. Sci.* **500**, 722 (2002)

[21] Book

[22] G. Binning, H. Rohrer, Ch. Gerber and E. Weibel, *Surf. Sci.* **131**, L379 (1983)

[23] D. E. Aspnes, J. P. Harbison, A. A. Studna and L. T. Florez, *J. Vac. Sci. Technol. A* **6**, 1327 (1988)

[24] J. P. Harbison, D. E. Aspnes, A. A. Studna, L. T. Florez and M. K. Kelly, *Appl. Phys. Lett.* **52**, 2046 (1988)

[25] W. Richter, *Phil. Trans. R. Soc.* A **344**, 453 (1993)

[26] C. Goletti, G. Bussetti, P. Chiaradia, R. Paolesse, C. Di Natale, E. Mazzone and A. D'Amico, *Phys. Status Solidi A* **188**, 1339 (2001)

[27] G. Bussetti, C. Goletti, P. Chiaradia, A. Sassella, M. Campione, S. Tavazzi and A. Borghesi, *Surf. Sci.* **601**, 4488 (2007)

[28] M. Scarselli, G. Ercolani, P. Castrucci, D. Monti, G. Bussetti, M. Russo, C. Goletti, P. Chiaradia, R. Paolesse and M. De Crescenzi, *Surf. Sci.* **601**, 2607 (2007)

[29] S. D. Silaghi and D. R. T. Zahn, *Appl. Surf. Sci.* **252**, 5462 (2006)

[30] N. Witkowski, O. Pluchery, S. Royer and Y. Borensztein, *Phys. Status Solidi C* **2**, 4053 (2005)

[31] M. Marsili, N. Witkowski, O. Pulci, O. Pluchery, P. L. Silvestrelli, R. Del Sole and Y. Borensztein, *Phys. Rev. B* **77**, 125337 (2008)

[32] S. Wenmackers, S. D. Pop, K. Roodenko, V. Vermeeren, O. A. Williams, M. Daenen, O. Douhéret, J. D'Haen, A. Hardy, M. K. Van Bael, K. Hinrichs, C. Cobet, M. van de Ven, M. Ameloot, K. Haenen, L. Michiels, N. Esser and P. Wagner, *Langmuir* **24**, 7269 (2008)

[33] P. Weightman, G. J. Dolan, C. I. Smith, M. C. Cuquerella, N. J. Almond, T. Farrell, D. G. Fernig, C. Edwards and D. S. Martin, *Phys. Rev. Lett.* **96**, 086102 (2006)

[34] M. C. Cuquerella, C. I. Smith, D. G. Fernig, C. Edwards and P. Weightman, *Langmuir* **23** 2078 (2007)

[35] C. P. Mansley, C. I. Smith, M. C. Cuquerella, T. Farrell, D. G. Fernig, C. Edwards and P. Weightman, *Phys. Status Solidi C* **5**, 2582 (2008)

[36] S. D. Silaghi, M. Friedrich, R. Scholz, T. U. Kampen, C. Cobet, N. Esser, W. Richter, W. Braun and D. R. T. Zahn, *Thin Solid Films* **455**, 505 (2004)

[37] S. D. Silaghi, M. Friedrich, C. Cobet, N. Esser, W. Richter, W. Braun and D. R. T. Zahn, *Phys. Status Solidi A* **242**, 3047 (2005)

[38] *Circular Dichroism and Linear Dichroism*, A. Rodgers and B. Nordén (Oxford: Oxford University Press, 1997)

[39] R. L. Johnson, J. Barth, M. Cardona, D. Fuchs and A. M. Bradshaw, *Nucl. Inst. Methods* A **290**, 606 (1990)

[40] R. L. Johnson, J. Barth, M. Cardona, D. Fuchs and A. M. Bradshaw, *Rev. Sci. Instrum.* **60**, 2209 (1989)

[41] D. S. Martin and P. Weightman, *Surf. Interface Anal.* **31**, 915 (2001)

[42] T. Farrell, P. Harrison, C. I. Smith, D. S. Martin and P. Weightman, *Appl. Phys. Lett.* **93**, 191102 (2008)

Chapter 3

The Au(110) Surface

An understanding of the Au(110) surface is a crucial prerequisite for the use of RAS to monitor the behaviour of biological molecules adsorbed at an Au(110)/electrolyte interface. This chapter works through the previous studies of the Au(110) surface both in UHV and electrochemical environments and discusses the electronic and physical structure of the surface. This chapter also introduces the three-phase model which is used in RAS simulations of the Au(110) surface and includes summaries of recent studies of the behaviour of the Au(110) surface reconstructions in varying electrolytes and electrode potentials.

3.1 Introduction

In this work a cubic crystal is used to obtain surface specificity, although amorphous substrates can also give rise to surface specificity. The Au(110) surface that is used throughout this thesis is one of the low index faces of the gold face centred cubic (FCC) crystal structure. Following the flame annealing preparation methods described in section 2.4, the Au(110) adopts the (1×2) reconstruction, alternatively known as the "missing row" reconstruction that is discussed in greater detail in section 3.3. The (1×2) reconstruction has the anisotropic structure required for monitoring surface sensitivity using RAS and this intrinsic anisotropy gives rise to an RA spectrum with substantial well-defined features. Conversely, the other low index faces of gold; the unreconstructed (100) and (111), have inherently isotropic surface structures which do not yield RA spectra.

The flame annealing process that is used to prepare the Au(110) crystals allows the sample to be prepared in conditions outside of a UHV environment. In particular this method of specimen preparation yields single crystal electrodes within electrochemical environments and facilitates the investigations of the adsorption of biological molecules which are discussed in this thesis.

3.2 Surface Phase Transitions

Phase transitions can occur in many physical systems. These transitions belong to two broad categories. There are the first-order transitions which are characterised by latent heats and arise primarily through "mixed phase" regimes whereby parts of the system have successfully undergone the transition but others are yet to achieve this state; an example of this type of system is the solid/liquid/gas transitions. Second-order transitions, sometimes known as continuous phase transitions, do not have a latent heat. This category of phase transitions includes the transitions to the superconducting and superfluid states when the temperature is lowered in some metals and in liquid He.

Phase transitions result from the tendency of systems in thermodynamic equilibrium, at constant temperature and volume, to minimise their free energy, F.

$$F = U - TS \tag{3.1}$$

The transitions arise at specific temperatures at which the free energy can be divided between the internal energy, U(T), and the entropy of the system, S(T), in different ways. To characterise a phase transition, it is necessary to define order parameters. These order parameters capture the change in the order of the system as the transition temperature, T_C, is reached. For second-order transitions, the order parameter varies by $(T-T_C)^{\beta}$, where β, the critical exponent, depends solely on the dimensionality of the order parameter, the dimensionality of space and the symmetry of the system.

3.3 The Physical Structure of the Au(110) Surface

The following subsections consider the Au(110) surface and the phase transition between the (1×2) surface reconstruction and the (1×1) surface structure. This phase transition can be stimulated by means of thermal treatment under UHV conditions or by the potentiostatic control encountered within an electrochemical cell.

The phase transition of the Au(110) surface has evoked considerable interest and a summary of previous investigations into the transition is given in this section, since it is important to have knowledge of the transitional behaviour of the Au(110) surface under various environments in order to understand the RA spectral profiles of the system as functions of applied electrode potential and sample temperature. The background literature of the conformational changes to the surface, experienced in both UHV and electrochemical environments, has been reviewed extensively by N. J. Almond [1] and A. Bowfield [2]. Their findings will be summarised in the following section together with more recent work.

3.3.1 Au(110) in UHV

Figure 3.1 shows a schematic of some of the low Miller index surfaces. Of the low Miller index surfaces, the (110) surface is the most open of a FCC crystal and because of this the (110) surface have the lowest atomic density and highest surface energy. This causes the (110) surface to have a susceptibility to reconstruct. An unreconstructed Au(110) surface is called the (1×1) surface structure, which reveals the atoms exposed when a FCC crystal is cut through the (110) plane.

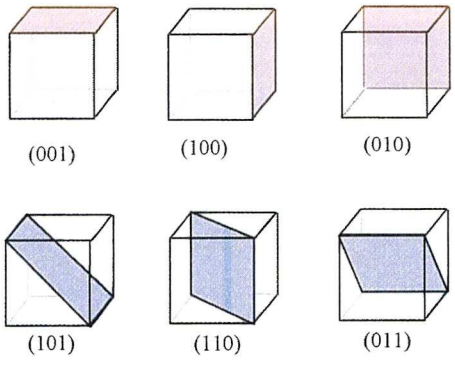

Figure 3.1: A schematic of some of the low index Miller surfaces.

Figure 3.2 (a) shows this unreconstructed (1×1) surface structure, highlighting the rows of gold atoms. The most common reconstruction is the (1×2) reconstruction. This configuration results from the removal of every other row of gold atoms along the $[1\bar{1}0]$ direction. This reconstruction is shown in figure 3.2 (b).

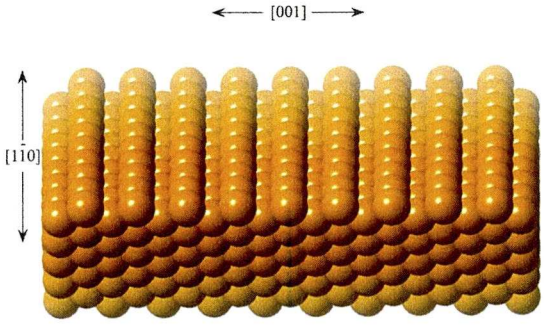

Figure 3.2 (a): A schematic of the Au(110)-(1×1) reconstruction.

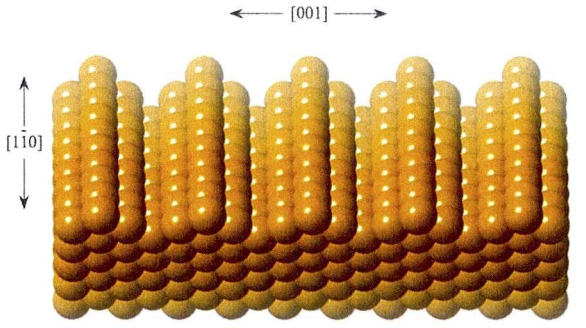

Figure 3.2 (b): A schematic of the Au(110)-(1×2) reconstruction.

The first technique used to reveal the (1×2) surface reconstruction [3,4] was LEED and this showed a reversible temperature dependent phase transition between the (1×2) and the (1×1) surface reconstructions in UHV conditions. In order for this transition to occur, a large scale reorganisation of the surface atoms needs to take place. Numerous models were given for this rearrangement, with each of them being tested [5] on the Ir(110)-(1×2) surface. Various models of the reconstructions were suggested including the paired rows model, the buckled surface model and the missing row model. The latter of these models was found to be the most probable after an R-factor analysis of X-Ray Diffraction (XRD) [6] results. At first sight the transition between the (1×1) surface structure and the (1×2) reconstruction would seem to require one half of the Au atoms on the surface to relocate by diffusion. However a comparison of the transition times and the self diffusion times revealed a 'mass transport problem' [7,8]. The transitions were too fast to be effected by the long range diffusion. Binnig *et al* [9] published an STM image which confirmed the missing row model of the (1×2) reconstruction. This model requires the removal of every second row of atoms along the [1$\bar{1}$0] direction, exposing (111) microfacets between the rows. It was suggested that the creation of the (111) microfacets facilitates the reconstruction by creating a more energetically stable surface structure. If two rows are removed from the (1×1) surface instead of just one, the surface adopts a (1×3) reconstruction which exposes greater (111) microfacets. The (1×3) surface reconstruction is shown in figure 3.3. STM studies have given an insight into the dynamics of surface structure throughout the (1×1) to (1×2) phase

transition. Studies have shown [10-16] the step structure to be of high importance to the phase transitions, whereby the mesoscopic "fish scale pattern" on the surface has been seen. The fish scale pattern relates to the anti-phase boundaries arising from the (111) step edges [14].

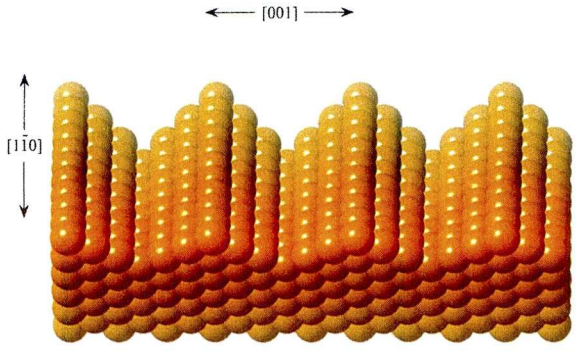

Figure 3.3: A schematic of the Au(110)-(1×3) reconstruction.

Monatomic steps on the Au(110) surface are restricted to the [1$\bar{1}$0] direction as steps along the [100] are impeded at room temperatures thus promoting the growth of large terraces. A disordered lattice gas phase model [17] was used to understand part of the (1×2) to (1×1) phase transition. The model only works if the surface only contains wall defects. If only steps were found on the surface then a roughening transition occurs. Regular surface step densities suggest a solution to the mass transport problem. If half of the surface atoms move as the surface changes from the (1×2) surface structure to the (1×1) surface structure, this indicates that the movement of steps and the growth of terraces on such a large scale would manifest itself in fluctuating step densities. Thus if one considers the (1×1) surface structure to be made up of a disordered half monolayer of surface atoms then all that is required to solve the mass transport problem associated with the (1×1) to (1×2) phase transition is for one half of the surface atoms to move on the order of one atomic space. As wall defects and steps are on the Au(110) surface, as the temperature is increased, the surface first undergoes a 2D Ising transition at a surface deconstruction temperature (T_D) followed by a roughening transition at a higher temperature (T_R). Figure 3.4 shows the excitations on the Au(110)-(1×2) surface with Ising and roughening transitions [18].

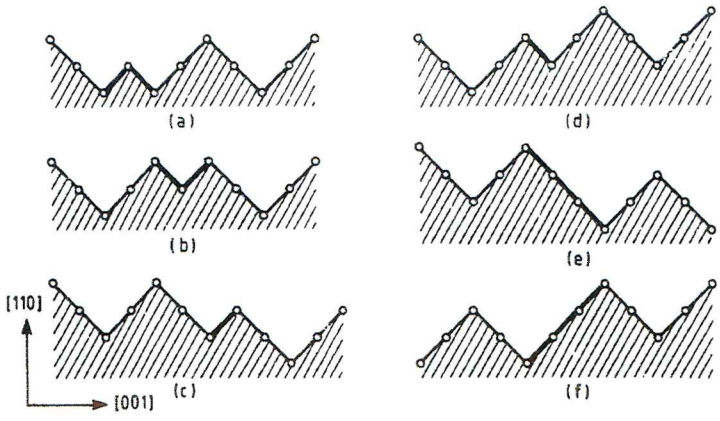

Figure 3.4: The excitations on the Au(110)-(1×2) surface structure taken from [18]. The heavy lines in (a) and (b) represent Ising-like excitations whereas in (c) to (f) they represent roughening transitions.

It is clear from models of the (1×2) reconstruction and confirmed by the results of STM studies that terraces that adopt the (1×2) reconstruction cannot be terminated by (111) microfacets on both sides of a step along the $[1\bar{1}0]$ direction. Instead one side of such terraces must be terminated by a (1×3) reconstruction that corresponds to an anti-phase boundary between (1×2) regions. It was found that the (1×2) surface reconstruction was stable at high temperatures close to T_R in the interior of terrace regions [15,19]. The effect of the deconstruction transition is to disorder the step edges. It is found that the temperature at which the (1×1) to (1×2) reconstruction occurs varies significantly; 850 K to 1080 K for different specimens, a result that is attributed to variations in crystal quality, crystal size and sample preparation.

Other *5d* FCC metals such as Iridium, Ir, and Platinum, Pt, have the same (1×2) surface structure as Au(110) [20,21] in UHV environments. The stabilisation of the (1×1) surface and the (1×2) surface reconstructions is determined by a balance between the reduction in kinetic energy, KE, of the *s-p* electrons [22], which is enhanced by the formation of (111) microfacets, and the increase in surface formed by the breaking of bonds necessitated by the formation of these facets. On the contrary, isoelectronic *3d* and *4d* FCC transition and noble metals do not exhibit a (1×2) reconstruction. These metals, such as Nickel, Ni, Copper, Cu and

Palladium, Pd, maintain the (1×1) surface structure when exposed to the same conditions.

The (1×2) surface reconstruction has been observed on Ag(110) as a result of the adsorption of sub-monolayer proportions of Potassium, K, [23]. This result has been attributed to charge transfer from the alkali metal atoms to the surface which increases the surface electronic charge density of the *s-p* surface electrons, and therefore leading to the need to reduce kinetic energy and reconstruct as the (1×2) surface structure.

3.3.2 The Electrochemistry of Au(110)

As a result of a variety of studies we now have a clear understanding of the (1×1) to (1×2) phase transition of the Au(110) surface in UHV. However the behaviour of the Au(110) surface under an electrochemical environment is much more difficult to comprehend because of the presence of the electrolyte. Important information on the Au(110) surface under electrochemical conditions has been obtained from electrochemical STM techniques. A study of an Au(110) electrode in aqueous perchloric acid ($HClO_4$) [24] demonstrated that the Au(110) surface shows similar behaviour when the applied potential was negative of the PZC to that observed by changes in temperature in a UHV environment. The PZC corresponds to the value of potential where the solid electrode in electrolyte has a zero net electrical charge on the surface. At an applied potential of -0.02 V vs. SCE, the Au(110) surface was found to be predominantly made up of (1×2) domains, but there were also small regions of the (1×3) surface reconstruction. When the applied potential was taken to -0.3 V, the (1×2) plus (1×3) structure was maintained. As in UHV conditions, the surface electronic charge density will be negative at the -0.02 V potential and this promotes the (1×1) to (1×2) phase transition in order to reduce the surface kinetic energy. A reversible transition to the unreconstructed (1×1) surface structure on a time scale of two seconds, is driven by the reduction in atomic density of the surface and facilitated by the requirement of only short range motion of the atoms.

A study of the Au(110) surface in perchloric acid and sulfuric acid (H_2SO_4) [24] showed 700 Å terraces of the (1×2) structure separated by monatomic steps. However these results revealed interesting differences between UHV and electrochemical environments. In an electrochemical environment anisotropic islands were dispersed across half of the terraces on the Au(110) surface, therefore creating only a few small regions of perfect (1×2) reconstruction. The (1×2) reconstructions were maintained at voltages below +0.05 V, however at +0.25 V the unreconstructed (1×1) surface was adopted. Between the two potentials, the surface consisted of a mixture of (1×1) and (1×2) regions.

The potential at which the (1×2) reconstruction is adopted is found [25] to be 0.3 V greater than the result presented by Gao *et al* [24]. The applied potentials close to the PZC were expected to give the most prevalent reconstruction which equates to that found in UHV conditions. At potentials greater than +0.2 V, steps occurred as well as holes and isotropically shaped islands. The positions of the holes correspond to the positions of the anisotropic islands that were found on the (1×2) reconstruction. At potentials of +0.8 V the surfaces roughen due to the substrate being oxidised.

The (111) microfacets aid the step structure stabilisation in electrochemical environments, even though the regions of (1×2) reconstruction are smaller than those found in UHV conditions. Magnussen *et al* [25] and a previous study [12] agree that anti-phase domain boundaries separate the (1×2) terraces, suggesting that the (1×3) domains play a vital part in the phase transition.

Ocko *et al* [26] obtained results from a surface X-ray scattering study that showed a reconstructed Au(110) surface in $HClO_4$ at 0.0 V vs. SCE and the Au(110) surface was primarily made up of regions of (1×2) with a few (1×3) domains. Various halide salt solutions were examined and they resulted in the (1×3) reconstructions at significantly negative voltages. However, at positive voltages the surface adopted the (1×1) unreconstructed structure. No (1×2) reconstruction was found between these two voltage regions. This direct transition from a (1×3) phase to a (1×1) phase has been found in UHV following the adsorption of minor amounts of alkali metals [27]. This and other work [28-30], supports the argument that at sufficiently negative surface charge the (1×3) surface reconstruction occurs. These

studies suggest that the Au(110) surface takes the form of the (1×2) reconstruction when approaching voltages of the PZC and that the surface adopts the (1×1) structure at more positive potentials. When immersed in alkaline solutions, the Au(110) adopts the (1×3) reconstruction due to greater negative excess charges within the electrolyte. To date is it unknown as to why in these conditions there is direct movement from the (1×3) structure to the (1×1) structure, whilst avoiding an intermediate (1×2) structure.

The fact that such intricate changes occur in the Au(110) surface structure emphasizes the importance of the varying mechanisms that promote surface phase transitions. Almost all of the experiments reported in this thesis are performed on Au(110) samples in liquid environments. The (111) microfacets are the key to the surface reconstructions and the adsorption of some biological molecules. In this work RAS is used to monitor these reconstructions and their corresponding optical responses. In order to understand the RA spectra of the Au(110) surface it is first necessary to understand the electronic structure of the surface.

3.4 The Electronic Structure of the Au(110) Surface

The RA spectrum of the Au(110) surface has been interpreted in terms of single particle excitations between states in its band structure. Some insight into the optical spectrum of the Au(110) surface can be obtained from electroreflectance spectroscopy (ERS). The ERS experiments [31] showed that the Au(110) surface was optically anisotropic when reconstructed. Liu *et al* [32] used ERS to investigate the optical transitions that occur on the low Miller index surfaces of gold. The data obtained were compared to theoretical results obtained from pseudo-potential calculations of the bulk and surface electronic structure. The theoretical results revealed the presence of surface states at particular symmetry points in the Surface Brillouin Zone (SBZ) and assumed a (1×1) unreconstructed surface. Ho *et al* [22] and Xu *et al* [33] extended the theoretical studies to include a (1×2) surface reconstruction thus halving the SBZ yielding results for the surface electronic structure supported by photoemission measurements [34]. Figure 3.5 is a

representation of the electronic structure of the Au(110) surface calculated by Xu *et al* [33].

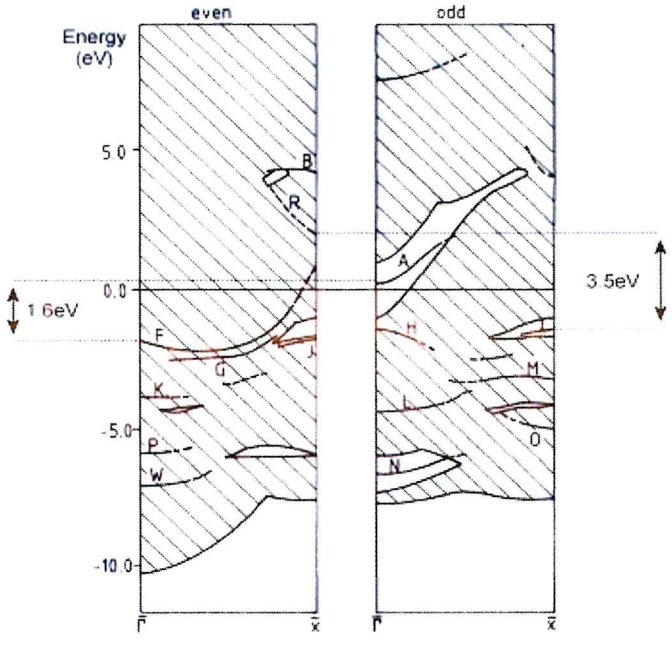

Figure 3.5 (a): The calculated electronic structure of Au(110) taken from Xu *et al* [33].

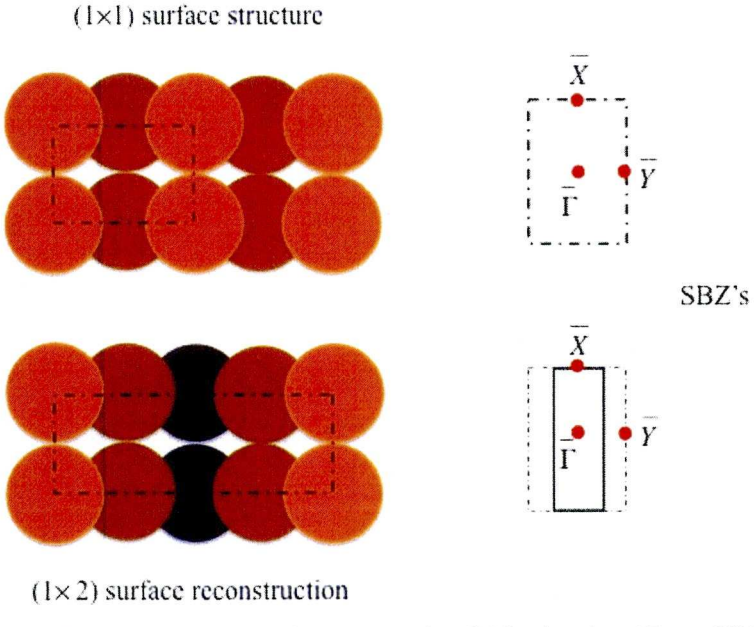

Figure 3.5 (b): The calculated electronic structure of Au(110) taken from Xu *et al* [33].

The centre of the SBZ is called the $\bar{\Gamma}$ point. The point at the edge of the SBZ in reciprocal space, which is perpendicular to the $\bar{\Gamma}$ point and in the [100] direction is called the $\bar{Y}$ point. These points are shown in figure 3.5 (b) and how the size of the SBZ varies between the surface reconstructions. Similarly, the point perpendicular to the $\bar{\Gamma}$ point but in the [110] direction is called the $\bar{X}$ point. Only certain transitions can occur at the $\bar{X}$ and $\bar{Y}$ points. If the transition has the correct energy at a point in reciprocal space, the polarisation that excites that transition depends on the symmetry and parity of the initial and final states. The condition that the orbital quantum number obeys, $\Delta\ell = \pm 1$, for an allowed optical transition must also be satisfied. This means that a transition only occurs at a point in reciprocal space when the two states involved in a transition are respectively even and odd with respect to reflection in a plane perpendicular to the polarisation of the E vector of the incident light.

3.5 RAS of the Au(110) Surface

To understand the RA spectra of the Au(110) surface reported in this thesis, theoretical simulations are required to support experimental results and to suggest further investigations. As the technique of RAS is still in its infancy there are no calculations of the RAS of the Au(110) surface from first principles.

3.5.1 Early RAS Studies of Au(110)

Early RAS work recorded the optical response of Ag(110) and Au(110) surfaces [35] and a sample RA spectrum of the Au(110)-(1×2) surface in UHV is shown in figure 3.6 (a). The primary RA spectrum of the Au(110) surface under ambient conditions was published in conjunction with a theoretical model based on the surface local-field effect (SLFE). The RA spectrum obtained in that work differs considerably from those produced by modern RA spectrometers. Surface sensitive RAS profiles of cubic crystals like the Au(110) surface can now be produced experimentally. Some initial calculations explained the electronic structure of the

Au(110) surface in UHV but they were unable to simulate the experimental RA spectra [36], however, reference 36 did show that the (1×1) to (1×2) phase transition was accompanied by an increase in the spectral feature at 2.5 eV. This increase is accredited to the screened local field on *d*-band transitions.

Mazine *et al* [37] disagreed with the results of the local field theory. Their STM and RAS study of Au(110) in sulfuric acid describes a decrease in the 2.5 eV feature in an electrochemical environment at -0.2 V. This result was due to a "poorly reconstructed" (1×2) reconstruction, but in a further publication [38], the same authors describe a RA spectrum as an "optical fingerprint" of the Au(110)-(1×2) reconstruction. The RA spectra from each of the studies carried out by Mazine and co workers [37,38] were very similar. Weightman *et al* [39] suggested the inconsistency in the labelling of the RA spectra in [37,38] occurred because of the change in surface morphology of the gold specimens used in each experiment.

Figure 3.6 (a) shows the RA spectral profile of an Au(110) sample under UHV conditions. It shows a positive feature between the energies of 1.5 eV and 2.3 eV, negative features arising at 2.5 eV and 3.5 eV and finally a positive feature between the energies of 4.0 eV and 5.0 eV. The first three features of the Au(110) RA spectrum described above and the origin of those features has been attributed to transitions occurring between states in the electronic structure of the surface and the few layers of atoms directly beneath the surface. The positive feature which begins at 4.0 eV requires deeper analysis. Martin *et al* [21] used RAS in association with STM and established that the positive feature found in an Au(110) RA spectrum starting at 4.0 eV was correlated with surface steps. Consequently this positive peak was attributed to the existence of monatomic high steps aligned parallel to the [1 $\bar{1}$0] axis of the Au(110). Figure 3.6 (b) is the STM image taken of the Au (110) sample under UHV conditions, displaying the (1×2) surface reconstruction and the monatomic steps. Figure 3.6 (b) corresponds to the RA spectrum of figure 3.6 (a).

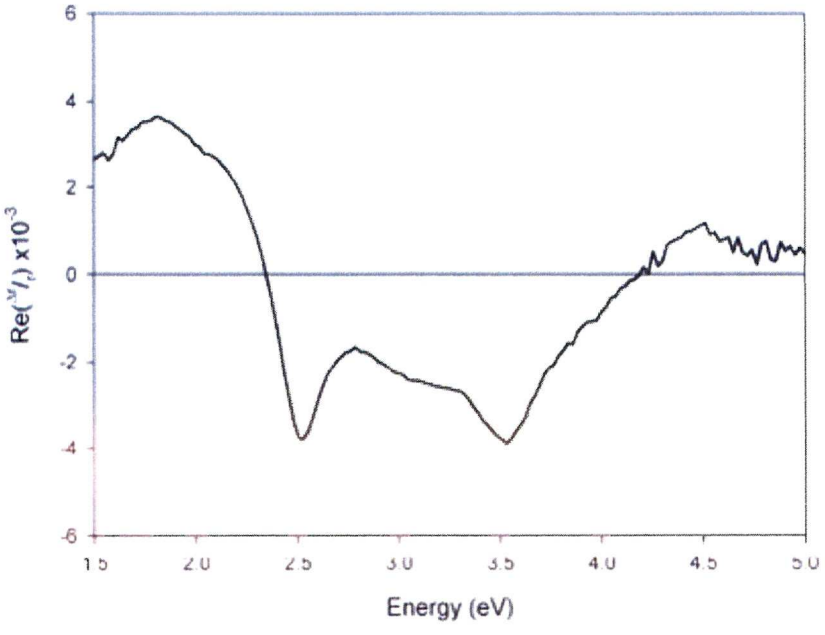

Figure 3.6 (a): RA profile of the Au(110) crystal the STM of the surface of which is shown in (b). From Martin *et al* [21].

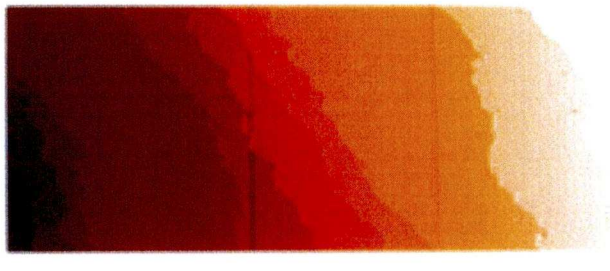

Figure 3.6 (b): STM image of Au(110) in UHV after annealing showing the monatomic steps and large terraces associated with the (1×2) reconstruction (100nm × 40nm). From Martin *et al* [21].

3.5.2 Interpreting the RAS of Au(110)

Sheridan *et al* [40] analysed the RA spectrum of the Au(110)-(1×2) surface in terms of optical transitions between states at the $\overline{\Gamma}$ and $\overline{X}$ points of the SBZ which were obtained from first principle calculations [33]. The results of the calculations of the surface electronic structure of Au(110) [33] had been compared with results obtained by inverse photoemission experiments [41]. It was suggested that the peak which features at ~2.5 eV on the RA spectrum arises from a transition at the $\overline{\Gamma}$ point

between an unoccupied surface resonance of odd symmetry, derived from *d* states of *yz* character, and an empty surface state that lies ~0.3 eV above the Fermi energy. It has been suggested that the region of the RA spectrum between 1.5 eV and 2.5 eV is sensitive to variations in the Au(110) surface electronic or physical structure because of a contribution to the optical response from a surface state [31]. The feature of the RA spectrum which occurs at ~3.5 eV was attributed to a transition between an empty state of even symmetry and mainly *sp* character, and a state of odd symmetry that is *d* derived. This feature at ~3.5 eV is not as sensitive to surface alterations as the feature at ~2.5 eV, a finding that is attributed to the states involved having significant contributions from the secondary layer of atoms.

3.5.3 Further Work on Au(110)

Following on from this investigation [40], the Au(110) surface was treated to a course of Argon ion bombardment for specific durations of time and was periodically probed by LEED, RAS and STM [21]. After just three minutes of exposure to Ar ions, the 3.5 eV feature was no longer visible on the RA spectra. After a similar period of time, the long step structures observed by STM on the clean Au(110) are no longer visible, suggesting they are sensitive to the surface morphology. Also, after only three minutes of bombardment, the spectral feature between 4.0 eV and 5.0 eV is lost, causing the RA spectrum of Au(110) to plateau in this energy region. The removal of the step structures by Ar ion bombardment was also observed in the RAS study of Cu(110) [42].

The region 1.5 eV to 2.3 eV of the Au(110) RA spectrum also undergoes a reduction in intensity corresponding to a reduction of surface layer anisotropy, leading to a smaller contribution from the surface state to the RA spectrum following Ar ion bombardment. Despite its loss in intensity, the peak at 2.5 eV maintains its definition after 36 minutes of bombardment, indicating the slow emergence of the (1×1) surface structure from the (1×2) reconstruction. These studies highlight the sensitivity of the 2.5 eV peak to the surface reconstructions but also its resistance to effects caused by the alteration of surface roughness. After

bombardment the Au(110) surface is different to the truncated surfaces of the reconstructed (1×2) and (1×3) surfaces. The contributions from the second and third layers are more likely to be disordered and do not give rise to any surface anisotropy. A reduced surface anisotropy leads to the removal of the surface modified bulk states. These bulk states contribute to the 2.5 eV region of the Au(110) RA spectrum. This interpretation is supported by previous studies [18,36] that suggest this feature of the RA spectrum is the result of inter-band transitions involving bulk *d* bands.

3.5.4 Thermal Studies of Au(110) in UHV

The temperature dependence of the RAS of the Au(110) surface in UHV has been studied by two groups [20,43]. It was found that the RAS features of the Au(110) surface became less defined as the temperature of the sample was increased to 800 K [20] and 1000 K [43] corresponding to temperatures which exceed both the T_C and T_R for this surface. The energies of features at 1.8 eV, 2.5 eV, 3.5 eV and 4.5 eV were monitored as a function of temperature. The feature at 1.8 eV was unchanged by the variation of sample temperature, although the region of the RA spectra between 1.8 eV and 2.5 eV, which is thought to have contributions from transitions involving surface states, does reduce in intensity, once again reinforcing the idea of disordering of the surface atomic structure throughout the phase transition that is anticipated in this temperature range. The feature at 2.5 eV is unchanged to temperatures of 580 K but experiences a slight increase in energy when the sample exceeds that temperature. When approaching the T_R, between 700 and 815 K, the 2.5 eV feature broadens to the point where it is no longer well defined. The features at 3.5 eV and 4.5 eV change markedly as the temperature is increased. Both features undergo significant broadening suggesting that the two features are linked in some way. In addition to the broadening of the 3.5 eV peak experiences a shift in peak energy to approximately 3.1 eV as the temperature of the Au(110) sample is taken towards the T_R.

The results obtained in the temperature variation experiments [43] were analysed using a model derived by Russow *et al* [44] and were found to be consistent with a thermovariation spectroscopy investigation [45] whereby the primary features of the bulk dielectric constant, ε_b, of the Au(110) sample are attributed to interband transitions situated close to the L point of the bulk Brillouin Zone (BZ). The agreement of the temperature dependent RAS results and the thermovariation spectroscopy results makes it possible to attribute the 3.5 eV and 4.5 eV features observed on the Au(110) RAS profile to specific transitions; the $E_F \rightarrow L_3$ and $L'_2 \rightarrow L^u_1$ transitions respectively. This correlation leads to the conclusion that the region of the Au(110) RAS profile between 2.5 eV and 4.5 eV originates from transitions involving surface modified bulk states.

3.5.5 Deposition on Au(110)

The underpotential deposition (UPD) of Cu onto Au surfaces has been investigated [46-52]. Smith *et al* [52] used RAS to study an Au(110) sample in a mixture of sulphuric acid and copper (II) sulphate ($H_2SO_4/CuSO_4$). In this study the optical response of the system was monitored as the potential was varied through an array of applied positive potentials. The study showed that at +0.1 V vs SCE, the RAS corresponds to one monolayer of Cu adsorbed at the interface but at an applied potential of +0.4 V vs SCE the RAS is used to show that there was no Cu adsorption. Determining whether the Cu adsorption occurs is dependent on the Au surface reconstruction. Cu adsorbs on the (1×2) surface reconstruction which occurs at +0.1 V vs SCE, but Cu does not adsorb at +0.4 V vs SCE when the Au surface now consists primarily of the unreconstructed (1×1) surface structure. The idea that the surface structure effects the Cu adsorption is suggested from the changes observed in the RAS profiles; more specifically the increase in the 3.5 eV feature and the small decrease in the feature at 2.5 eV. Data of the Au(110) surface in H_2SO_4 at +0.1 V vs SCE and + 0.4 V vs SCE, both with and without the $CuSO_4$, indicated that the variations in optical response were due to the UPD layer and not to a more reconstructed surface. The Cu layer causes the termination of the top layer of

Au atoms causing the surface of the Au to act more like bulk material, thus leading to the increase of the 3.5 eV feature. A two monolayer deposition of Pd onto the Au(110) surface was found to migrate below the surface of the Au [53], which resulted in a decrease in the intensity of the feature found at 3.5 eV probably because the Au/Pd mixed layer did not have an ordered anisotropy. N. J. Almond [1] used the three phase model to analyse the changes observed in the Cu study [52] and attributed these changes to a (1×1) to (1×2) phase transition under electrolyte. This result indicates that the UPD of Cu onto the Au(110) surface does not inhibit the phase transition.

The studies discussed in this subsection demonstrate that RAS is an experimental technique that provides surface sensitive information of the Au(110) surface.

3.6 The Three-Phase Model

The Jones matrix formalism described in section 2.2 describes the behaviour of the polarised light after it has been reflected from the sample's surface. However in order to understand RA spectra there is a need to understand the change in polarisation of the incident light when it is reflected from the surface.

As there are very few *ab initio* theoretical treatments derived from first principles for the RAS response of materials, McIntyre and Aspnes [54] introduced a linear approximation that can be used in reflectivity calculations for multiphase stratified systems like the interfacial surface region of an Au(110) sample in UHV or electrochemical environments. This model was developed further by Cole *et al* [55]. The model assumes the reflecting surface can be represented by the three regions as shown in figure 3.7. The three regions are an anisotropic surface in between an isotropic semi-infinite bulk and an ambient/vacuum layer.

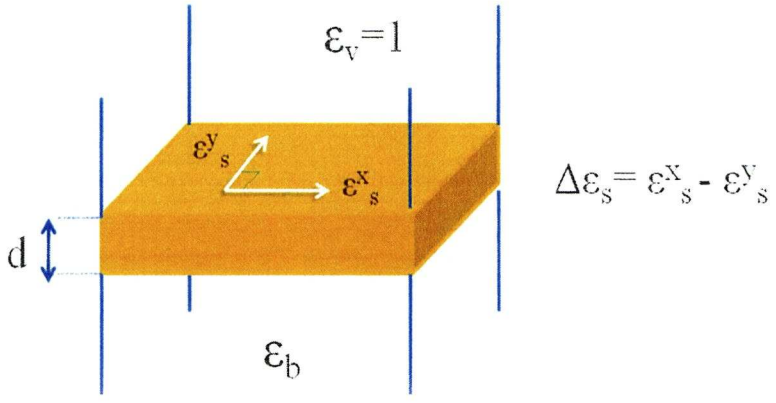

Figure 3.7: A schematic of the three phase model.

3.6.1 The Dielectric Function

The interaction of light with a material can be described by the dielectric function, ε [56]. The three phase model discussed in the previous section treats this interaction in terms of three differing media; the ambient/vacuum layer, the surface of the sample and the bulk of the sample, each having their own distinct dielectric function. The dielectric functions of the semi-infinite bulk (ε_b) and the ambient/vacuum layer (ε_v) are both isotropic, while the dielectric function of the surface is split into two principle directions (ε^y_s, ε^x_s) and ε^y_s and ε^x_s may not be equal due to the anisotropy of the sample. This possible difference between the dielectric response in the x and y directions, $\Delta\varepsilon$, is also known as the surface dielectric anisotropy (SDA). This difference results in an RAS response when $\varepsilon^y_s \neq \varepsilon^x_s$. If it is assumed that $d << \lambda$ and that the dielectric function for the ambient/vacuum layer, $\varepsilon_v = 1$, the RAS equation can be expressed in terms of the surface and bulk dielectric functions, as shown in equation 3.2.

$$\frac{\Delta r}{r} = -\frac{2i\omega d}{c}\left[\frac{\varepsilon_s^x - \varepsilon_s^y}{1-\varepsilon_b}\right] \tag{3.2}$$

where ω is the angular frequency and c is the speed of the wave. Equation 3.2 links (Δr/r), an experimentally measurable quantity, to the material property $\Delta\varepsilon_s$. The RA spectra that are given in this thesis correspond to the real part of the RAS signal. Therefore equation 3.2 can be expressed in terms of the real parts:

$$\mathrm{Re}\left(\frac{\Delta r}{r}\right) = \frac{2\omega d}{c}\mathrm{Im}\left[\frac{\Delta\varepsilon_s}{1-\varepsilon_b}\right] \tag{3.3}$$

3.6.2 The Lorentzian Transition Model

In order to simulate RA spectra, the optical transitions can be approximated by Lorentz contributions. In order to do this, the bulk dielectric function in terms of functions $A(\omega)$ and $B(\omega)$ given by equation 3.4.

$$A(\omega) - iB(\omega) = \frac{1}{1-\varepsilon_b(\omega)} \tag{3.4}$$

$A(\omega)$ and $B(\omega)$ are determined from the bulk dielectric function, which itself is derived from the refraction coefficient, n, and the extinction coefficient, k, in the expression $\varepsilon = N^2$, whereby N is the refractive index and is in turn given as $N = n - ik$. Using SE [57], the values of n and k for the Au(110)-(1×1) can be determined. The data produced by Blanchard *et al* [58,59] is used for the range from 1.5 eV to 5.0 eV and the lower resolution data from Palik [57] is utilised for the energy range beyond 5.0 eV. Equation 3.4 can be substituted into equation 3.2, thus resulting in an equation 3.5 in terms of the $A(\omega)$ and $B(\omega)$ functions.

$$\mathrm{Re}\left(\frac{\Delta r}{r}\right) = -\frac{2\omega d}{c}\left[A(\omega)\mathrm{Im}(\Delta\varepsilon_S) + B(\omega)\mathrm{Re}(\Delta\varepsilon_S)\right] \tag{3.5}$$

Equation 3.5 makes it possible to simulate RA spectra in terms of the bulk optical response of the Au sample and provides a representation of the transitions involving the surface. The RAS is simulated by choosing transitions within the surface layer of atoms, ε^x_s and ε^y_s, in the x or y directions respectively, and of the energy, ω_t, intensity, S, and the full width at half maximum (FWHM), Γ, [55]. Each simulated transition takes the form of a Lorentzian, as shown in equation 3.6.

$$\varepsilon^x_s = 1 + \frac{S/\pi}{\omega_t - \omega + i\Gamma/2}\ ,\quad \varepsilon^y_s = 1 \tag{3.6}$$

This equation, in conjunction with appropriately chosen empirical lineshape parameters (energy, intensity and FWHM), is used to simulate RA spectra. The values of ε^x_s and ε^y_s are not equal in order to produce the SDA described in section 3.6.1 and hence an RAS response.

Figure 3.8 shows the $A(\omega)$ and $B(\omega)$ functions as defined by equation 3.4 where $\varepsilon_b(\omega)$ is imaginary. The small discontinuities observed at 5.0 eV are the result of the change in data sets.

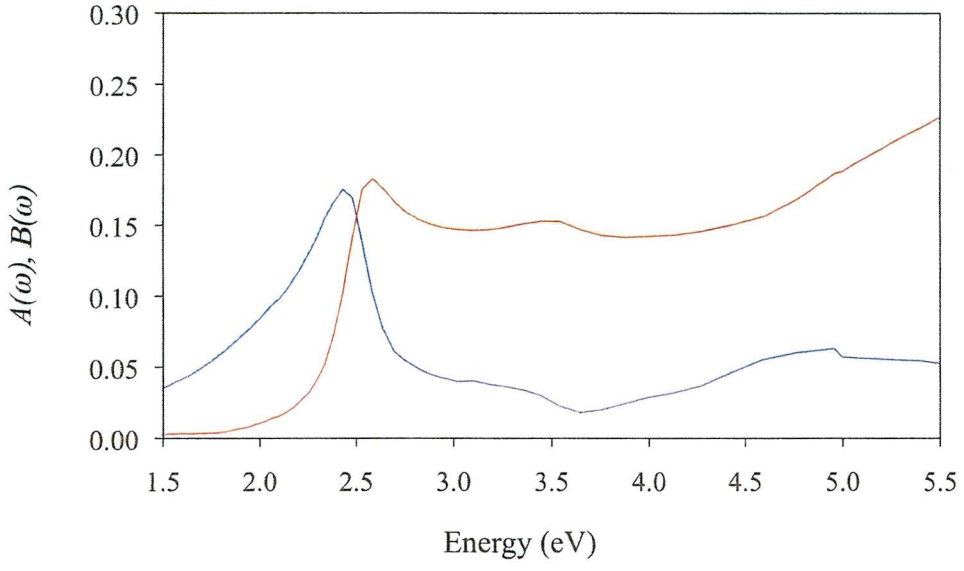

Figure 3.8: The shape of the $A(\omega)$ function (blue line) and the $B(\omega)$ function (red line).

3.7 RAS Simulations

This subsection is an introduction to the theoretical fitting method which is used to simulate RA spectra. In order to make these simulations as physically plausible as possible boundaries are assigned for each set of parameters used to characterise a transition.

The RA spectra of the Au(110) surface have been found to be successfully simulated by five transitions each of which have three variables that effect the shape of the simulation; the transition energy, intensity and FWHM. It has been shown in several publications [1,2,40,60] that these transitions and their respective variables can be confined to a fixed range of values. Table 3.1 shows the five transitions used for the Au(110) RAS simulations and the upper and lower boundaries of their transition energies.

In order to keep the simulation reasonable, the FWHM Lorenztian shape width of each of the transitions, is confined to 0.3 eV – 2.5 eV. However, the absolute intensities of these transitions are not confined to a fixed range.

Transition	Energy Range (eV)
1	1.6 – 2.0
2	3.3 – 3.6
3	3.8 – 4.1
4	4.3 – 4.8
5	5.4 – 5.8

Table 3.1: A list of the transition energy ranges.

Of course the three variables have different influences on the contribution of a transition to a simulated RAS profile. The transition energy naturally determines the region of the spectrum where a transition contributes most strongly. However the FWHM is inversely proportional to the peak intensity of the transition, and determines the sharpness of the transition.

The development of an RAS instrument which extends the spectrum into the UV range has lead to the number of transitions necessary to simulate the RAS of the Au(110) to be increased and also some modification of the previously labelled fourth and fifth transitions of the RAS of Au(110) [61]. These changes to the simulations and the reasoning behind these alterations are discussed later on in this chapter.

This thesis focuses on the adsorption of biological molecules onto the Au(110) surface. The adsorption of these biological molecules affects the optical response of the Au(110) and previous work on cytosine [60] has shown the necessity to add two further transitions to the RAS simulations in order to obtain an empirical description of the optical response. The previous work [60] maintained the energies of the transitions for the initial Au(110) simulated RA spectrum but allowed the intensity and FWHM values to vary so that the RA spectra could be simulated.

3.8 Spectral Signatures of the Au(110) Surface Reconstructions

It is difficult to identify RAS profiles corresponding to the three surface structures of the Au(110) surface. This difficulty is exacerbated by the variation in RAS profiles obtained from the flame annealed Au(110) surfaces, a variation attributed to the slight differences in surface morphology [1,37-40].

In addition to this there are variations in the RA spectra of the Au(110)/electrolyte interface which have been assigned to the differing anions present in electrolytes. Stronger adsorbing anions like SO_4^{2-} have a much greater effect on the Au(110) surface in comparison to weaker adsorbing anions such as ClO_4^- [25,51,62-67]. Potentials positive of the PZC are anticipated to result in the anions from the electrolyte being specifically adsorbed onto the crystal surface. In an attempt to minimise the systematic error and to categorise the changes in the optical response of the Au(110) that arose from variations in anions, a series of experiments were carried out on a flame annealed Au(110) single crystal using three different electrolytes; $H_2SO_4/NaSO_4$ (pH 1.36), $NaClO_4/HClO_4$ (pH 1.18) and $NaClO_4$ (pH 6.14). This series of experiments enables direct comparisons to be made between the effects arising from a variation in anion and pH on the Au(110) surface reconstructions.

An experiment was conducted whereby the Au(110) sample experienced cyclic potential variations from 0.0 V → 0.6 V → 0.0 V → 1.2 V → -0.6 V → 0.0 V in discrete 0.1 V increments. This was done in order for the Au(110) crystal to be taken through the reversible (1×1) to (1×2) phase transition at potentials below oxidation, then through oxidation and then on to experience the negative potential induced (1×3) surface reconstruction before returning to a neutral potential to re-establish the original surface morphology and (1×2) surface reconstruction [70]. The reasons behind this cyclic experiment were that it has been shown that applied electrode potentials below the PZC result in the surface displaying a (1×3) surface reconstruction as its lowest energy state [26,28-30]. Moreover, the (1×2) to (1×1)

phase transition is believed to be entirely reversible [3,4,24,25,37,38] and that oxidation of the surface leaves the surface reconstruction undamaged [1,68].

Grey areas persist with regard to the effects of specific anion adsorption onto surface structures as well as the difference between this action and that of changing applied electrode potentials. It is unclear whether or not the ClO_4^- anions in perchloric acid are very weakly adsorbing or whether they do not adsorb at all at potentials positive of the PZC. The lifting of the (1×2) surface reconstruction at positive potentials was attributed to the specific adsorption of the anions, after Kolb and Schneider [69] performed a CV capacitance and ERS study of the Au(110) surface in perchlorate. This interpretation of the results was based on evidence showing the surface reconstruction is lifted at higher potentials when the surface was under a ClO_4^- environment as opposed to when the sample was in the presence of the more strongly adsorbing SO_4^{2-} or Cl^- anions. This study shows the anion effect is greater than the effect of the surface charge upon the surface reconstruction. Borkowska and Stimming [70] then went on to show that the lowering of the PZC and the increase in the potential of oxidation were free from the effect of electrolyte concentration. This result was explained in terms of the low bond strength of the perchlorate anion which enables the hydroxide anion to replace it as quickly as possible.

3.9 A Comparison of the (1×1), (1×2) and (1×3) Surface Reconstructions Under Varying pH and In Differing Electrolytes

This section is an overview of the study undertaken to investigate the anion induced surface reconstructions by A. Bowfield [2]. The following subchapters will discuss the conditions of each experiment, describe the RA spectra produced and attempt to highlight the spectral profiles of each of the three surface reconstructions and compare each of them with the corresponding reconstructions under the different electrolytes.

3.9.1 Au(110) in 0.1 M H_2SO_4/Na_2SO_4

The work of A. Bowfield [2] and Magnussen *et al* [25], showed that at 0.0 V in H_2SO_4/Na_2SO_4, the RA spectrum corresponds to that of the Au(110)-(1×2) surface reconstruction. The main features of the RA profile of the Au(110)-(1×2) surface reconstruction in H_2SO_4/Na_2SO_4 are the broad feature observed below 2.5 eV, two negative peaks of similar intensity at 2.5 eV and 3.5 eV which are connected by a plateau. Finally there is also the peak observed at 4.5 eV.

It was also shown [2] that the features of RA spectra of the Au(110) surface in H_2SO_4/Na_2SO_4 at +0.4 V represents the (1×1) surface structures. This profile includes a reduction in intensity of the feature below 2.5 eV in comparison to that of the (1×2) surface structure, a slight increase in energy position of the 2.5 eV peak, an increase in the intensity of the 3.5 eV peak and the complete removal of the plateau that connected these two peaks in exchange for a significant trough.

The spectral profile of the (1×3) surface structure was also determined in [2]. The RA spectrum of Au(110) in H_2SO_4/Na_2SO_4 at -0.6 V was labelled as the RA profile of the (1×3) surface reconstruction. It is apparent that the peak at 2.5 eV deteriorates rapidly as the electrode potential becomes increasingly more negative. At the same time, the broad feature below 2.5 eV becomes more intense as the electrode potential becomes more negative. The peak at 3.5 eV does reduce in intensity but not at the same rate of reduction as the 2.5 eV peak, resulting in it maintaining definition even to a potential of -0.6 V. The spectral profiles of the three reconstructions of Au(110) in 0.1 M H_2SO_4/Na_2SO_4 are highlighted in figure 3.9.

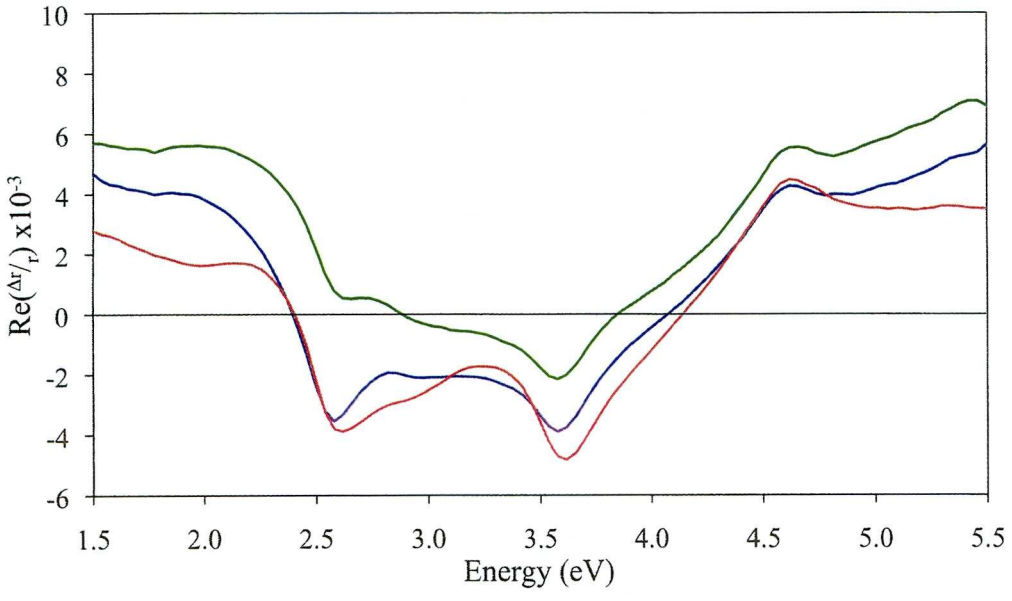

Figure 3.9: The RA spectra of Au(110) in 0.1 M H_2SO_4/Na_2SO_4 showing the spectral profiles of the different surface reconstructions: (1×1) +0.4 V (red line), (1×2) 0.0 V (blue line) and (1×3) -0.6 V (green line). Data taken from [2].

3.9.2 Comparing the Au(110) Reconstructions Under Varying Electrolytes and pH.

A summary of the previous study [2] is described in this section in order to determine whether the results found in section 3.9.1 were indicative of the surface structure or had contributions from the anion used. The previous study [2] compared the results to similar experiments in which different electrolytes were employed and the pH of the solution varied.

The first comparison was to change the anion but maintain an acidic pH by changing the electrolyte to 0.1 M $NaClO_4/HClO_4$. This experiment found that the RA spectra of the Au(110) were similar to those shown in the previous section but with greater changes between the RA spectra of different electrode potentials, more so in the positive electrode potentials. It found that the alterations to the spectral features at 2.5 eV, 3.5 eV and 4.5 eV were similar to those from the sulfate investigation indicating that the surface reconstructions of the Au(110) gave rise to

similar RA spectra. Figure 3.10 illustrates the RA spectra of the Au(110) in 0.1 M $NaClO_4/HClO_4$ showing the spectral profiles of the different surface reconstructions. When compared to the RA spectra of the sulfate investigation in figure 3.9, it can be seen that there are only minor differences between the two data sets, therefore supporting the view that the Au(110) surface behaves similarly in the two electrolytes.

The next experiment conducted in the previous study [2] used the same anions but then changed the pH of the electrolyte. It was changed from 0.1 M $NaClO_4/HClO_4$ at pH 1.18 to 0.1 M $NaClO_4$ at pH 6.14. This experiment should establish whether variations in the pH would result in any changes of the RAS of Au(110) that can be attributed to the variations of the surface structure. It was found that the pH did appear to affect the cyclic behaviour of the experiments and lead the author to suggest that there exists a pH dependent hysteresis of the RAS of Au(110) before the surface entered oxidation. Some small changes in the RA spectra of Au(110) were observed but the characteristic RA profiles of the (1×1) surface structure and the (1×2) and (1×3) surface reconstructions were still produced. Figure 3.11 shows the RA spectra of Au(110) in 0.1 M $NaClO_4$ showing the spectral profiles of the different surface reconstructions. The RA profile of the (1×1) surface structure holds its positive slope between the 2.5 eV and 3.5 eV peaks.

The RA profile of the (1×2) surface structure keeps the plateau between the same two peaks, whereas the RA profile of the (1×3) surface structure maintains its characteristic lack of definition for the peak at 2.5 eV. The study [2] also discussed that the CV associated with this particular experiment generated an interesting result. It showed that oxidation of the Au(110) surface occurs at a potential of +1.0 V whereas the acidic experiments maintain oxidation at +1.2 V, this suggests that the pH bears a direct effect on the oxidation of Au(110).

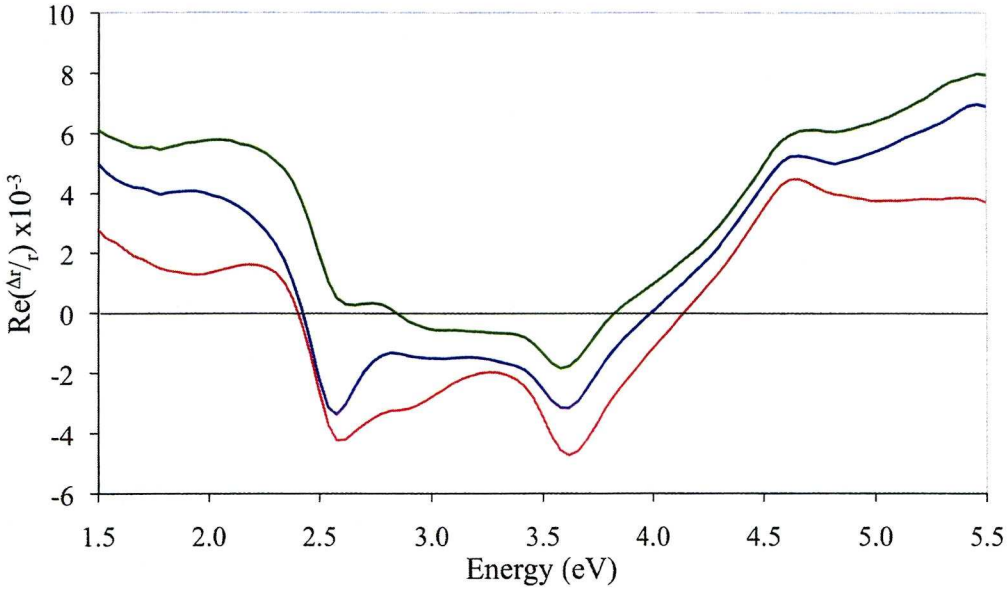

Figure 3.10: The RA spectra of Au(110) in 0.1 M $NaClO_4/HClO_4$ showing the spectral profiles of the different surface reconstructions: (1×1) +0.4 V (red line), (1×2) 0.0 V (blue line) and (1×3) -0.6 V (green line).

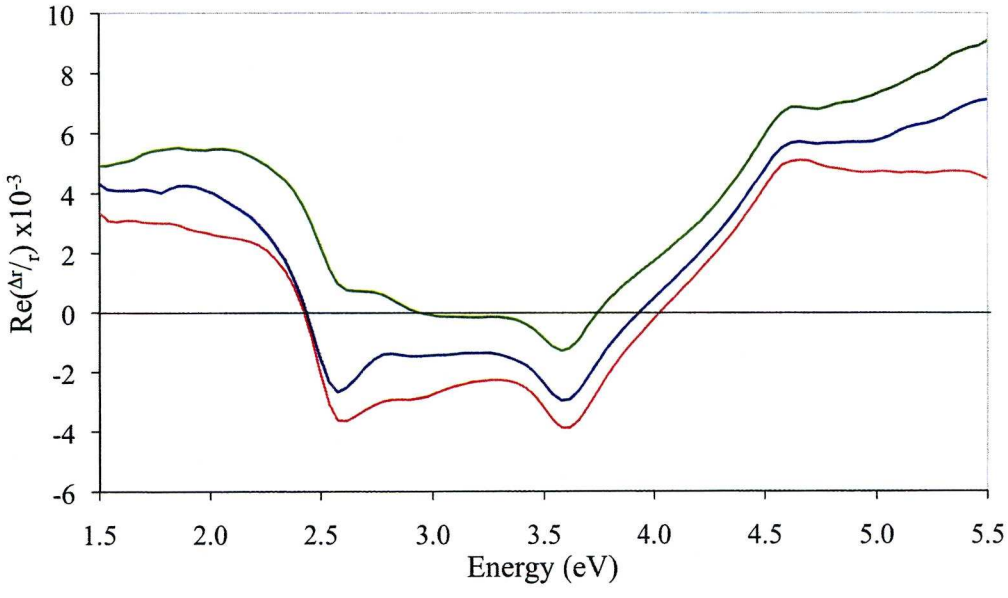

Figure 3.11: The RA spectra of Au(110) in 0.1 M $NaClO_4$ showing the spectral profiles of the different surface reconstructions: (1×1) +0.3 V (red line), (1×2) 0.0 V (blue line) and (1×3) -0.6 V (green line).

3.9.3 Comparing the RAS profiles of the Au(110) Surface Structures in Differing pH and Electrolyte.

The RA spectra of the Au(110) surface under differing electrolytes and at varying pH can now be compared and provide insight into the influence of particular anions or pH effects on the optical response of the Au(110) sample.

Figure 3.12 illustrates the three (1×1) RA spectra produced under the differing electrolytes and pH. At an electrode potential of +0.4 V, the Au(110) surface is anticipated to adopt a mainly (1×1) surface structure [25]. In the energy region beyond 2.5 eV; the region associated with surface modified bulk states and the monatomic steps, the two acidic electrolytes differ slightly in their response. The region between 1.5 eV and 2.5 eV produces a noticeable variation between the RAS responses from the acidic electrolytes and the neutral electrolyte. This has been assigned to the (1×2) not being fully removed from the surface [2]. The complete removal of the flat region between the peaks at 2.5 eV and 3.5 eV under acidic electrolytes would suggest a complete removal of the (1×2) reconstruction and a full adoption of the unreconstructed (1×1) surface structure. This removal of the plateau is not seen to the same extent in the neutral electrolyte, leading to the belief that in the neutral perchlorate solution at +0.4 V, the Au(110) surface is a mixture of primarily (1×1) regions and (1×2) surface regions.

Figure 3.13 illustrates the RAS profiles of the (1×2) surface reconstruction. As expected at 0.0 V in electrolyte, the Au(110) adopts the (1×2) surface structure [24-26]. The RA spectra of all three experiments are almost identical up to the energy of 2.6 eV and all three have the flat region between 2.5 eV and 3.5 eV. The variation arises after 2.6 eV whereby the RA spectrum in neutral electrolyte begins to map the path of the Au(110) RA spectrum in the acidic perchlorate electrolyte. The perchlorate electrolyte gives rise to a greater intensity for both the 2.5 eV and 3.5 eV peaks, therefore indicating that there is an anion and pH effect with the SO_4^{2-} sulfate electrolyte resulting in a greater interaction with the surface. It induces the (1×2) reconstruction more than with the perchlorate anion, possible due to the sulfate anion adsorbing more strongly.

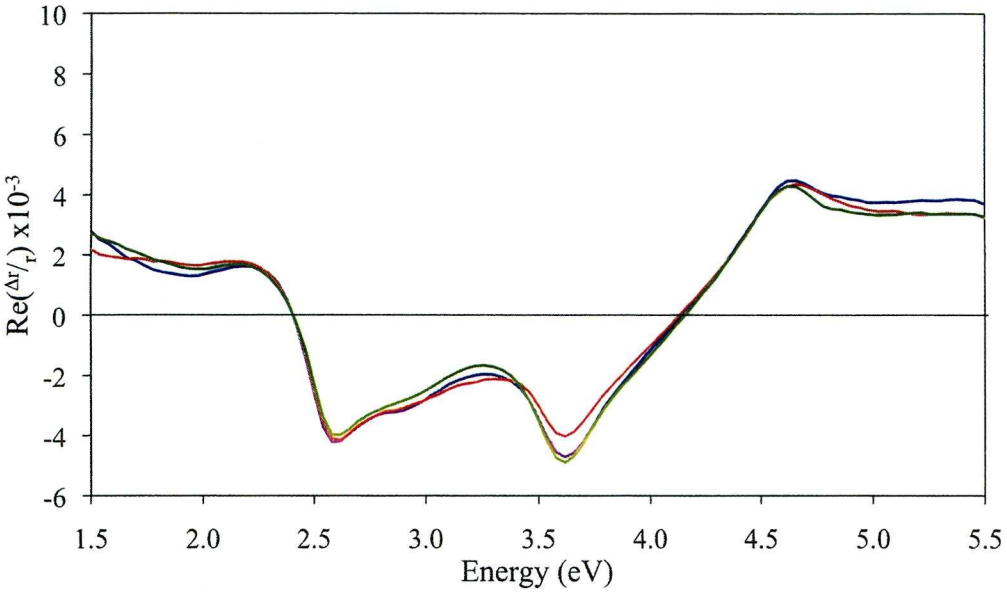

Figure 3.12: The RA spectra of the Au(110)-(1×1) surface structure at +0.4 V vs SCE in 0.1 M $H_2SO_4/NaSO_4$ at pH 1.36 (green line), $HClO_4/NaClO_4$ at pH 1.18 (blue line) and $NaClO_4$ at pH 6.14 (red line).

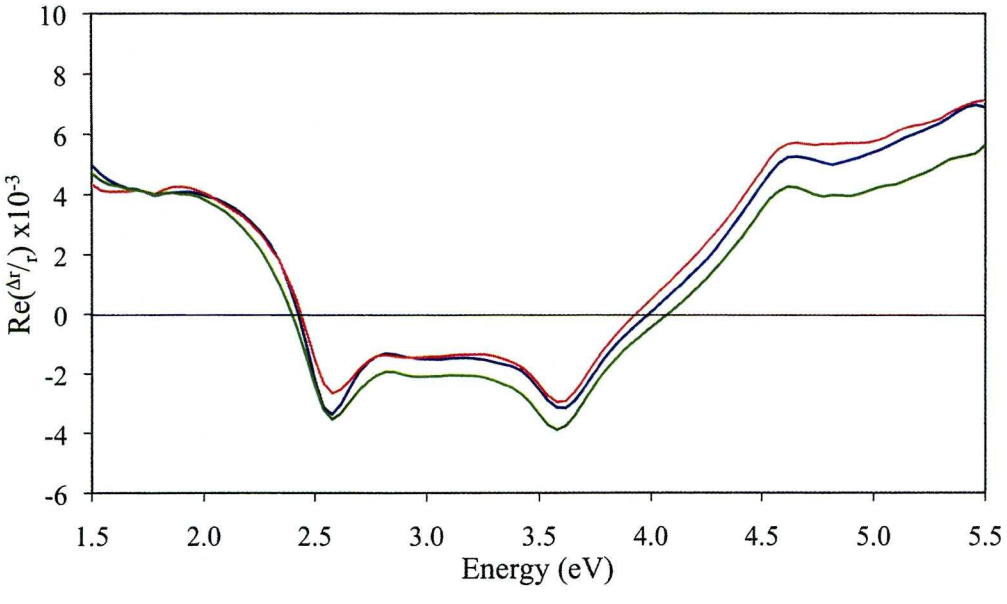

Figure 3.13: The RA spectra of the Au(110)-(1×2) surface structure at 0.0 V vs SCE in 0.1 M $H_2SO_4/NaSO_4$ at pH 1.36 (green line), $HClO_4/NaClO_4$ at pH 1.18 (blue line) and $NaClO_4$ at pH 6.14 (red line).

Figure 3.14 compares the (1×3) reconstruction. The (1×3) reconstruction behaves similarly to the (1×2) in the sense that the three RA spectra in the three different electrolytes produce almost identical spectra up to 2.6 eV. The differences occur when they reach the region affected by the surface modified bulk states (3.0 eV).

The main variation in the (1×3) RA spectra, albeit small, occurs at the energies around the 4.5 eV peak. This region is related to the steps on the surface and the variations in the step structure can be accounted for by the variations in the surface morphology when undergoing the flame annealing preparation process. A possible contribution to this variation in the steps could be the stronger absorbing anions from the two acidic electrolytes. Nevertheless, all three RA spectra from the exhibit the typical profile connected to the (1×3) surface reconstruction.

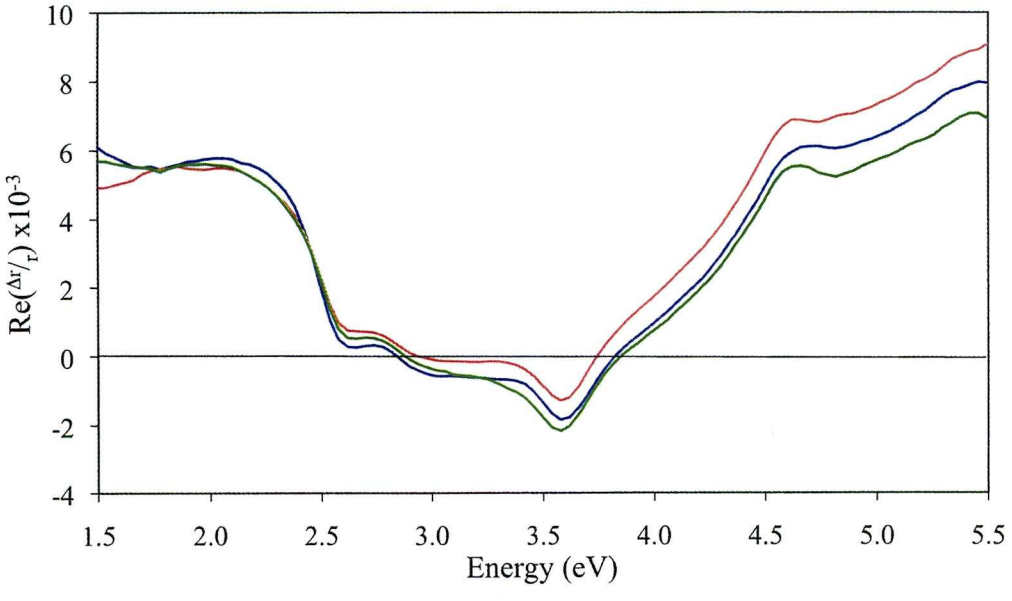

Figure 3.14: The RA spectra of the Au(110)-(1×3) surface structure at -0.6 V vs SCE 0.1 M $H_2SO_4/NaSO_4$ at pH 1.36 (green line), $HClO_4/NaClO_4$ at pH 1.18 (blue line) and $NaClO_4$ at pH 6.14 (red line).

3.10 Simulations of the RA Spectra of the Varying Au(110) Surface Structures

The following sections move on from the work of A. Bowfield [2] and describe new work undertaken for this thesis.

In order to get an idea of how the RAS of surfaces consisting of mixed reconstructions would appear, the RAS data given by a simple simulation of the results described in the previous section was made using equation 3.7 and equation 3.8. This simulation used the experimental data of the RAS of the Au(110) for the (1×1), (1×2) and (1×3) surface reconstructions.

$$RAS(50\%(1\times3)) = \frac{1}{2}RAS(1\times2) + \frac{1}{2}RAS(1\times3) \tag{3.7}$$

$$RAS(50\%(1\times1)) = \frac{1}{2}RAS(1\times2) + \frac{1}{2}RAS(1\times1) \tag{3.8}$$

Equation 3.7 gives a simulation of the RAS of an Au(110) surface which consists of 50% of its area to be (1×2) and 50% to be (1×3). This is achieved by reducing the magnitude of each data point of the (1×2) RA spectrum and the (1×3) RA spectrum by 50% and then adding them together. Equation 3.8 provides a similar simulation of the RAS of an Au(110) surface area consisting of 50% (1×1) and 50% (1×2). Figures 3.15 (a) and (b) illustrate the results of these simulations; the former showing the simulated RA spectra of a half (1×2) half (1×3) sample, the latter showing the simulated RA spectra of a half (1×2) half (1×1) Au(110) sample.

In order to demonstrate the value of the simulations they are compared to experimental RAS data in figures 3.16 (a) and 3.16 (b). Figure 3.16 (a) compares the simulated RA spectrum of Au(110) 50% (1×2) and 50% (1×3) and the RA spectrum of Au(110) in Na_2SO_4/H_2SO_4 at -0.2 V vs SCE. As the Au(110) in this electrolyte has been shown to adopt the (1×2) and (1×3) surface reconstructions at 0.0 V and -0.6 V respectively, one would assume that at some electrode potential in between the two, the surface would become half of each of the reconstructions.

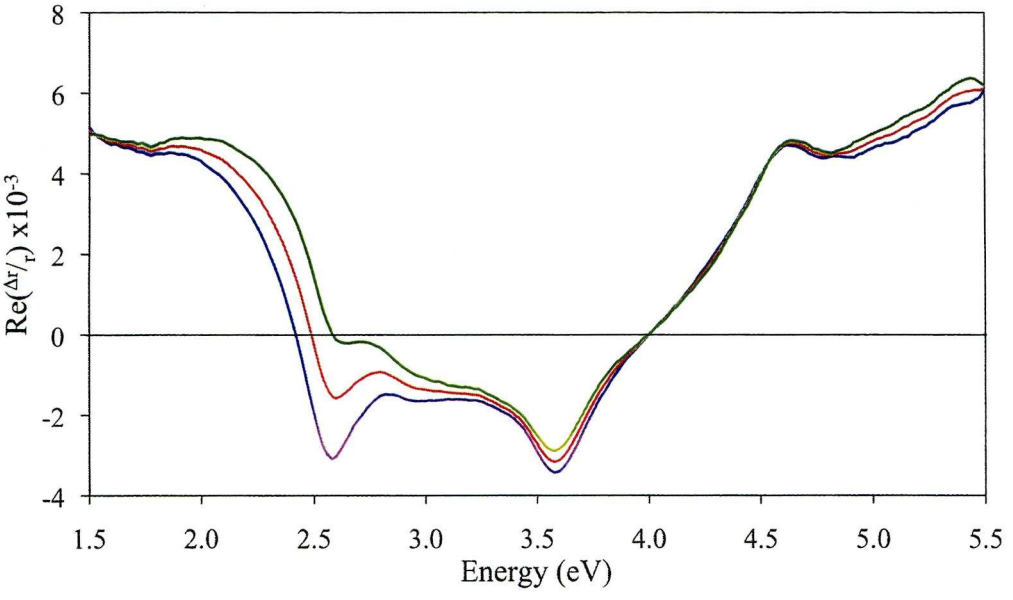

Figure 3.15 (a): The RA spectra of the Au(110)-(1×3) surface structure (green line), the Au(110)-(1×2) surface structure (blue line) and the simulated RA spectra of the Au(110) surface with 50% (1×2) and 50% (1×3) (red line).

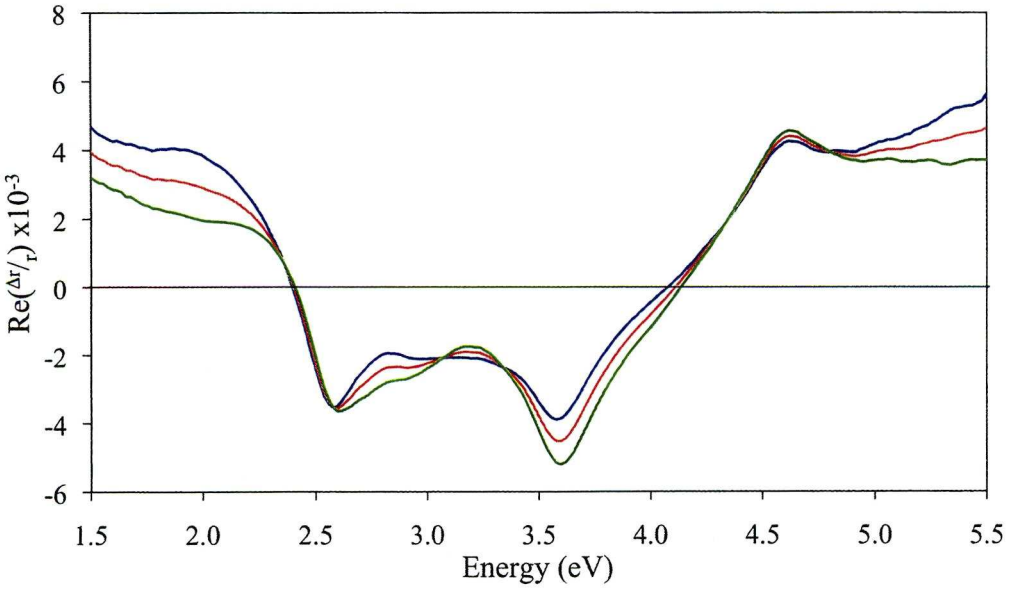

Figure 3.15 (b): The RA spectra of the Au(110)-(1×1) surface structure (green line), the Au(110)-(1×2) surface structure (blue line) and the simulated RA spectra of the Au(110) surface with 50% (1×2) and 50% (1×1) (red line).

Figure 3.16 (a) indicates that the Au(110) sample in Na_2SO_4/H_2SO_4 at -0.2 V vs SCE is slightly more than 50% (1×2) as the 2.5 eV peak is larger than that observed in the simulation. In a similar fashion, figure 3.16 (b) compares the simulated RA spectrum of Au(110) 50% (1×2) and 50% (1×1) and the RA spectrum of Au(110) in Na_2SO_4/H_2SO_4 at +0.2 V vs SCE. As previous discussions have concluded, the (1×1) reconstruction is adopted at potentials above +0.25 V. Therefore at potentials between 0.0 V; where the (1×2) reconstruction presides, and +0.25 V, the Au(110) crystal should adopt a mixture of the two reconstructions. Figure 3.16 (b) indicates that the sample has a greater than 50% coverage of (1×1) domains and less (1×2) domains. This is made apparent by the experimental data displaying a more intense peak at 3.5 eV and less of the expected plateau between the peaks of 2.5 eV and 3.5 eV. However, as both figures 3.16 (a) and (b) show that the simulations are close to mapping the experimental data, it would suggest that the calculations used to generate the simulations of mixed reconstruction Au(110) surfaces are reasonably valid.

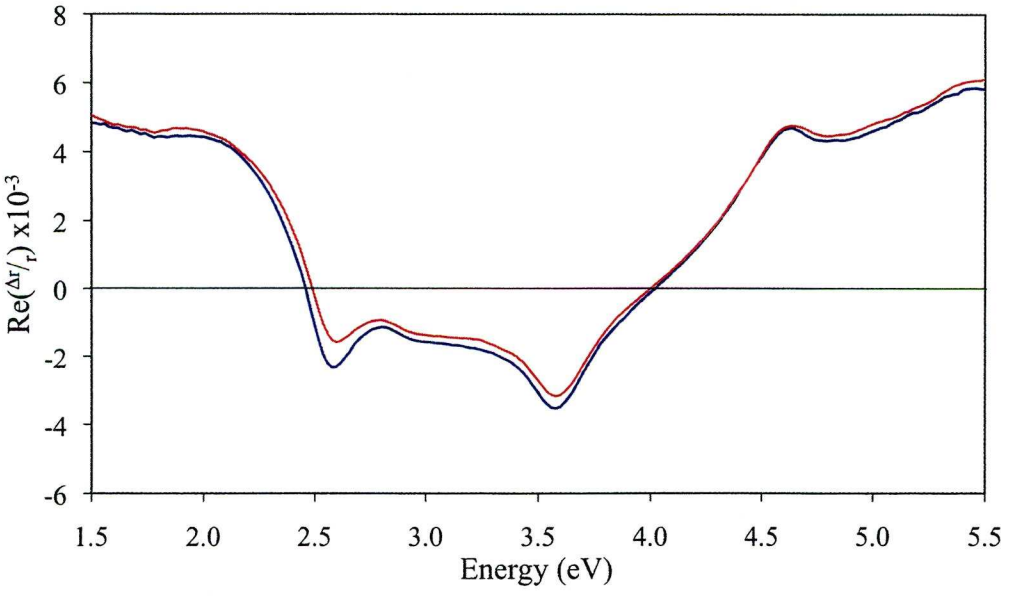

Figure 3.16 (a): The simulated RA spectrum of Au(110) 50% (1×2) and 50% (1×3) (red line) and the RA spectrum of Au(110) in Na_2SO_4/H_2SO_4 at -0.2 V vs SCE (blue line).

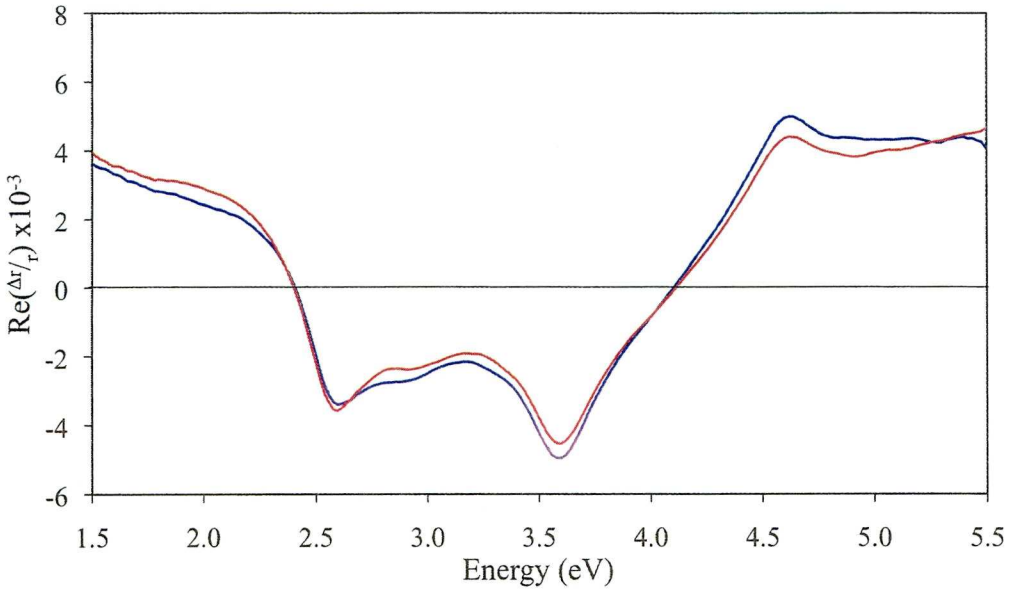

Figure 3.16 (b): The simulated RA spectrum of Au(110) 50% (1×2) and 50% (1×1) (red line) and the RA spectrum of Au(110) in Na_2SO_4/H_2SO_4 at +0.2 V vs SCE (blue line).

3.11 An Extension of the Au(110) RA Spectra into the UV Range

With the development of a new UV RAS instrument it became possible to explore the optical response of the Au(110) crystal into the UV region of the electromagnetic spectrum. The instrument usually used for the RAS experiments obtained data between 1.5 eV and 5.5 eV. Figure 3.17 shows the RA spectrum for the Au(110)/electrolyte interface over the range 1.5 eV to 5.5 eV that we have obtained in the UV-VIS instrument and which is in agreement with previous work in UHV and under liquid [36,39,40,71-77]. In figure 3.15 the key features of the Au(110) RA spectrum are displayed. It should be noted that the region above 4.5 eV appears different to the RA spectra of Au(110) seen previously in this chapter. The reason for the steady decrease in intensity above 4.5 eV in this RA spectrum, and not in previously displayed spectra, is that the instrument began to lose sensitivity above this energy. The RA spectra displayed in the rest of this chapter were obtained after a

time where the RAS instrument had a new detector installed, giving improved more detailed RAS data.

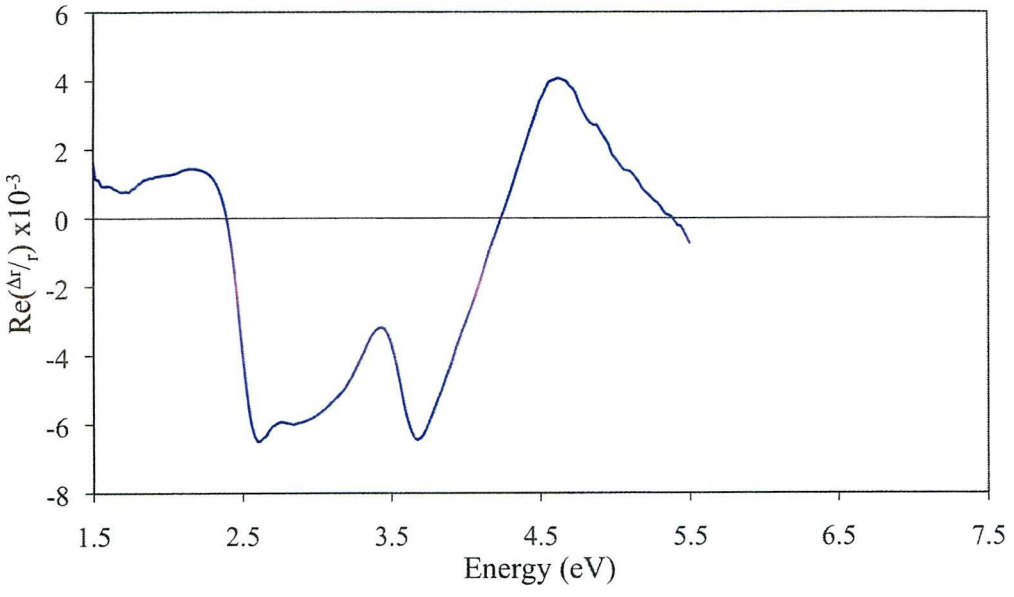

Figure 3.17: RA Spectrum of Au(110) in 0.1M NaH_2PO_4/K_2HPO_4 in the range 1.5 to 5.5 eV.

Figure 3.18 shows the RA spectrum of Au(110) in the extended range (4.0 eV to 7.0 eV) instrument. There are major differences between the spectra of figure 3.17 and figure 3.18 in the energy range 4.6 eV to 5.5 eV. The sharp peak observed at 4.6 eV in the UV-VIS instrument is replaced by a smooth plateau that remains until 5.8 eV following which it descends into a small broad trough at 6.4 eV.

The composite spectrum, figure 3.19, covering the range 1.5 eV - 6.8 eV was obtained by using the matching procedure described earlier in section 2.5 with the same scaling factor deduced from the comparison of the results obtained with Si(110); the translation factor, which was determined from setting the Re(Δr/r) to zero at 2.4 eV (UV-VIS) and using the same polariser angle as with Si(110) in the far UV instrument, was also the same as that used with Si(110). The mean value was used in the overlap range. We note that the translation factor is very small compared with the magnitudes of the features in both the Si(110) and the Au(110) spectra.

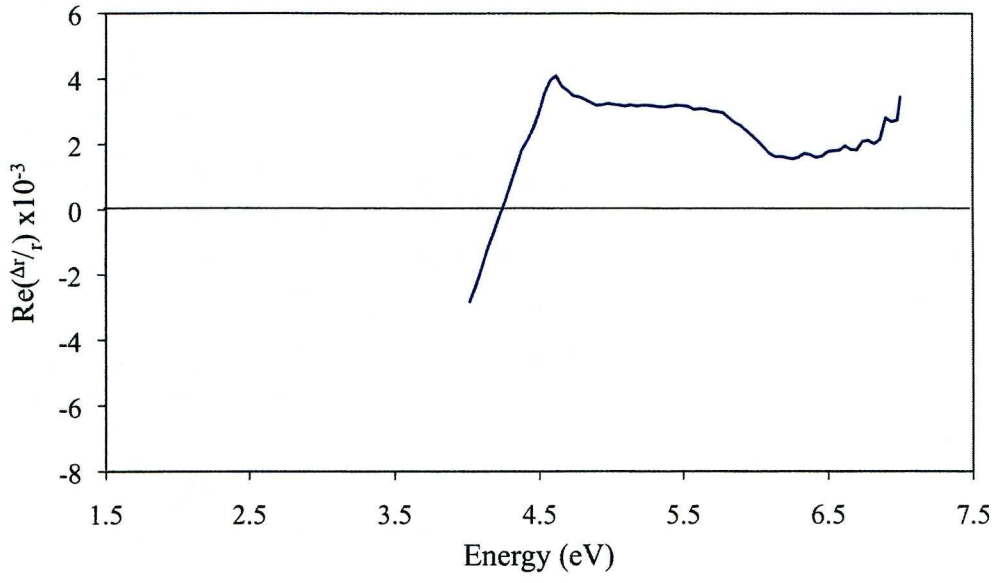

Figure 3.18: RA Spectrum of Au(110) in 0.1M NaH_2PO_4/K_2HPO_4 in the range 4.0 to 7.0 eV.

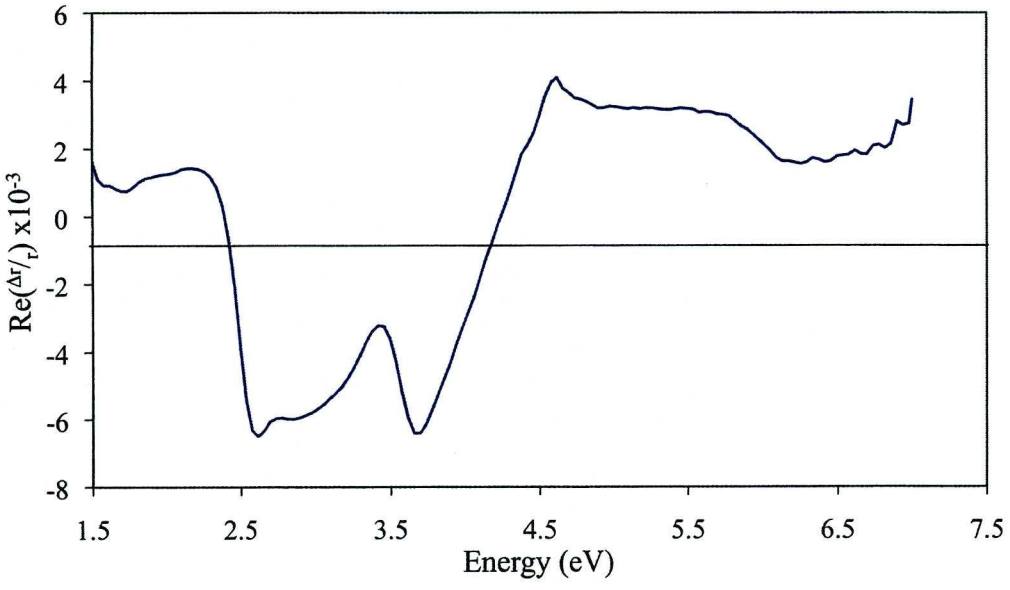

Figure 3.19. Composite Spectrum of Au(110) in 0.1M NaH_2PO_4/K_2HPO_4 in the range 1.5 to 7.0 eV.

A key feature of previous work on RAS studies of the adsorption of biological molecules at Au(110)/electrolyte interfaces [38,76] was the fitting of the RAS of both the Au(110)/interface and that of the adsorbed molecule to an empirical model. In order to facilitate studies in the future and to gain insight into the origins of the extended range RAS of the Au(110)/electrolyte interface, analysis of the RAS profile of figure 3.19 is required, using the empirical approach of Cole *et al* [55] deduced from the three-phase model. As with the earlier work [38,76] five transitions were required for a good simulation of the normal range spectrum and six were essential to get a good simulation of the extended range spectrum. This simulation is shown in figure 3.20 while table 3.2 lists the parameters needed to simulate the normal range spectrum and the extended range spectrum. Table 3.2 shows that of the three parameters that describe each transition, the simulation is generally most sensitive to the transition energy. It is to be expected that the simulation would be less sensitive to the transitions occurring near the extremities of the spectral range and this is observed. Nonetheless changes in the three parameters governing the sixth transition gave visibly poorer simulations at energies above 6.4 eV without noticeably affecting the simulation at lower energies. As expected there is a correlation between the strength of the transitions and the sensitivity of the simulation to variations in the parameters of the transition; generally the stronger the transition the more sensitive is the fit to changes in the parameters describing the transition.

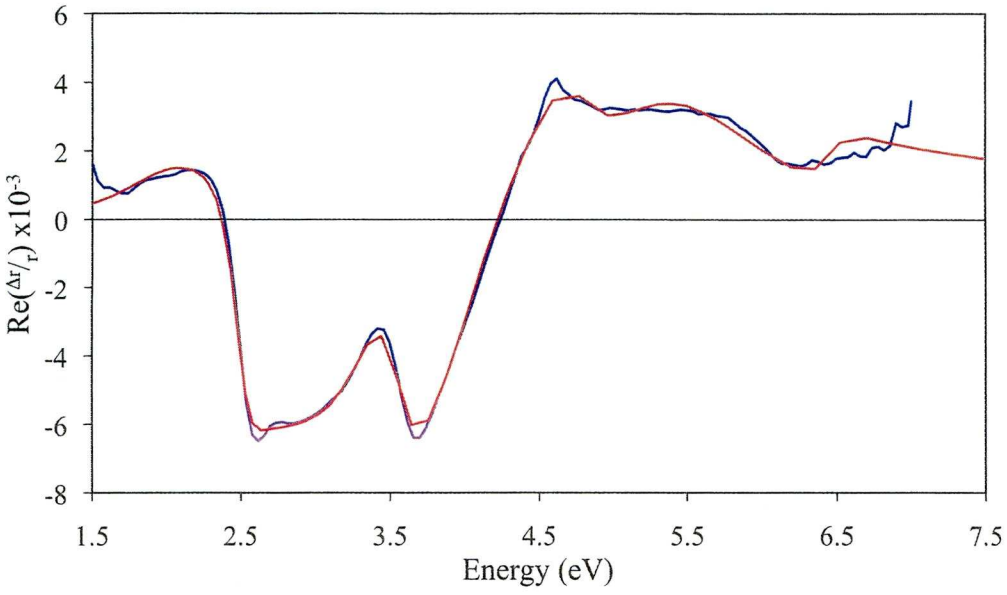

Figure 3.20. Extended range RA Spectrum of Au(110) (blue line) and the simulation obtained using the empirical model (red line).

Range, eV	Transition	1	2	3	4	5	6
	Direction	[001]	[001]	[1 $\bar{1}$0]	[001]	[001]	[1 $\bar{1}$0]
1.5 – 5.5	ω_t/eV	1.88 ± 0.10	3.55 ± 0.02	3.73 ± 0.03	4.71 ± 0.05	5.07 ± 0.06	…
	Γ/eV	2.10 ± 0.18	0.44 ± 0.05	2.12 ± 0.18	0.48 ± 0.09	0.90 ± 0.14	…
	S[a]	1.00 ± 0.06	0.02 ± 0.03	1.36 ± 0.05	0.07 ± 0.01	0.12 ± 0.02	…
1.5 – 6.8	ω_t/eV	1.94 ± 0.11	3.55 ± 0.03	3.73 ± 0.34	4.74 ± 0.07	5.51 ± 0.12	6.43 ± 0.01
	Γ/eV	1.93 ± 0.20	0.47 ± 0.06	2.00 ± 0.20	0.66 ± 0.14	2.03 ± 0.24	0.42 ± 0.01
	S[b]	1.00 ± 0.05	0.22 ± 0.02	1.61 ± 0.04	0.10 ± 0.02	0.22 ± 0.03	0.01 ± 0.00

[a,b]Relative intensities. Absolute intensities of transition 1 are 4789 (1.5 - 5.5 eV range), 4386 (1.5 – 6.8 eV range).

Table 3.2: The parameters for the simulated RA spectra of Au in the normal and extended energy ranges.

Recalling that the sensitivity of the normal range instrument starts to fall above 4.5 eV and the sensitivity of the UV instrument increases rapidly above 4.2 eV and begins to fall above 6.5 eV, the extended range spectrum formed from the combination of the results from the two instruments, will be more representative over the whole range. The first four transitions are very similar in the two

simulations as shown in table 2.2; there is a small difference in energy of transition one but in each case the simulation is less sensitive to the transition energy than transitions two, three and four. The real difference between the two simulations is with transition five and the appearance of a weaker transition in the [1 $\bar{1}$ 0] direction above 6.4 eV in the extended spectrum. The relatively weak and narrow transition at 5.1 eV in simulations of the RAS obtained with the normal instrument is replaced by a much stronger, wider transition at 5.5 eV, which like the additional transition at 6.4 eV is outside the range of the standard instrument. The reason for this difference is two-fold. The falling sensitivity of the UV-VIS instrument above 4.5 eV has the effect of sharpening any high-energy features and introducing a shift to lower energies. The curve fitting is restricted to transitions that sit within the range of the instrument; clearly a 5.5 eV transition cannot be detected with the standard instrument. The peak sensitivity in the far UV instrument occurs between 5.5 eV and 6.5 eV; 5.5 eV is well removed from the extremities of the extended range.

3.12 Summary

This chapter has described the physical and electronic structure of Au(110). The three surface structures of the Au(110) surface; the (1×1) structure and the (1×2) and (1×3) reconstructions, and the conditions under which each occurs have been described. It was noted that the anion and the pH of the electrolyte can affect the RAS observed from the Au(110) surface. The variation in the RAS observed from different Au(110) surfaces were also described. A theoretical model was used to represent the transitions observed in the optical response of the Au(110) sample and a simple simulation routine was used to show how the RAS observed from samples of mixed surface reconstructions can be fabricated from the experimental data of the RAS observed from two surface structures. This chapter concluded with a section highlighting data obtained from a new instrument which extended the energy range of RAS experiments providing new data about the higher energy RAS of Au(110).

3.13 References

[1] N. J. Almond, *Ph. D. Thesis*, The University of Liverpool (2008)

[2] A. Bowfield, *Ph. D. Thesis*, The University of Liverpool (2009)

[3] D. G. Fedaks and N. A. Gjoste, *Acta Metallurgica* **15**, 23 (1967)

[4] D. G. Fedaks and N. A. Gjoste, *Surf. Sci.* **8**, 77 (1967)

[5] C-M. Chan, M. A. Van Hove, W. H. Weinberg and E. D. Williams, *Surf. Sci.* **91**, 440 (1980)

[6] I. K. Robinson, *Phys. Rev. Lett.* **50**, 1145 (1983)

[7] J. R. Noonan and H. L. Davis, *J. Vac. Sci. Technol.* **16**, 587 (1979)

[8] B. Reihl and B. T. Dunlap, *Appl. Phys. Lett.* **37**, 941 (1980)

[9] G. Binning, H. Rohrer, Ch. Gerber and E. Weibel, *Surf. Sci.* **131**, L379 (1983)

[10] Y. Kuk, P. J. Silverman and H. Q. Nguyen, *J. Vac. Sci. Technol. A* **6**, 524 (1988)

[11] K. Gimzewski, R. Berndt and R. R. Schlittler, *Surf. Sci.* **247**, 327 (1991)

[12] T. Gritsch, D. Coulman, R. J. Behm and G. Ertl, *Surf. Sci.* **257**, 297 (1991)

[13] R. Koch, M. Borbonus, O. Hasse and K. H. Rieder, *Appl. Phys. A* **55**, 417 (1992)

[14] S. Speller, S. Molitor, C. Rothig, J. Bomermann and W. Heiland, *Surf. Sci.* **312**, L748 (1994)

[15] M. Sturmat, R. Koch and K. H. Rieder, *Phys. Rev. Lett.* **77**, 5071 (1996)

[16] R. Koch, M. Sturmat and J. J. Schulz, *Surf. Sci.* **454**, 543 (2000)

[17] J. C. Campuzano, M. S. Foster, G. Jennings and R. F. Willis, *Phys. Rev. Lett.* **54**, 2684 (1985)

[18] J. Villain and I. Vilfan, *Surf. Sci.* **199**, 165 (1988)

[19] C. Hofner and J. W. Rabalais, *Surf. Sci.* **400**, 189 (1998)

[20] K. Stahrenberg, Th. Herrmann, N. Esser, W. Richter, S. V. Hoffman and Ph. Hofmann, *Phys. Rev. B* **65**, 035407 (2001)

[21] D. S. Martin, N. P. Blanchard and P. Weightman, *Surf. Sci.* **532-535**, 1 (2003)

[22] K. M. Ho and K. P. Bohnen, *Phys. Rev. Lett.* **59**, 1833 (1987)

[23] J. W. M. Frenken, R. L. Krans and J. F. van der Veen, *Phys. Rev. Lett.* **59**, 2307 (1987)

[24] X. Gao, A. Hamelin and M. J. Weaver, *Phys. Rev. B* **44**, 10983 (1991)

[25] O. M. Magnussen, J. Wiechers and R. J. Behm, *Surf. Sci.* **289**, 139 (1993)

[26] B. M. Ocko, G. Helgesen, B. Schardt, J. Wang and A. Hamelin, *Phys. Rev. Lett.* **69**, 3350 (1992)

[27] P. Härberle, P. Fenter and T. Gustafsson, *Phys. Rev. B* **39**, 5810 (1989)

[28] X. Gao and M. J. Weaver, *Surf. Sci.* **313**, L775 (1994)

[29] I. M. Tidswell, N. M. Marković and P. N. Ross, *Surf. Sci.* **317**, 241 (1994)

[30] X. Gao, G. J. Edens, A. Hamelin and M. J. Weaver, *Surf. Sci.* **318**, 1 (1994)

[31] R. Koffman, P. Cheyssac and R. Richard, *Surf Sci.* **77**, 537 (1978)

[32] S. H. Liu, C. Hinnen, C. Nguyen, N. R. De Tacconi and K. M. Ho, *J. Electroanal. Chem.* **176**, 325 (1984)

[33] C. H. Xu, K. M. Ho and K. P. Bohnen, *Phys. Rev. B* **39**, 5599 (1989)

[34] M. Sastry, K. C. Prince, D. Cvetko, A. Morgante and F. Tommansi, *Surf. Sci.* **271**, 179 (1992)

[35] W. L. Mochán, R. G. Barrera, Y. Borensztein and A. Tadjeddine, *Physica A* **207**, 334 (1994)

[36] J-K. Hansen, J. Bremer, L. Seime and O. Hunderi, *Physica A* **298**, 46 (2001)

[37] V. Mazine, Y. Borensztein, L. Cagnon and P. Allongue, *Phys. Status Solidi A* **175**, 311 (1999)

[38] V. Mazine, Y. Borensztein, *Phys. Rev. Lett.* **88**, 147403 (2002)

[39] P. Weightman, C. I. Smith, D. S. Martin, C. A. Lucas, R. J. Nichols and S. D. Barrett, *Phys. Rev. Lett.* **92**, 199707 (2004)

[40] B. Sheridan, D. S. Martin, J. R. Power, S. D. Barrett, C. I. Smith, C. A. Lucas, R. J. Nichols and P. Weightman, *Phys. Rev. Lett.* **85**, 4618 (2000)

[41] R. A. Bartynski and T. Gustafsson, *Phys. Rev. B* **33**, 6588 (1986)

[42] J. Bremer, J-K. Hansen and O. Hunderi, *Surf. Sci.* **436**, L735 (1999)

[43] D. S. Martin, R. J. Cole, N. P. Blanchard, G. E. Isted, D. S. Roseburgh and P. Weightman, *J. Phys. Condens. Matter* **16**, S4375 (2004)

[44] U. Rossow, L. Mantese and D. E. Aspnes, *J. Vac. Sci. Technol. B* **14**, 3070 (1996)

[45] P. Winsemius, F. F. van Kampen, H. P. Lengkeek and C. G. van Went, *J. Phys. F: Met. Phys.* **6**, 1583 (1976)

[46] M. J. Bennahmias, S. Lakkaraju, B. M. Stone and K. Ashley, *J. Electroanal. Chem.* **280**, 429 (1990)

[47] O. M. Magnussen, J. Hotlass, R. J. Nichols, D. M. Kolb and R. J. Behm, *Phys. Rev. Lett.* **64**, 2929 (1990)

[48] X. H. Xia, L. Nagle, R. Schuster, O. M. Magnussen and R. J. Behm, *Phys. Chem. Chem. Phys.* **2**, 4387 (2000)

[49] M. Cappadonia, U. Linke, K. M. Robinson and U. Stimming, *J. Electroanal. Chem.* **405**, 227 (1996)

[50] O. M. Magnussen, J. Hotlass, G. Breitel, D. M. Kolb and R. J. Behm, *J. Vac. Sci. Technol. B* **9**, 969 (1991)

[51] M. S. Zei, G. Qiao, G. Lehmpfuhl and D. M. Kolb, *Phys. Chem.* **91**, 349 (1987)

[52] C. I. Smith, T. Farrell, C. A. Lucas, R. J. Nichols and P. Weightman, *Phys. Status Solidi B* **242**, 2595 (2005)

[53] N. J. Almond, N. P. Blanchard, D. S. Martin and P. Weightman, *Phys. Status Solidi C* **2**, 4003 (2005)

[54] J. D. E. McIntyre and D. E. Aspnes, *Surf. Sci.* **24**, 417 (1971)

[55] R. J. Cole, B. G. Frederick and P. Weightman, *J. Vac. Sci. Technol. A* **16**, 3088 (1998)

[56] C. Kittel, *Introduction to Solid State Physics*, seventh edition (John Wiley & Sons, New York, 1996)

[57] *Handbook of Optical Constants of Solids*, edited by E. D. Palik, Vol. 1 (Academic, New York, 1985 and 1991)

[58] N. P. Blanchard, C. I. Smith, D. S. Martin, D. J. Hayton, T. E. Jenkins and P. Weightman, *Phys. Status Solidi C* **0**, 2931 (2003)

[59] N. P. Blanchard, *Ph. D. Thesis*, The University of Liverpool (2004)

[60] P. Weightman, G. J. Dolan, C. I. Smith, M. C. Cuquerella, N. J. Almond, T. Farrell, D. G. Fernig, C. Edwards and D. S. Martin, *Phys. Rev. Lett.* **96**, 086102 (2006)

[61] C. P. Mansley, T. Farrell, C. I. Smith, P. Harrison, A. Bowfield and P. Weightman, *J. Phys. D: Appl. Phys.* **42**, 115303 (2009)

[62] D. M. Jaffery and R. J. Madix, *Surf. Sci.* **258**, 359 (1991)

[63] J. X. Wang, G. M. Watson and B. M. Ocko, *J. Phys. Chem.* **100**, 6672 (1996)

[64] O. M. Magnussen, *Chem. Rev.* **102**, 679 (2002)

[65] A. Hamelin, *J. Electroanal. Chem.* **407**, 1 (1996)

[66] A. Hamelin, M. J. Sottomayor, F. Silva, S-C. Chang and M. J. Weaver, *J. Electroanal. Chem.* **295**, 291 (1990)

[67] Z. Borkowska and U. Stimming, *J. Electroanal. Chem.* **312**, 237 (1991)

[68] C. I. Smith, N. J. Almond and P. Weightman, *J. Electrochem. Soc.* **154**, F90 (2007)

[69] D. M. Kolb and J. Schneider, *Electrochim. Acta* **31**, 929 (1986)

[70] Z. Borkowska and U. Stimming, *J. Electroanal. Chem.* **312**, 237 (1991)

[71] C. I. Smith, A. J. Maunder, C. A. Lucas, R. J. Nichols and P. Weightman, *J. Electrochem. Soc.* **150**, E233 (2003)

[72] C. I. Smith, G. J. Dolan, T. Farrell, A. J. Maunder, D. G. Fernig, C. Edwards and P. Weightman, *J. Phys. Condens. Matter* **16**, S4385 (2004)

[73] C. I. Smith, A. Bowfield, G. J. Dolan, M. C. Cuquerella, C. P. Mansley, D. G. Fernig, C. Edwards and P. Weightman, *J. Chem. Phys.* **130**, 044702 (2009)

[74] R. LeParc, C. I. Smith, M. C. Cuquerella, R. L. Williams, D. G. Fernig, C. Edwards, D. S. Martin and P. Weightman, *Langmuir* **22**, 3413 (2006)

[75] M. C. Cuquerella, C. I. Smith, D. G. Fernig, C. Edwards and P. Weightman, *Langmuir* **23**, 2078 (2007)

[76] C. P. Mansley, C. I. Smith, M. C. Cuquerella, T. Farrell, D. G. Fernig, C. Edwards and P. Weightman, *Phys. Status Solidi C* **5**, 2582 (2008)

Chapter 4

The Determination of the Structure of Cytosine Monolayers Adsorbed at the Au(110)/Electrolyte Interface

RAS has been successfully applied to study the preferential orientation of cytosine and its corresponding monophosphate (cytidine 5′-monophosphate (CMP)) molecules adsorbed at the Au(110)/electrolyte interface. This chapter describes the behaviour of the cytosine and CMP molecules at the Au(110)/electrolyte interface within different environments that include varying electrode potential and solution pH. In addition to this is are the RA spectra for varying concentrations of cytosine and CMP molecules in solution and how the adsorption of these molecules affect the Au(110) surface below.

4.1 Introduction

The adsorption of DNA and DNA bases at metal/liquid interfaces has potential as a structural basis for "bottom up" fabrication of inorganic and organic molecular devices [1] and in biomimetic materials science and molecular electronics. An understanding of the interactions between nucleic acids and metal surfaces, which is best studied in a liquid environment required by biological molecules for their stability and functional activity, can also provide insight into complex intermolecular processes relevant to the origin of life [2]. It is also important in DNA bioarray technology where the surface environment affects DNA hybridisation [3] and the intensity of the fluorescence signal from tagged strands [4].

This chapter describes the orientation and behaviour of the nucleic acid base cytosine at the Au(110)/electrolyte interface in various electrochemical environments using RAS. This chapter extends an earlier study [5] of cytosine and its monophosphate CMP adsorbed at saturation coverage at Au(110)/liquid interfaces. In the previous study [5] it was demonstrated using RAS that cytosine molecules give rise to ordered structures in which the base is orientated vertically to the surface and parallel to the $[1\,\bar{1}0]$ axis of the Au(110) plane. Figure 4.1 shows the structure of cytosine and CMP molecules.

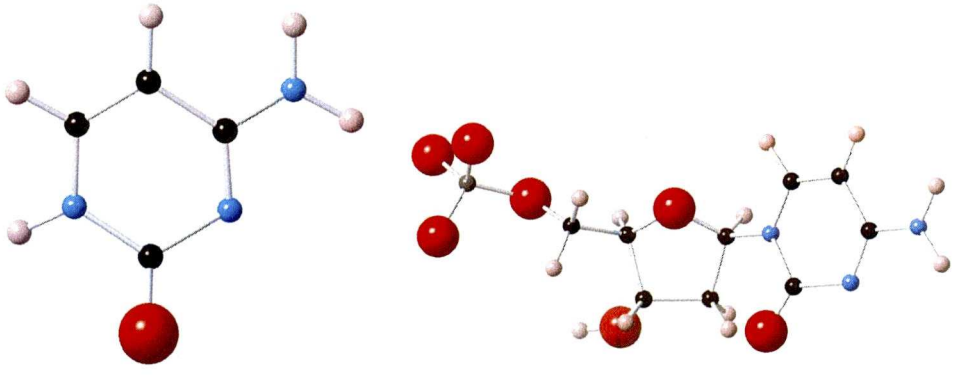

Figure 4.1: The structure of cytosine (left) and CMP (right). Key: oxygen - red spheres, carbon - black spheres, nitrogen - sky blue spheres, hydrogen - beige spheres and phosphorous - dark grey sphere.

The adsorption of nucleic acids was widely studied initially on mercury and carbon electrodes by electrochemical methods such as a.c. polarography [6], differential capacity [7] and CV [8]. With the introduction of imaging techniques on the molecular level such as Atomic Force Microscopy (AFM) and STM, there have been a variety of investigations of the nature of the monolayers formed on graphite [9], gold [10,11] and copper [12]. Previous work on the adsorption of cytosine at solid/liquid interfaces has included studies on silver [13,14] and gold [15,16] substrates using a variety of techniques such as Infra-Red Reflection Adsorption Spectroscopy (IRRAS) [17], Surface Enhanced Raman Spectroscopy (SERS) [18], Specular Reflectivity [19], LEED [20] and Electron Spectroscopy for Chemical Analysis (ESCA) [10]. These studies have shown that the type of the underlying substrate used has a strong influence on the behaviour of cytosine. There is evidence of structural phase transitions on the graphite, gold and mercury electrodes while on silver the cytosine only adsorbs vertically.

4.2 The Electronic Structure of Cytosine

The earlier study [5] proves that cytosine molecules adsorbed onto a surface assume an anisotropic alignment across the Au(110) substrate. The optical response of the cytosine molecules arises from defined dipole transitions whose orientation with respect to the structure of the cytosine molecule are known. This facilitates the determination of the orientation of the molecules' preferential ordering on the substrate. This subsection describes the optical response of cytosine and describes the dipole transitions which give rise to the RA spectra reported in the previous study [5].

Extensive studies [21,22] of cytosine have been conducted and give rise to interesting discussions about the transition energies and directions of the transition dipoles with respect to the molecular axes. Cytosine is essentially a planar molecule that has an optical spectrum that consists of two types of transitions, $n \rightarrow \pi^*$ that are polarised at right angles to the plane of the cytosine molecule, and $\pi \rightarrow \pi^*$ transitions which are polarised parallel to the molecular plane. The $n \rightarrow \pi^*$

transitions are located on the nitrogen atoms of the six membered ring and are of significantly lower intensity than the $\pi \rightarrow \pi^*$ transitions, approximately one thousandth of the intensity and are orientated perpendicular to the molecule [23]. From hereon in the $n \rightarrow \pi^*$ transitions are overlooked in the RAS analysis. The $\pi \rightarrow \pi^*$ transitions have been calculated using gradient corrected density-functional theory (DFT-GGA) [24] using ultra soft psuedopotentials and give rise to transitions with approximate energies of 4.6 eV, 5.5 eV and 6.2 eV. These transitions energies are similar to those published by Fülscher and Roos [22] who used complete active space self-consistent field method (CASSCF) to obtain energies of 4.4 eV, 5.4 eV and 6.2 eV for the $\pi \rightarrow \pi^*$ transitions of the cytosine molecule.

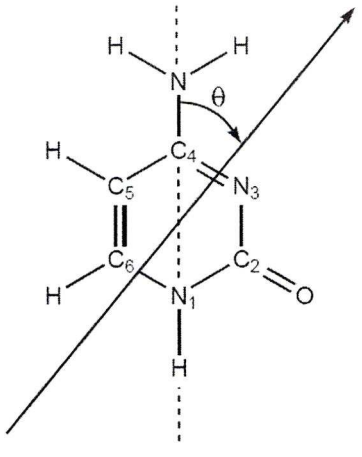

Figure 4.2: The DeVoe-Tinoco convention of molecular transition directions [26] of cytosine. The azimuth angle θ is measured from the N(1)-C(4) axis towards the N(3) atom.

The experimental and theoretical studies yield similar results for the transition energies, however the two disagree with regards to the directions of these dipole transitions. The angles, θ, specifying the directions of the $\pi \rightarrow \pi^*$ transitions that are polarised in the plane of the six membered ring are defined by the DeVoe-Tinoco convention [25] with respect to the N(1)-C(4) axis as shown in figure 4.2. Positive angles are measured towards the N(3) atom of the molecular ring. Fülscher and Roos [22] suggest that the angles for the 4.4 eV and 5.4 eV transitions are 60° and -5° respectively, whereas Žaloudek *et al* [26] suggest that their experiments yield angles of 6° and -46°. In addition to this disagreement in the angles of the

dipole transitions, the character of the 5.4 eV transition is also debated. Fülscher and Roos [22] describe the second transition as n $\rightarrow$ π^* from their theoretical calculations, but Žaloudek *et al* [26] did not find any evidence of the n $\rightarrow$ π^* transition. An important agreement between the two studies is that both find that the direction of the transitions at 4.4 eV and 5.4 eV are separated by approximately 50°.

The analysis of the electronic structure of cytosine gives rise to an optical transition at 4.4 eV that lies within our experimental spectral range of RAS. The 5.4 eV transition is also with the spectral range of our RA spectrometer but the sensitivity of the apparatus at this energy diminishes to give rise to less reliable data.

4.3 Concentration Effect of Cytosine Adsorption

RAS is sensitive to the steps, surface states and reconstructions of the Au(110) surface with the result that it is difficult to obtain reproducible results from the flame annealing process [27-32]. However by careful attention to the duration and sequence of the flame annealing process good reproducibility was achieved as may be seen from a comparison of the RAS from the results shown in figure 4.3 for four different Au(110) surfaces employed in this study.

The Au(110) crystal was prepared as described in Chapter 2. The solution used in the electrochemical cell used in the experiments reported in this subsection was a phosphate buffer solution made from NaH_2PO_4, K_2HPO_4 (BDH, Analar grade) and Millipore ultra-pure water (18 MΩcm). The buffer solution was then purged with Argon before the insertion of the Au(110) crystal in order to remove any oxygen from the electrochemical cell.

In the separate experiments various volumes of a 1 mM cytosine (Aldrich) solution were added to the electrochemical cell to give final concentrations of 0.1 μM, 0.5 μM, 20 μM and 100 μM with the Au electrodes held at 0.0 V and the resulting RAS profiles are shown in figure 4.4 (a). In the previous study [5] results were only reported for a 100 μM solution. As discussed previously, the addition of 100 μM of cytosine led to an increase in negative intensity across the entire spectrum, with the appearance of an additional negative shoulder at 4.2 eV and the

loss of the positive 4.6 eV peak (figure 4.4 (a)). The RA spectra obtained from the Au(110) surface after the addition of cytosine to give the final concentrations of 0.1 μM, 0.5 μM and 20 μM are also shown in figure 4.4 (a). A comparison of figure 4.3 and figure 4.4 (a) can be used to highlight the change in RAS between the RA spectra of Au(110) and the RA spectra of Au(110) + cytosine. The RAS of the Au(110) and Au(110) + cytosine between 1.5 eV and 2.5 eV remain similar throughout the separate experiments. At energies above 2.5 eV, the overall negative intensity of the RA spectra of Au(110) + cytosine is increased in comparison to the four clean Au(110) RA spectra and the overall negative intensity of the RA profile of Au(110) + cytosine correlated with the strength of the cytosine concentration and the largest changes were observed when going from the 0.5 μM to the 20 μM solution. In addition to the overall increase in RAS intensity, the results of these experiments reproduced the same shoulder at 4.2 eV and the loss of the positive 4.6 eV peak as seen in previous work [5] with the size of the shoulder being proportional to the concentration of the cytosine in solution.

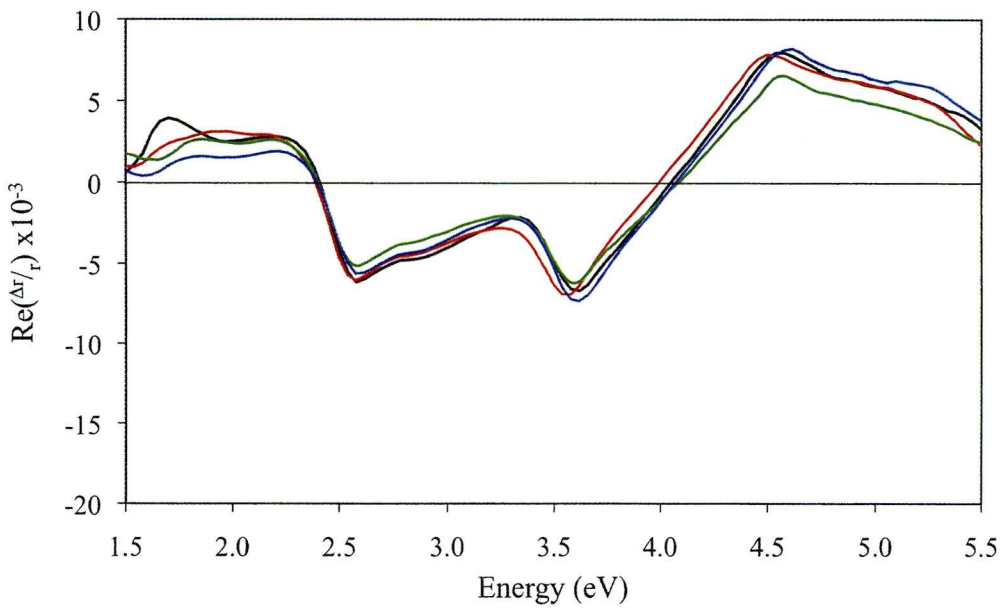

Figure 4.3: The RA spectra of Au(110) used with varying concentrations of cytosine solution, 0.1 μM (black line), 0.5 μM (red line), 20 μM (green line) and 100 μM (blue line) experiments.

The difference spectra obtained by subtraction of the RA spectra of Au(110) from the RA spectra of Au(110) + cytosine are shown in Figure 4.4 (b). The difference spectra show that a broad negative feature developed at 4.6 eV as the cytosine concentration increased.

The RA spectra of figures 4.4 (a) and (b) show that the intensity of the negative peak at 2.6 eV in the spectra of the Au(110) surface increased as the concentration of cytosine is increased. Figure 4.5 shows the variation in the intensity of the 2.6 eV peak as a function of time starting from the addition of cytosine to the electrochemical cell. There are clear differences in the time dependence of the intensity of the 2.6 eV peak for the four cytosine concentrations and as the concentration of cytosine in the solution was increased, the maximum intensity reached by the 2.6 eV RA peak also increased.

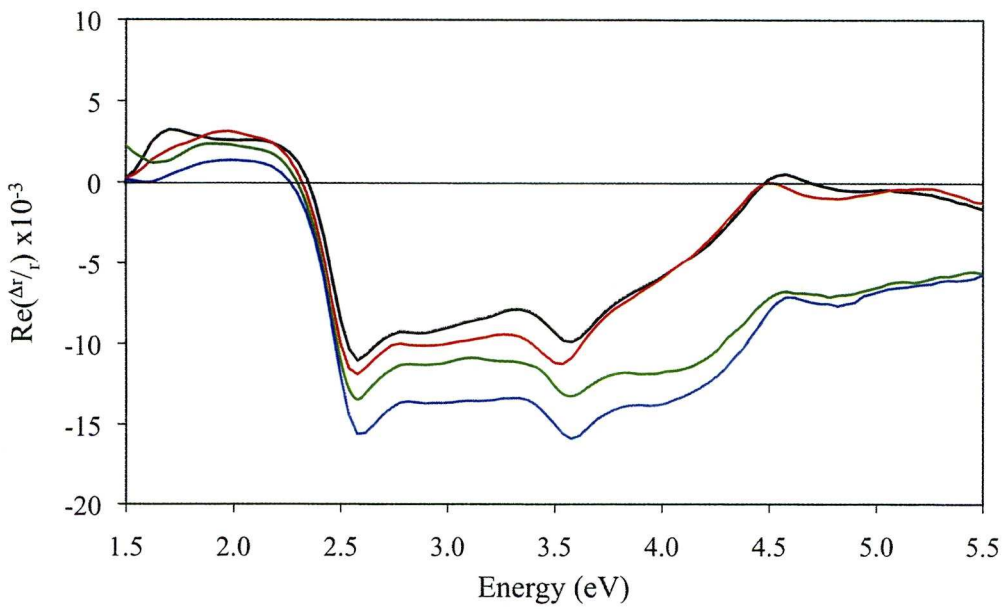

Figure 4.4 (a): The RA spectra of Au(110) + 0.1 μM (black line), + 0.5 μM (red line), + 20 μM (green line) and +100 μM (blue line) of cytosine at 0.0 V vs SCE at pH 7.1.

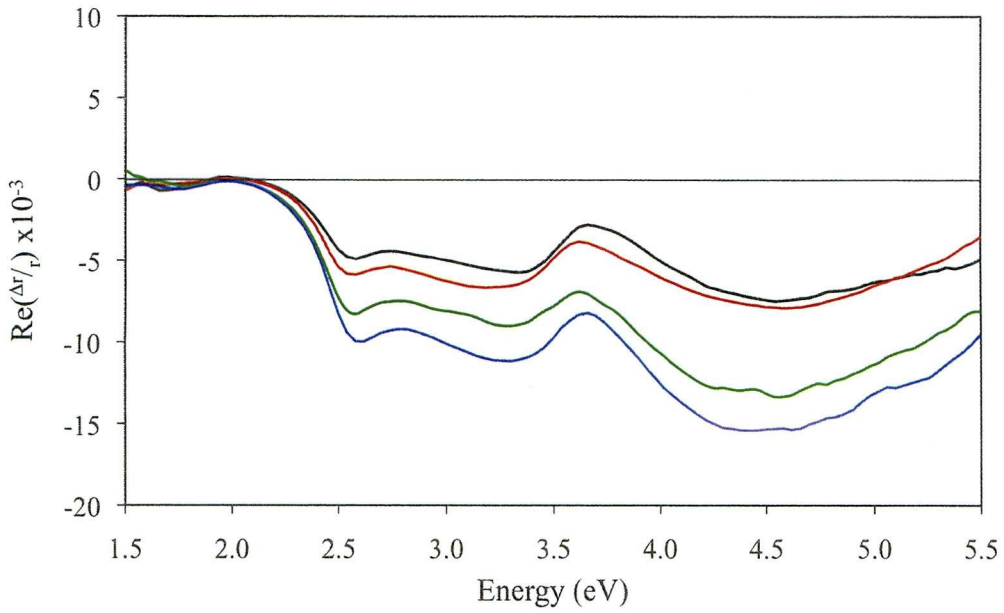

Figure 4.4 (b): The spectra of cytosine generated by the subtraction of the corresponding Au(110) spectra shown in 4.3 from the respective Au(110) + cytosine spectra shown in 4.4 (a). 0.1 μM (black line), 0.5 μM (red line), 20 μM (green line) and 100 μM (blue line).

The increase in the RAS of the Au(110)/electrolyte interface at 2.6 eV following the addition of cytosine to the electrochemical cell (figure 4.5) can be explained by assuming the cytosine adsorbs on the Au(110) surface until either saturation coverage is reached or the solution is exhausted of molecules. The results of figure 4.5 are used to suggest that a monolayer is only achieved when the Au(110) sample is immersed in the fourth concentration of 100 μM and that at the lower concentrations the solutions are exhausted. These results differ from those obtained from similar studies of the adsorption of adenine on Au(110) where only the lowest concentration failed to saturate the solution [33]. It is calculated that within the electrochemical cell at the 0.1 μM solution of cytosine, there are 3×10^{15} molecules. The area of the Au(110) is 0.5 cm^2 so if all of these molecules are adsorbed onto the available area, then the density of molecules would be three molecules per 5 $Å^2$. On Au(111) two orientations are possible [9,15]; the area of the unit cell of cytosine when adsorbed horizontally and vertically on the surface are ~ 100 $Å^2$ [9] and ~ 63 $Å^2$ [15] respectively which are both considerably greater than the maximum packing density achievable if all the available molecules adsorb on

the Au(110) structure. However, it is likely that the molecules also adsorb onto the back face of the crystal and the glass walls of the electrochemical cell which would bring the saturated surface concentration down to levels in keeping with the deduction from electron spectroscopy that one cytosine molecule occupies the area of about six gold atoms [10].

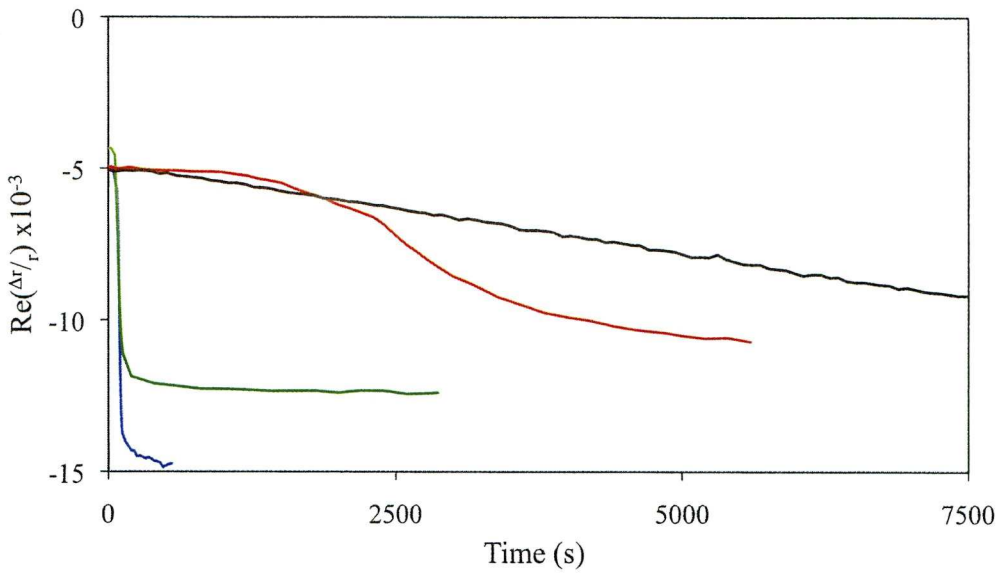

Figure 4.5: RA spectra showing the changes in the intensity of the 2.6 eV peak as a function of time for addition of 0.1 μM (black line), 0.5 μM (red line), 20 μM (green line) and 100 μM cytosine (blue line) to Au(110) in 0.1 M NaH_2PO_4/K_2HPO_4 (pH 7.1) at 0.0 V vs. SCE.

The addition of cytosine molecules clearly affects the RA spectra of the Au(110) surface and this is shown by the difference spectra of figure 4.4 (b). In order for there to be an optical response of the cytosine that is measurable by RAS, the cytosine molecules must have a preferential ordering at the Au(110)/electrolyte interface. If the anisotropic alignment did not exist then the spectra displayed in figure 4.4 (b) would be featureless.

In conclusion the data reported in this subsection show that the concentration of cytosine molecules in solution does effect the RA response of the Au(110) surface and as the concentration of cytosine solution in the electrochemical cell increases so too does the intensity of the RA spectra of Au(110) + cytosine. The

data also shows that monolayer coverage of the cytosine molecules onto the Au(110) surface is only achieved at the highest concentration.

4.4 Simulations of Sub-Monolayer Au(110) + Cytosine

In the previous subsection it was shown that the addition of 100 μM of cytosine to the electrochemical cell resulted in a greater change to the RA response of Au(110) than when only 0.1 μM of cytosine was added. It is clear from figure 4.4 (a) that the RA profiles obtained from all four concentrations have similar line shapes but vary in intensity. Assuming that the 100 μM case gives rise to a complete monolayer, and the other three are sub-monolayer coverage then the differences between these RA spectra could arise from a significant contribution to the RAS from areas of the Au(110) surface which are not covered by cytosine molecules. If this is the case and also that the orientation of the cytosine molecule does not change with coverage then it should therefore be possible to represent the lower concentration RA spectra as a linear summation of the RAS of the full monolayer coverage and the RAS of the Au(110)-(1 × 1) surface. The equation used takes the form:

$$\begin{aligned} \text{RAS}\ \{\text{Au(110)} + \text{C}\ \mu\text{M}\} = \text{A} * \{\text{RAS}\ [\text{Au(110)}]\} \\ + \text{B} * \{\text{RAS}\ [\text{Au(110)} + 100\ \mu\text{M}]\} \end{aligned} \qquad (4.1)$$

where C is the concentration of less than 100 μM, and A and B are non-independent multiplication factors. Simulations of the experimental results obtained using these procedures are shown in figure 4.6 and the parameters used in the simulations are shown in table 4.1.

Figure 4.6 shows that there is good correlation between the simulations and the experimental data. This indicates that the cytosine adsorbs in the same orientation at lower concentrations as well as at higher concentrations. This result also demonstrates that there is no phase transition as a function of cytosine concentration.

Concentration	A	B	% Gold
0.1 μM	0.50	0.50	50
0.5 μM	0.53	0.47	47
20 μM	0.90	0.10	10

Table 4.1: The multiplicity factors used in the simulations and the equivalent percentage of uncovered gold.

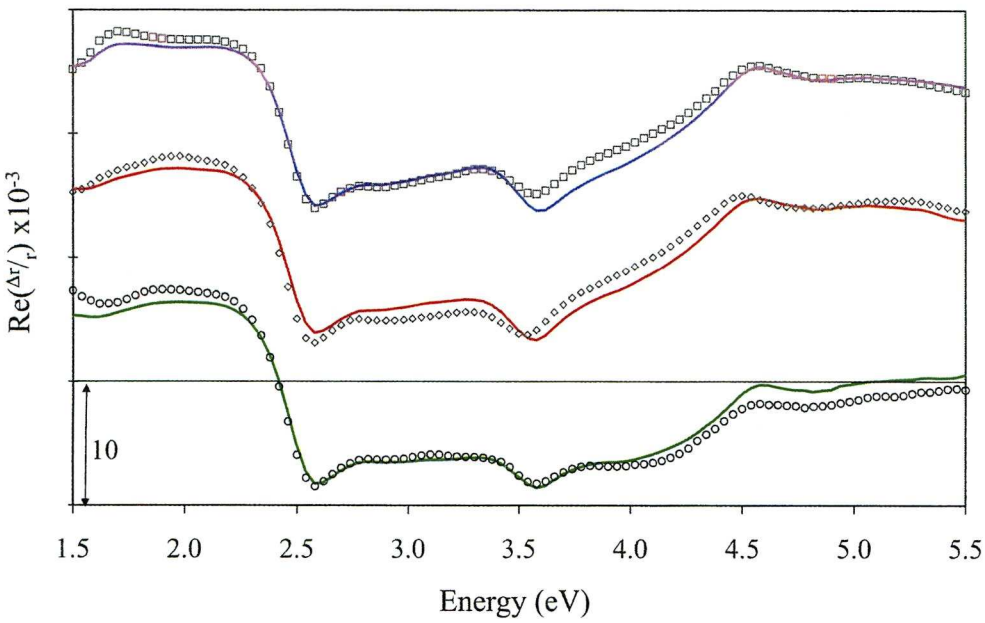

Figure 4.6: Simulation of 0.1 μM (□), 0.5 μM (◇) and 20 μM (○) RA spectra of Au(110) + cytosine with the corresponding simulation in solid coloured lines. The graphs have been offset for clarity and units displayed on the y-axis.

4.5 Angular Variation

The technique of rotating a sample about the axis of the incident light between each RA spectrum is known as Azimuth-Dependent RAS (ADRAS). Earlier studies [5,34-36] have given details of how the alignment of the optical axes of an adsorbed molecule on a surface can be obtained by using ADRAS. The initial orientation of the Au(110) crystal is such that the principal axes of the crystal are aligned 45° to

the plane of polarisation of the incident light. Orientating the crystal this way produces the 'maximum' intensity RA response. When the crystal is rotated in the plane of its surface the angle separating the substrate axes and the plane of polarisation of the incident light vector (the *azimuthal* angle) will change.

Figure 4.7 shows the ADRAS of a clean Au(110) crystal at 0.0 V in phosphate buffer. The intensity of RA spectra for Au(110) varies as a function of cos(2θ) where θ is the angle of rotation away from the initial 45° position. This means that as θ tends towards 45°, the intensity of the subsequent RA spectra tend towards zero due to the loss of anisotropy in the reflected light as the polarisation direction of the incident light is parallel to one of the optical axes and perpendicular to the other. As θ is increased from 45° to 90°, the intensity of the RA spectra become negative and produce mirror images of the RA spectra from 90° down to 45°, resulting in the 90° spectrum having the maximum negative intensity and being the mirror image of the spectrum obtained with the Au(110) crystal positioned at θ = 0°. The mirror imaging occurs because of the anisotropic response resulting from $r_{[001]} - r_{[1\bar{1}0]}$ instead of $r_{[1\bar{1}0]} - r_{[001]}$. As the Au(110) sample is rotated further the intensity of the RA spectra will become zero as θ = 135° and return to a maximum positive RA intensity at θ = 180°.

If an ordered molecular adlayer forms on a crystal surface it is not certain that it will have the same optical axes as the substrate. If the adlayer does not have the same optical axes then the ADRAS becomes more complex due to the two sets of contributions from the two anisotropies competing as the angle of rotation is varied.

Figure 4.7 shows that the RA response of the Au(110) sample tends towards zero when the polarisation plane becomes parallel to one of the surface directions. If the optical axes of an adlayer were not aligned in the same directions as the optical axes of the substrate then there would never be a featureless RA spectrum as there would be a contribution from the adlayer regardless of whether the RA response of the substrate tended towards zero. Macdonald *et al* [36] used ADRAS to calculate the angle separating two competing optical axes by recording RA spectra at a single wavelength as a function of θ.

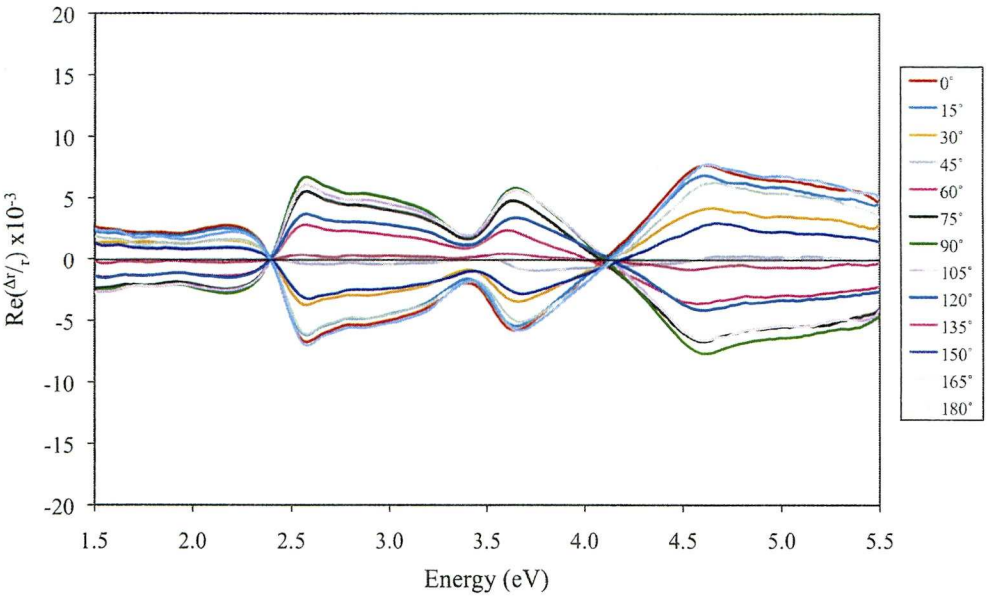

Figure 4.7: RA spectra of Au(110) as a function of angular rotation, θ, from 0° to 90° at 0.0 V vs SCE and pH 7.1.

Figure 4.8 shows the angular variation of the RA spectra of Au(110) + 100 μM of cytosine as the crystal is rotated azimuthally about the direction of the incident light. The molecules are added at 0.0 V, left to adsorb and then the sample is rotated through 90°, whilst taking an RA spectrum at 10° intervals. The results show mirror images through the *x*-axis and the intensity at all energies showed a cos(2θ) dependence [5,37]. It is important to note that the spectra fall to zero across the entire spectral range for θ = 45° when the polarisation of the incident light is parallel to one of the crystal axes in the surface plane. Previous work [5] showed that at saturation coverage cytosine adsorbs to form an ordered structure at the Au(110)/electrolyte interface in which the base interacts with the surface through the N(3) atom, as shown in figure 4.2, and is orientated vertically to the surface with the long axis of the molecule parallel to the [1 $\bar{1}$0] axis of the Au(110) plane. The conclusion that the cytosine molecules adsorbed vertically on the Au(110) surface arises from the fact that the two transitions from the cytosine molecule are 50° apart. The only way that the RA spectra can go to zero across the whole spectral range is if

the molecule is vertical. If the cytosine molecule was not vertical then at least one of the transitions would produce an RA response at any given orientation.

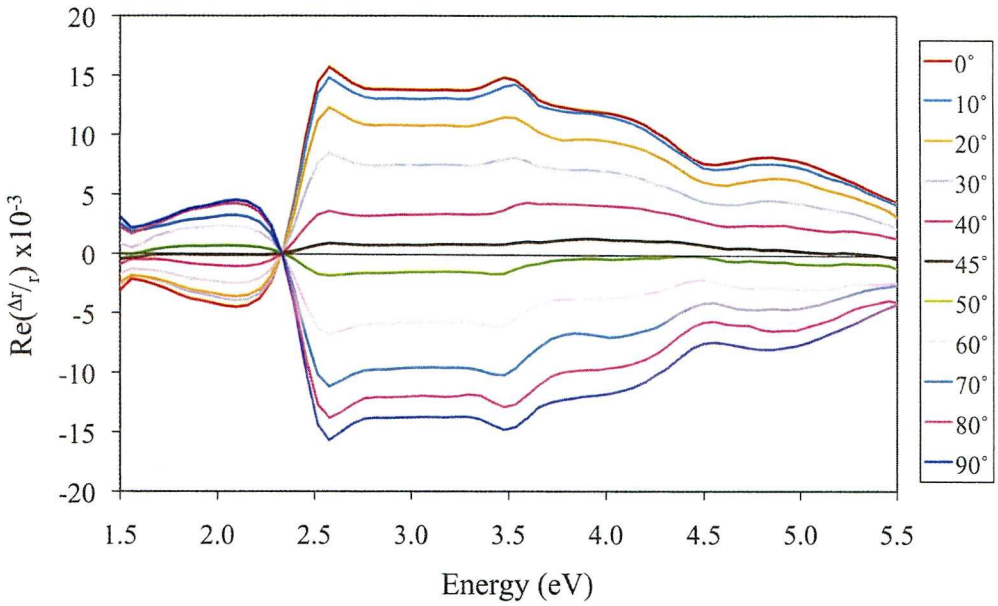

Figure 4.8: RA spectra of Au(110) + 100 μM of cytosine as a function of angular rotation, θ, from 0° to 90° at 0.0 V vs SCE and pH 7.1.

Figure 4.9 shows the RA spectra generated by investigating the effect on the RA response of an Au(110) crystal after the addition of 100 μM of CMP. This experiment was undertaken in order to compare the orientation of the cytosine and CMP molecules at the Au(110)/electrolyte interface.

A comparison of figures 4.8 and 4.9 highlights the similarities of RA spectra of Au(110) + cytosine and the RA spectra of Au(110) + CMP. The addition of CMP results in an overall increase in spectral intensity compared to the Au(110) spectra as well as the emerging shoulder at 4.2 eV and the loss of the positive 4.6 eV peak that is observed after the addition of cytosine. In addition to these similarities, the intensity of the RA rotation data sets of Au(110) + cytosine and Au(110) + CMP both decrease to zero at $\theta = 45°$, which gives rise to the result that CMP also aligns itself along one of the optical axes of the Au(110) substrate.

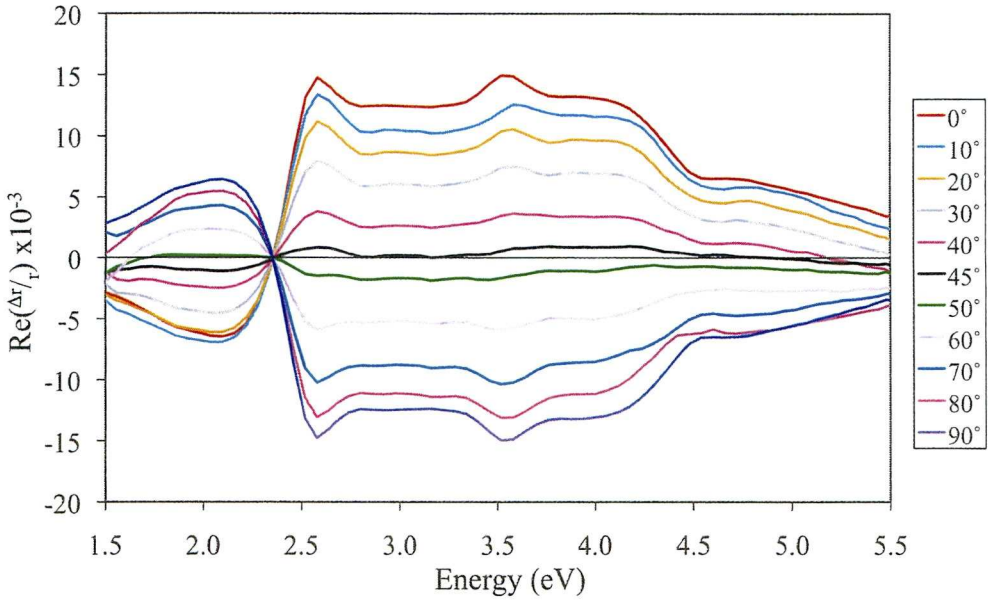

Figure 4.9: RA spectra of Au(110) + 100 μM of CMP as a function of angular rotation, θ, from 0° to 90° at 0.0 V vs SCE and pH 7.1.

The difference between a cytosine molecule and a CMP molecule is that the CMP molecule is the cytosine base attached to a sugar and phosphate group as shown in figure 4.1. The sugar and the phosphate of the CMP molecule do not have optical transitions in the spectral range of the RA spectrometer and thus only the dipole transitions from the base contribute to the RA spectra. Although the optical response of the cytosine and the CMP are the same to first order, it does not necessarily mean the two molecules would give rise to similar RA spectra as they may have orientated differently on the Au(110) surface. However the Au(110) + cytosine and Au(110) + CMP do yield very similar RA spectra, a result that is used to suggest that the cytosine and the base section of the CMP molecules align in the same way on the Au(110) surface.

The adsorption of cytosine molecules onto the Au(110) surface gives rise to an increase in the RA response of the Au(110) between 2.5 eV and 3.5 eV. The increase in signal between these energies is attributed to the dipole transitions of the bases coupling to the dielectric response of the Au(110) [34] since the cytosine and CMP give rise to similar RA spectra then the molecules must adsorb onto the Au(110) surface via bonding sites found on the base. The comparison of the RA

spectra of ss-DNA and ds-DNA in previous works [37,38] shows and describes how the ss-DNA experiences a similar increase in RA response to that of the Au(110) + cytosine when the bases of the ss-DNA were the points of adsorption onto the Au(110) surface. Conversely the increase in RA response of the ds-DNA was much less than that observed with the adsorption of ss-DNA. This smaller response in RAS from the ds-DNA is attributed to the bases being prohibited from coupling to the Au(110) surface because of the phosphate groups separating the bases and the substrate.

In conclusion, cytosine and CMP bond to the Au(110) substrate via sites on the bases resulting in similar RA spectra for both sets of molecular adsorption. The idea of the cytosine and CMP molecules adsorbing vertically onto the Au(110) surface is reinforced by Ataka and Osawa [15] who used in situ surface-enhanced infrared absorption spectroscopy and CV experiments to declare that cytosine attaches to an Au electrode vertically via the N(3)-O-NH_2 sites. Their paper also references another study by Koglin *et al* [18] who use SERS to determine that CMP on Ag is adsorbed via the cytosine base at negative potentials.

4.6 The Effect of Electrode Potential on the RAS of Adsorbed Cytosine

The experiments in this subsection were conducted using 100 μM solution of cytosine and all voltage are vs SCE. Figure 4.10 (a) shows the RA spectra of the Au(110) surface in a 0.1 M phosphate buffer solution (pH 7.1) as the potential applied to the electrode was varied in the sequence of 0.0 V, 0.2 V, 0.4 V, 0.6 V, -0.2 V, -0.4 V and -0.6 V. As has been observed previously [5,37-40] the RAS of the Au(110)/liquid interface changes significantly as the voltage on the electrode is varied. As the potential becomes more positive, the magnitude of the 2.6 eV peak increases while the magnitude of the 3.6 eV peak decreases. As the potential is taken to more negative values the feature at 2.0 eV becomes more intense, the intensity of the peak at 2.6 eV decreases and becomes less defined and the intensity of the

3.6 eV decreases. Figure 4.10 (b) shows the RA spectra of Au(110) + 100 μM cytosine after the addition of cytosine at 0.0 V, the applied potential was cycled from 0.0 V to 0.6 V, then from 0.0 V to -0.6 V in 0.2 V steps. The RA spectra for the applied potentials of -0.2 V up to 0.6 V are almost identical, however the RA spectra obtained at -0.4 V and -0.6 V are different and show decreasing overall intensities respectively.

The RAS profile of the Au(110) surface is very sensitive to its morphology and both the RAS profile and the morphology of this surface are known to vary with the voltage applied to the Au(110) electrode in an electrochemical cell [27-30]. The variation of the RAS with applied voltage is not understood in detail but the surface is thought to adopt a (1×1) reconstruction at 0.0 V vs SCE and the spectra observed at 0.0 V vs SCE (figure 4.3) are very similar to those observed in other studies of the Au(110) surface [33,37-40]. In previous work on the adsorption of adenine [33], the sulphur containing amino acids [35] and single and double stranded DNA adsorbed on Au(110) [37,38] it was found that varying the voltage applied to the Au(110) electrode resulted in a change in the RAS profiles of the adsorbed molecules. In these systems the assumption was made that at each voltage the observed spectrum of the adsorbed molecules was a linear sum of the spectrum of the Au(110) surface and the "intrinsic" spectrum of the molecule. There is no way of checking this assumption empirically and it is known to fail for molecules adsorbed on the Si(100) surface where it has been shown that the electronic structure of the gas phase molecules and the semiconductor bulk wave-functions are strongly modified by the adsorption process and give rise to new optical fingerprints [41,42]. However for adenine adsorbed on Au(110) this procedure works rather well and in spite of the changes in the RAS of the Au(110) surface with applied voltage (figure 4.10 (a)) it gives rise to rather similar intrinsic profiles for the adsorbed molecules the small differences between which can be understood in terms of changes in the orientation of the molecule in a plane perpendicular to the Au(110) surface as the voltage is varied [5,43].

In contrast to the results obtained on other systems the RAS profile of cytosine adsorbed on the Au(110)/liquid interface at 0.0 V changes very little when the voltage is varied in the range from +0.6 V to -0.2 V (Figure 4.10 (b)). When the

voltage is varied to -0.4 V and then -0.6 V the RAS profile reduces in intensity but maintains the same basic profile which suggests that the molecules are desorbing from the surface at these voltages and that the remaining molecules do not change their orientation on the surface. In previous studies [38,39] it has been shown that the "intrinsic" RAS profiles of adsorbed molecules can be obtained by the subtraction of the RA spectrum of Au(110) from the RA spectrum of Au(110) + molecule at corresponding voltages. Figure 4.10 (c) shows the "intrinsic" RAS profile of the adsorbed cytosine molecules. Almost all of these differences can be attributed to the voltage dependence of the RAS of the Au(110)/liquid surface. Assuming that the adsorption of the cytosine "freezes" the Au(110)/liquid interface in the structure prevailing when the molecules are introduced into the electrochemical cell then a subtraction of the RAS of the Au(110)/liquid interface obtained at 0.0 V from the RAS of the adsorbed molecules at voltages between +0.6 V and -0.2 V should show the same intrinsic spectral profile for the cytosine. This is indeed the case as shown in Figure 4.10 (d). Furthermore these RAS profiles are remarkably similar to those shown in figure 4.4 (b) for the spectra obtained by adding different concentrations of cytosine to the electrochemical cell. Applying the same subtraction to the RAS of adsorbed cytosine observed at -0.4 V and -0.6 V yields profiles of very similar shape to those obtained for the other voltages (Figure 4.10 (d)) though much reduced in intensity suggesting that at these voltages some cytosine has desorbed but that the remaining molecules maintain their orientation on the surfaces. The RAS profile deduced for cytosine at -0.6 V differs from the others in that the peak at ~ 2.6 eV changes from a weak negative feature to a weak positive feature (Figure 4.10 (d)). This result can be explained by assuming that at this voltage the concentration of cytosine on the Au(110) is so low that the RAS of the clean Au(110)/liquid interface dominates the subtraction.

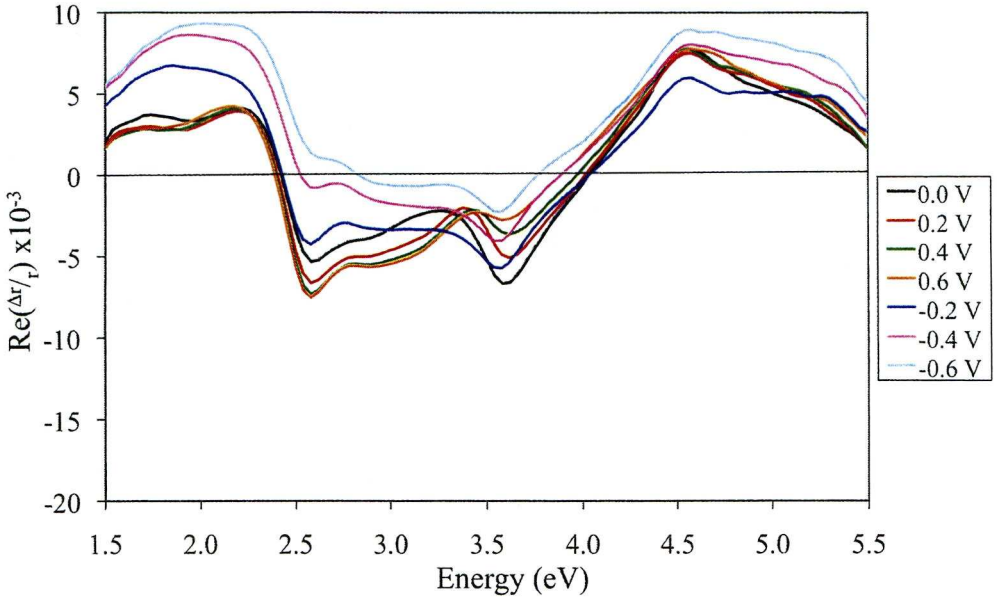

Figure 4.10 (a): RA spectra of Au(110) from 0.6 V to -0.6 V vs. SCE.

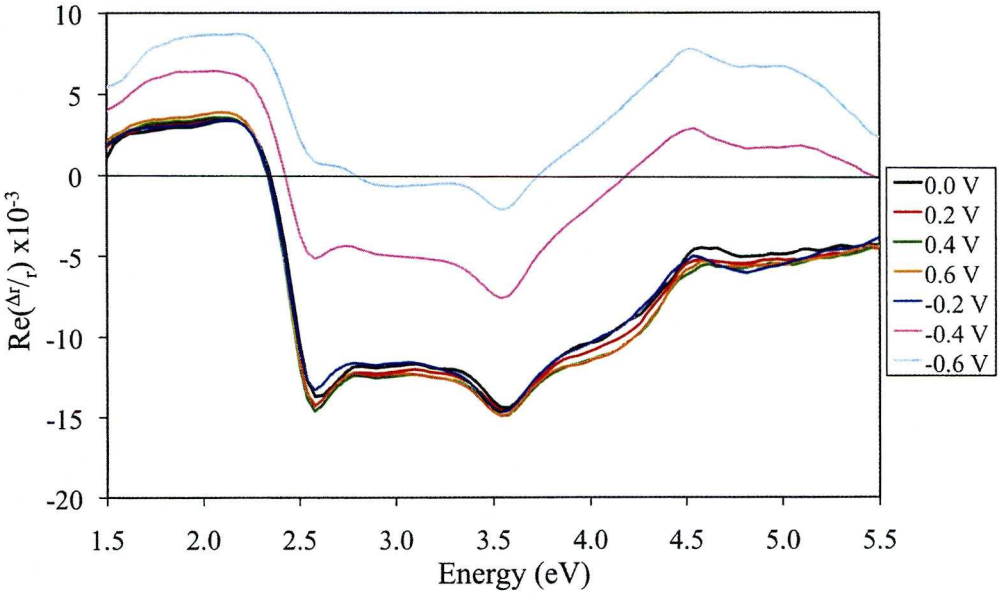

Figure 4.10 (b): RA spectra of Au(110) + 100 μM of cytosine from 0.6 V to -0.6 V vs. SCE

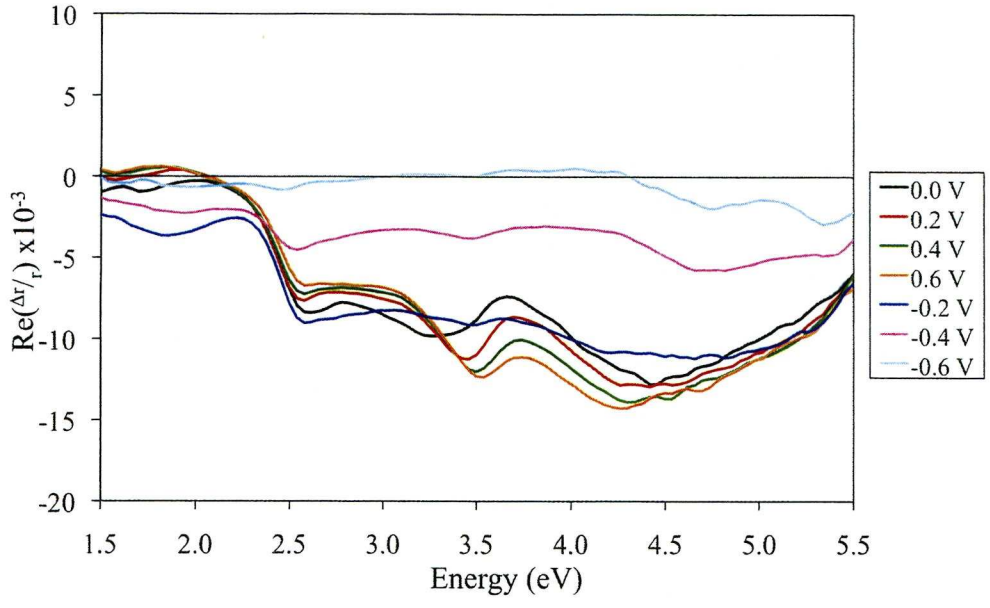

Figure 4.10 (c): RA spectra of cytosine from 0.6 V to -0.6 V vs. SCE

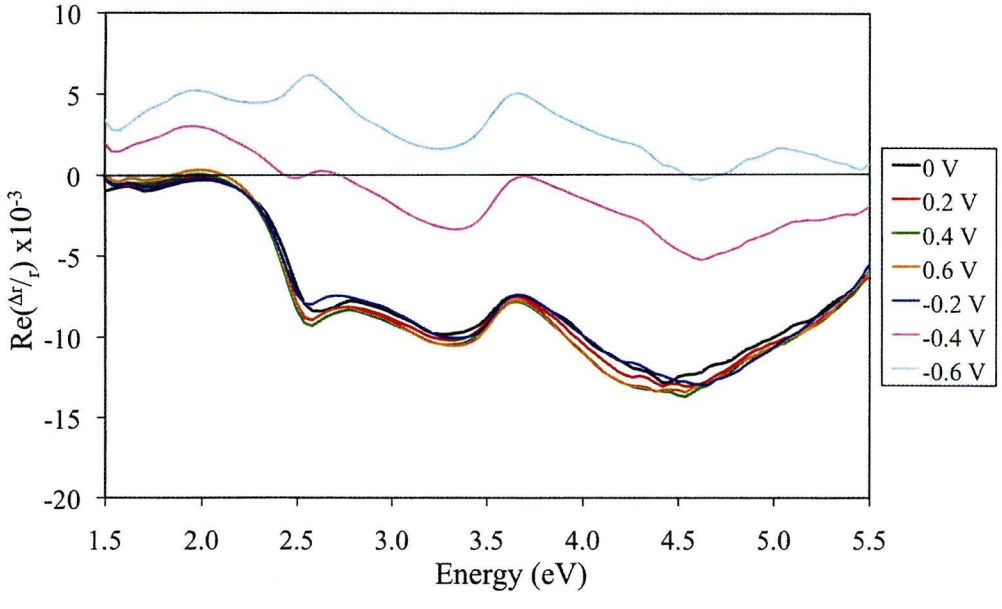

Figure 4.10 (d): RA spectra of cytosine obtained from subtracting the RA spectra of Au(110) at 0.0 V from each of the RA spectra of Au(110) + cytosine at each voltage.

The (1×1) reconstruction of the Au(110) surface is characterised by rows of gold atoms in the [1 $\bar{1}$ 0] direction separated by 2.88 Å along the row and separated from adjacent parallel rows by 4.08 Å. An adsorption geometry in which cytosine molecules are orientated with the long axis of the molecules along the [1 $\bar{1}$ 0] direction and with the molecule bonding through the NH_2 group, the N(3) site and possibly the O(8) site to three gold atoms at the top of the Au [1 $\bar{1}$ 0] rows as shown in figure 4.11 (a) suggests a mechanism for the "freezing" of the Au(110) surface structure. The distance across the length of three gold atoms is ~7.8 Å and is large enough to accommodate the NH_2-N(3)-O(8) group which has a length of ~6.3 Å. The unit cell of a vertically orientated cytosine molecule on the Au(111) is found to be 7.3 ± 0.3 Å by 8.7 ± 0.3 Å, resulting in the occupation of six gold atoms [11,16] consistent with the experimental results on the orientation of the molecules on the surface [5]. This adsorption geometry would "pin" the cytosine molecule to three atoms along the top rows of the [1 $\bar{1}$ 0] direction. Furthermore the distance between parallel cytosine molecules adsorbed on the top [1 $\bar{1}$ 0] atomic rows, is comparable to the separation of adjacent bases in the stacking structure observed on Au(111) [16] ~ 5.7 Å which is larger than the base stacking found in DNA, ~3.4 Å [44] but less than the ~6.8 Å separation [45] between bases when the DNA is stretched. Such an arrangement would still provide a stable structure since the π-π bonding of cytosine rows and the hydrophobic nature of the cytosine ring would act to prevent the transformation of the Au(110) surface to the more open (1×2) and (1×3) reconstructions. It is only when a significantly negative charge is applied to the surface that the π-π stacking is disrupted and this together with the electronegativity of the oxygen atom causes the cytosine molecules to be driven from the gold surface. The removal of the cytosine molecules at negative voltages should facilitate the formation of the Au(110)−(1×3) surface reconstruction on the free Au(110) surface. This suggestion predicts that the RAS profiles obtained for the cytosine on the Au(110)/liquid interface observed at -0.4 V and -0.6 V should be a sum of the Au(110) + cytosine profile obtained at 0.0 V and the Au(110) profiles at -0.4 V and -0.6 V respectively, in each case weighted by the amount of free and cytosine covered surface. The various RAS profiles obtained at -0.4 V should then obey the following expression

RAS {Au(110) + cytosine at -0.4 V} = RAS {Au(110) at -0.4 V} +
RAS {Au(110) + cytosine at 0.0 V} (4.2)

This was found to be the case and yielded the result that 63% of the Au(110) surface was free of cytosine at -0.4 V. A similar analysis showed that at -0.6 V 99% of the Au(110) surface was free of cytosine.

It has been shown that on a mercury electrode [6] and on the Au(111) surface [16] there is a phase transition between a physisorbed (planar) and chemisorbed (vertical) orientation of cytosine on the electrode surface as the potential on the electrode is changed from negative to positive. Since the RAS profile of cytosine [5], like that of adenine [40], is very sensitive to the orientation of the molecule on the surface the results of figure 4.10 (b) where shape of the RAS profile is shown to be independent of the applied voltage establishes that there is no voltage induced phase transition on this surface.

The RAS studies of Au(110) + cytosine give rise to different results to those arising from the RAS studies of Au(110) + adenine when both experience varying the electrode potentials. It is clear that at saturation and sub-saturation coverage both molecules form base stacked rows in which individual molecules are oriented vertically on the surface and with their long axis along a [1 $\bar{1}$ 0] direction. However the two molecules differ in that cytosine "freezes" the Au(110) surface when it is adsorbed at 0.0 V whereas adenine does not. These results are used to suggest that the cytosine adopts an adsorption geometry in which molecules are orientated with the long axis of the molecules along the [1 $\bar{1}$ 0] direction and with the molecule bonding through the NH_2 group, the N(3) site and possibly the O(8) site to three Au atoms at the top of the Au [1 $\bar{1}$ 0] rows as shown in figure 4.11 (a). In contrast to this work on the RAS of cytosine on Au(110) the equivalent RAS experiments of adenine did not show the same freezing of the underlying Au(110)–(1×1) surface structure [40]. This could be attributed to the relative size and charge of the cytosine being larger as well as having the three hydrogen bonding sites compared to only two in adenine. The presence of the oxygen atom in cytosine facilitates a greater attraction to the Au(110) surface. Figure 4.11 shows the different arrangements of the two bases on the (1×1) unreconstructed surface.

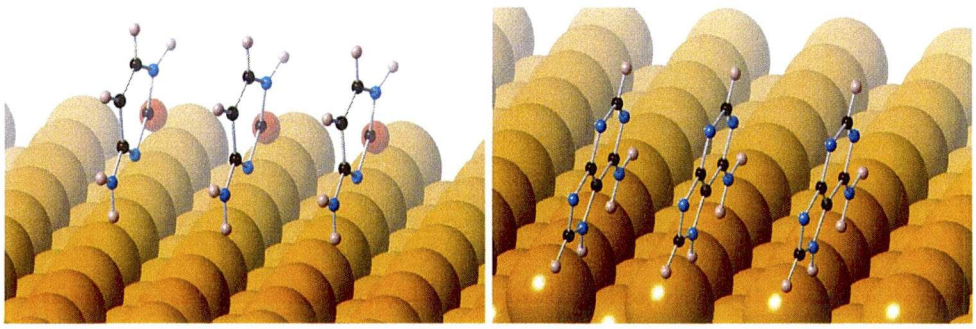

Figure 4.11: Shows the proposed stacking arrangement of cytosine (left) and adenine (right) on the Au(110) surface.

4.7 The Effect of pH on the RAS of Cytosine on Au(110)

This subsection describes the influence of pH on the RAS observed following the adsorption of cytosine onto the Au(110) surface. The Au(110) crystal was prepared as previously described and added to the electrochemical cell on three separate occasions each of which contained either a neutral solution of 0.1 M NaH_2PO_4/K_2HPO_4 (pH 7.1), an acidic solution of 0.1 M H_2SO_4 (pH 1.2) or a basic solution of 0.1 M of KOH (pH 12.8). For each experiment the final concentration of cytosine in solution was 100 μM.

The previous study [5] showed the RAS of Au(110) after the adsorption of cytosine at pH 7.1. Figure 4.12 (a) shows the RA spectra of Au(110) in each of the three pH solutions. As already described in Chapter 3, there are clear differences between the RA spectra of the Au(110) in acidic, basic and neutral pH solutions. Figure 4.12 (b) shows the RA spectra of the Au(110) + cytosine in pH 1.2 (blue line), pH 7.1 (red line) and pH 12.8 (green line). Figure 4.12 (c) shows the difference spectra obtained by subtracting the RA spectra of Au(110) in each solution from the corresponding RA spectra of Au(110) + cytosine.

There is a major difference between the RA spectra of Au(110) + cytosine in the varying pH solutions. Figure 4.12 (b) does not show the expected and previously observed cytosine shoulder between 4.0 eV and 4.5 eV when at pH 1.2. However at

pH 12.8, the shoulder on the RA spectrum is observed which suggests the cytosine molecules are ordered across the Au(110) surface.

Previous studies [15,16] show that cytosine does adsorb at acidic pH values regardless of the cytosine being protonated. The difference in results shown in this study and those described in [15,16] can be attributed to the fact that RAS can detect down to $1/200^{th}$ of a monolayer if the molecules are adsorbed in an ordered manner. Since the previous work [15,16] indicated that adsorption does occur at pH 1 then it is reasonable to conclude that the cytosine monolayer is random and therefore undetectable with RAS. There is some evidence to suggest that cytosine can form dimers on the surface, which would have transitions that would align themselves in the opposite sense thereby cancelling the effect.

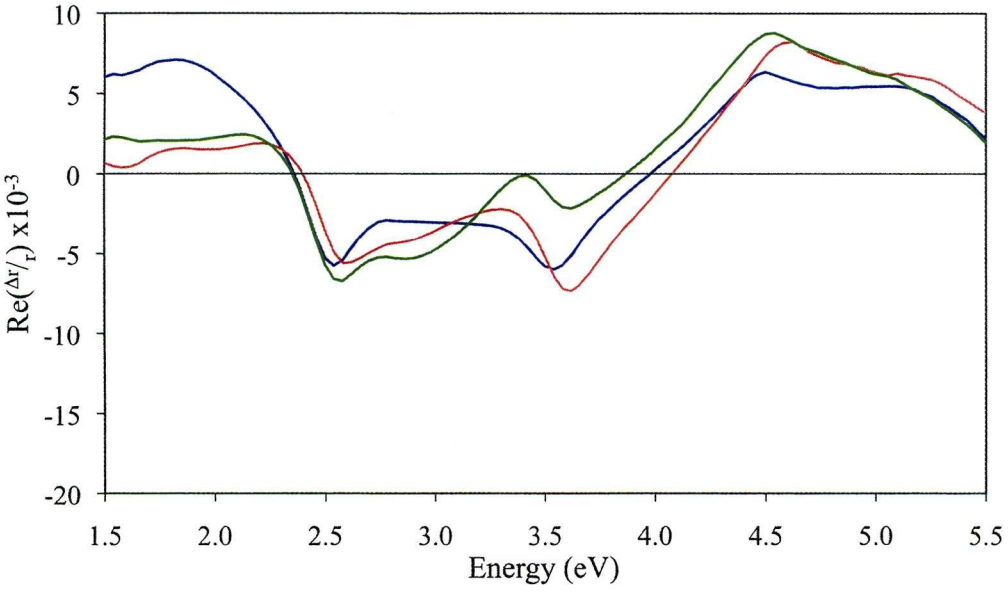

Figure 4.12 (a): The RA spectra of Au(110) in pH 1.2 (blue line), pH 7.1 (red line) and pH 12.8 (green line).

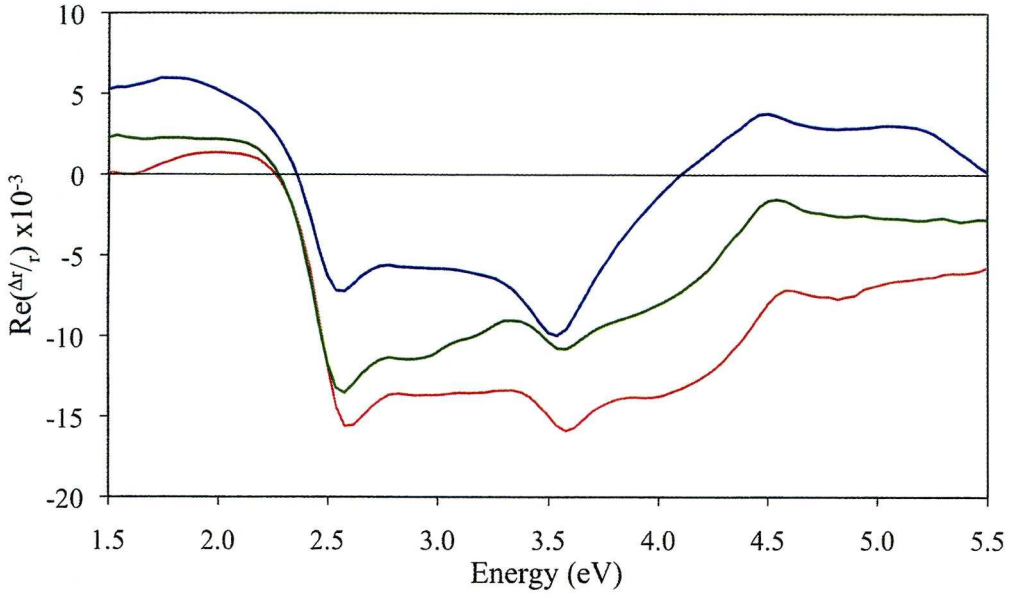

Figure 4.12 (b): The RA spectra of Au(110) + 100 μM of cytosine in pH 1.2 (blue line), pH 7.1 (red line) and pH 12.8 (green line).

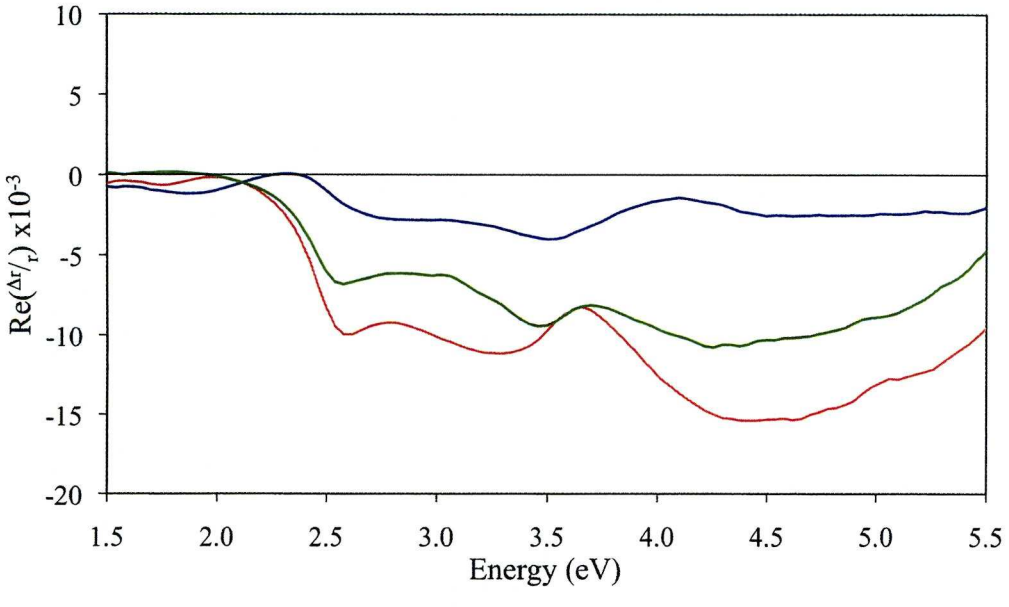

Figure 4.12 (c): The RA spectra of cytosine at pH 1.2 (blue line), pH 7.1 (red line) and pH 12.8 (green line) obtained from subtracting the RA spectra of Au(110) from the corresponding RA spectra of Au(110) + cytosine.

4.8 Theoretical Modelling of the RAS of Au(110) + Cytosine

The RA spectra of Au(110) and Au(110) + cytosine were simulated using the Lorentzian Transition Model described in Chapter 3. Figures 4.13 (a) and (b) show the RA spectra of Au(110) and Au(110) + 0.1 μM of cytosine, the smallest concentration of cytosine used, with the simulated RA spectra respectively. Figures 4.13 (c) and (d) show the RA spectra of Au(110) and Au(110) + 100 μM of cytosine, the largest concentration of cytosine used, with their simulated RA spectra respectively. Table 4.2 lists the parameters used to generate these simulations as well as the parameters used to simulate the RA spectra of Au(110) after the addition of the two intermediate concentrations, 0.5 μM and 20 μM of cytosine. The simulated RA spectra of Au(110) were generated with four transitions that are polarised along the [001] direction, 1.60 ± 0.20 eV, 3.45 ± 0.06 eV, 4.60 ± 0.07 eV and 5.64 ± 0.15 eV, and the final transition directed along the $[1\,\bar{1}\,0]$ at an energy of 3.90 ± 0.07 eV. The simulations of the RAS of Au(110) were accurate representations of the experimental data with the exception of the two extremes of the simulations (1.5 eV to 2.2 eV and 5.0 eV to 5.5 eV). The two regions difficult to simulate, 1.5 eV to 2.2 eV and 5.0 eV to 5.5 eV, are the regions where the DC component of the experiment is either climbing or falling respectively, therefore the experimental data within these regions may not give as accurate representation of the optical response of the sample due to the limitations of the apparatus. In spite of the limitations of the apparatus, the transition energies used for the simulations were relatively consistent with one and other and only slight changes were necessary for the values of FWHM, Γ, and the relative intensities, S.

The objective of the simulations is to interpret the change in RAS of the substrate after the adsorption of the molecules. As expected from subsection 4.2, there are two optical transitions that occur within the energy range of the RA spectrometer, one at 4.30 eV and the other at 5.50 eV. The adsorption of cytosine onto the Au(110) surface gives rise to an increase in intensity of the RA spectra an affect which spreads across a broad energy range of the spectrum (2.40 eV -

5.50 eV). The changes to the RA spectra of Au(110) induced by the adsorption of cytosine can successfully be simulated by the Lorentzian Transition Model with the addition of two transitions to the five existing transitions used to simulate the clean Au(110) surface; the two transitions occur at 4.30 ± 0.05 eV and 5.50 ± 0.06 eV. The previous study [5] simulated the RAS obtained after the addition of 100 μM of cytosine to the Au(110) interface and the parameters used in their simulation are comparable to those used for this simulation. This chapter reports an extension of the work by Weightman *et al* [5] by obtaining experimental and theoretical representations of sub-saturation coverage of cytosine at the Au(110)/electrolyte interface.

The results shown in table 4.2 indicate that the cytosine molecules are aligned along the $[1\,\bar{1}\,0]$ direction and that the energies of the two optical transitions used to simulate the RA spectra are consistent with those that occur in the cytosine molecule. In addition, the relative strength of the optical transition at 4.30 eV increases as the concentration of cytosine increase and the relative strength of the 5.50 eV transition, for the two highest concentrations of cytosine is much larger than those of the two lowest concentrations of cytosine adsorption.

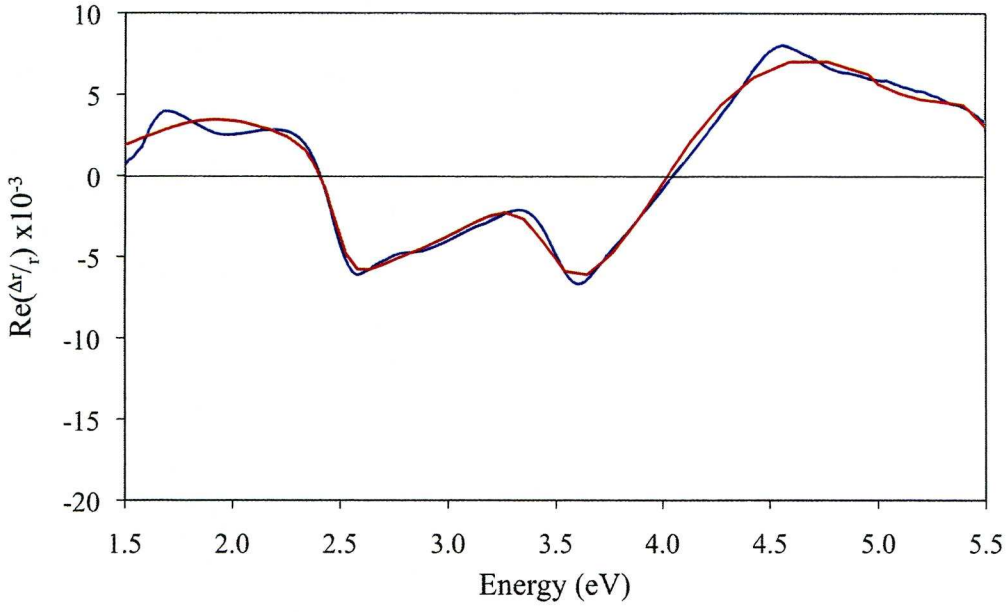

Figure 4.13 (a): The RA spectra of Au(110) in pH 7.1 before the addition of 0.1 μM of cytosine (blue line) and the corresponding simulated RA spectra (red line)

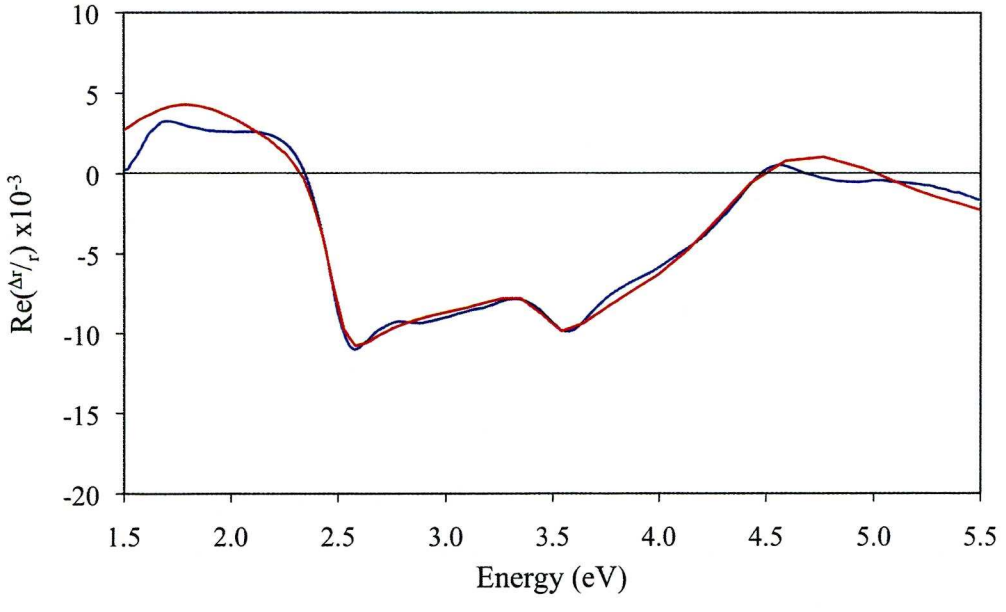

Figure 4.13 (b): The RA spectra of Au(110) in pH 7.1 after the addition of 0.1 μM of cytosine (blue line) and the corresponding simulated RA spectra (red line).

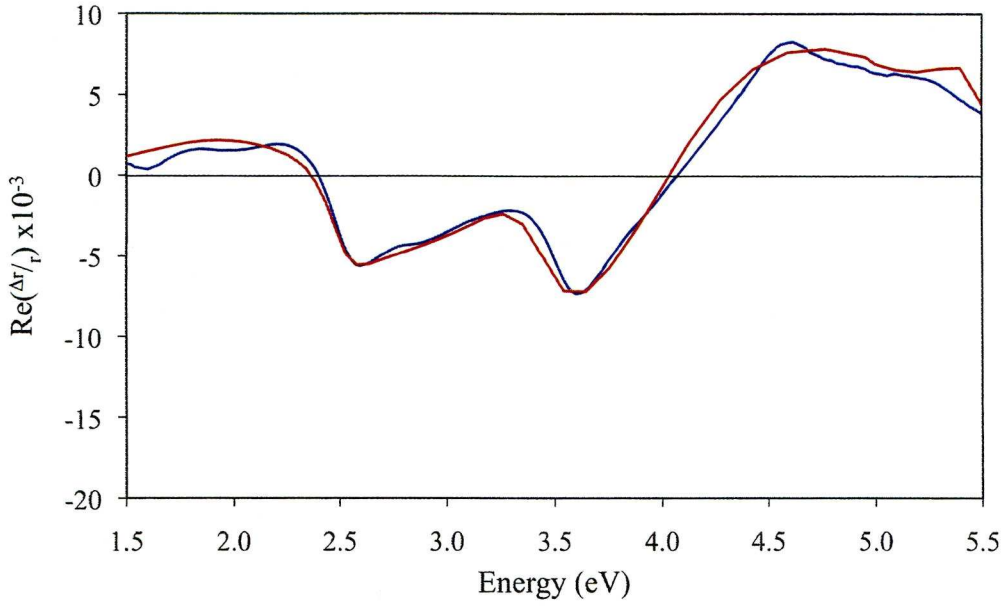

Figure 4.13 (c): The RA spectra of Au(110) in pH 7.1 before the addition of 100 μM of cytosine (blue line) and the corresponding simulated RA spectra (red line).

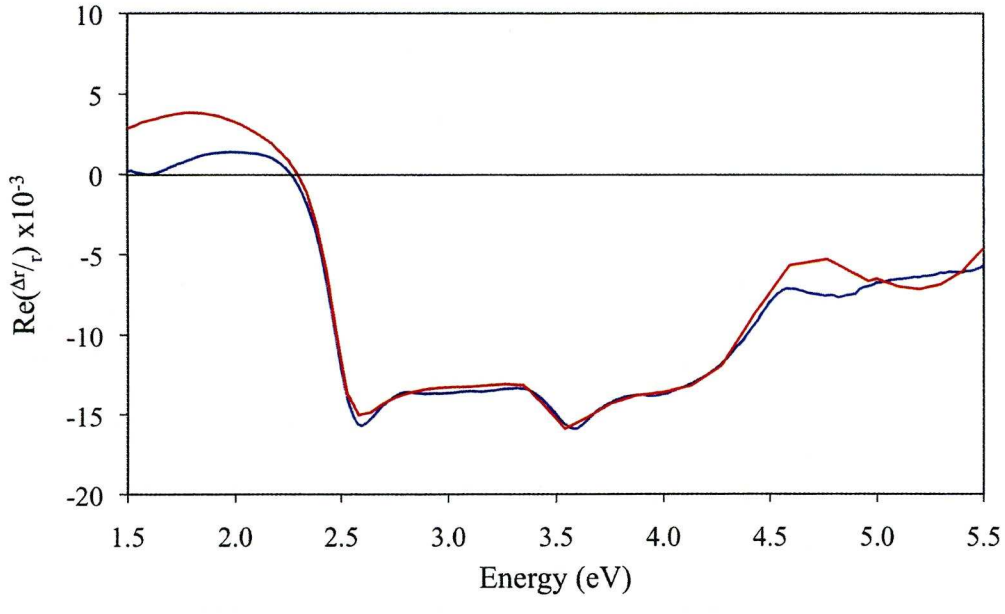

Figure 4.13 (d): The RA spectra of Au(110) in pH 7.1 after the addition of 100 μM of cytosine (blue line) and the corresponding simulated RA spectra (red line).

Table 4.2: The parameters for the simulated RA spectra of Au and Au + cytosine.

0.1 μM	Transition	1	2	3	4	5	6	7
	Direction	[001]	[001]	[1 $\bar{1}$ 0]	[001]	[001]	[1 $\bar{1}$ 0]	[1 $\bar{1}$ 0]
Au	ω_t/eV	1.60 ± 0.20	3.45 ± 0.06	3.90 ± 0.07	4.60 ± 0.07	5.64 ± 0.15	…	…
	Γ/eV	1.10 ± 0.20	0.62 ± 0.13	1.92 ± 0.15	2.11 ± 0.15	0.54 ± 0.07	…	…
	S^a	1.00 ± 0.10	0.27 ± 0.03	1.66 ± 0.08	1.36 ± 0.13	0.15 ± 0.01	…	…
Au / C	ω_t/eV	1.60 ± 0.10	3.45 ± 0.07	3.90 ± 0.15	4.75 ± 1.00	5.60 ± 1.00	4.30 ± 0.05	5.50 ± 0.06
	Γ/eV	0.80 ± 0.25	0.38 ± 0.05	2.00 ± 0.20	2.00 ± 0.30	0.70 ± 0.30	0.70 ± 0.10	2.00 ± 0.06
	S^b	1.00 ± 0.10	0.06 ± 0.01	0.80 ± 0.07	0.51 ± 0.02	0.02 ± 0.01	0.09 ± 0.01	0.18 ± 0.04

[a,b]Relative intensities. Absolute intensities of transition 1 are 6000 (Au), 6900 (Au/C).

0.5 μM	Transition	1	2	3	4	5	6	7
	Direction	[001]	[001]	[1 $\bar{1}$ 0]	[001]	[001]	[1 $\bar{1}$ 0]	[1 $\bar{1}$ 0]
Au	ω_t/eV	1.60 ± 0.20	3.40 ± 0.06	3.90 ± 0.08	4.60 ± 0.07	5.64 ± 0.14	…	…
	Γ/eV	1.10 ± 0.20	0.58 ± 0.08	1.90 ± 0.15	2.11 ± 0.15	0.54 ± 0.08	…	…
	S^a	1.00 ± 0.11	0.24 ± 0.03	1.65 ± 0.09	1.37 ± 0.14	0.11 ± 0.02	…	…
Au / C	ω_t/eV	1.50 ± 0.10	3.41 ± 0.07	3.90 ± 0.12	4.80 ± 0.70	5.60 ± 1.00	4.25 ± 0.04	5.50 ± 0.06
	Γ/eV	1.00 ± 0.20	0.43 ± 0.08	2.00 ± 0.30	2.00 ± 0.30	0.70 ± 0.40	2.20 ± 0.07	1.00 ± 0.06
	S^b	1.00 ± 0.10	0.06 ± 0.01	0.90 ± 0.08	0.34 ± 0.03	0.01 ± 0.05	0.18 ± 0.01	0.07 ± 0.04

[a,b]Relative intensities. Absolute intensities of transition 1 are 6000 (Au), 7250 (Au/C).

20 µM	Transition	1	2	3	4	5	6	7
	Direction	[001]	[001]	[1 $\bar{1}$ 0]	[001]	[001]	[1 $\bar{1}$ 0]	[1 $\bar{1}$ 0]
Au	ω_t/eV	1.55 ± 0.10	3.45 ± 0.05	3.95 ± 0.06	4.59 ± 0.06	5.60 ± 0.15	...	...
	Γ/eV	1.10 ± 0.20	0.60 ± 0.09	1.92 ± 0.15	2.20 ± 0.15	0.40 ± 0.07	...	...
	S[a]	1.00 ± 0.12	0.24 ± 0.03	1.57 ± 0.07	1.46 ± 0.13	0.09 ± 0.02	...	...
Au / C	ω_t/eV	1.55 ± 0.10	3.45 ± 0.10	3.90 ± 0.20	4.65 ± 1.00	5.60 ± 1.00	4.38 ± 0.04	5.50 ± 0.05
	Γ/eV	0.65 ± 0.20	0.40 ± 0.12	1.80 ± 0.40	2.00 ± 0.40	0.70 ± 0.40	0.60 ± 0.10	2.00 ± 0.10
	S[b]	1.00 ± 0.10	0.04 ± 0.01	0.76 ± 0.06	0.71 ± 0.02	0.03 ± 0.07	0.22 ± 0.02	1.10 ± 0.09

[a,b]Relative intensities. Absolute intensities of transition 1 are 5800 (Au), 5900 (Au/C).

100 µM	Transition	1	2	3	4	5	6	7
	Direction	[001]	[001]	[1 $\bar{1}$ 0]	[001]	[001]	[1 $\bar{1}$ 0]	[1 $\bar{1}$ 0]
Au	ω_t/eV	1.60 ± 0.09	3.44 ± 0.06	3.92 ± 0.07	4.60 ± 0.05	5.56 ± 0.15	...	...
	Γ/eV	1.25 ± 0.20	0.55 ± 0.09	1.85 ± 0.15	1.90 ± 0.15	0.40 ± 0.09	...	...
	S[a]	1.00 ± 0.08	0.27 ± 0.02	1.78 ± 0.10	1.27 ± 0.11	0.11 ± 0.02	...	...
Au / C	ω_t/eV	1.60 ± 0.15	3.45 ± 0.10	3.90 ± 0.20	4.65 ± 1.00	5.60 ± 1.00	4.38 ± 0.04	5.50 ± 0.10
	Γ/eV	0.80 ± 0.30	0.35 ± 0.15	2.05 ± 0.40	2.00 ± 0.40	0.70 ± 0.40	0.75 ± 0.07	1.70 ± 0.10
	S[b]	1.00 ± 0.11	0.06 ± 0.01	1.30 ± 0.09	0.50 ± 0.01	0.04 ± 0.05	0.28 ± 0.04	1.09 ± 0.04

[a,b]Relative intensities. Absolute intensities of transition 1 are 5500 (Au), 5500 (Au/C)

4.9 Conclusions

This chapter shows that as the concentration of the cytosine solution added to the electrochemical cell increases, the affect on the RA spectrum of Au(110) increases and that saturation of the exposed Au(110) surface occurs with the addition of the maximum concentration of cytosine, 100 μM. At the lower concentrations of cytosine, the surface of the sample consisted of regions of clean Au(110) and regions covered with aligned cytosine molecules. Simulations of the sub-saturation coverage were generated by the linear summations of the clean Au(110) RA spectrum and the RA spectrum of Au(110) + 100 μM of cytosine.

The application of ADRAS establishes that the optical axes of cytosine and CMP, at the Au(110)/electrolyte interface, are in alignment with the principal axes of the Au(110) substrate irrespective of whether there is saturation coverage of cytosine or sub-saturation coverage. In addition the results indicate that the cytosine molecule adsorbs to the Au(110) surface via the bonding sites located between the NH_2, N(3) and O sections of the molecule and that the adsorption of cytosine prevents the reconstruction of the Au(110) substrate, an effect which is not observed after the adsorption of adenine.

As a final point, experiments at variable pH were used to show that cytosine adsorbs at the Au(110)/electrolyte interface at 0.0 V when in either a neutral (pH 7.1) or basic (pH 12.8) solution but does not adsorb under acidic (pH 1.2) solutions.

4.10 References

[1] K. Tanaka, A. Tengeiji, T. Kato, N. Toyama and M. Shionoya, *Science* **299**, 1212 (2003)

[2] S.J. Sowerby, P.A. Stockwell, W.M. Heckl and G.B. Peterson, *Orig. Life Evol. Biosph.* **30,** 81 (2000)

[3] E. Southern, K. Mir and M. Shchepinov, *Nature Genet.* **21**, 5 (1999)

[4] Z. Guo, R. A. Guilfoyle, A. J. Thiel, R. Wang and L. M Smith, *Nucl. Acids Res.* **22**, 5456 (1994)

[5] P. Weightman, G. J. Dolan, C. I. Smith, M. C. Cuquerella, N. J. Almond, T. Farrell, D. G. Fernig, C. Edwards and D. S. Martin, *Phys. Rev. Lett.* **96**, 086102 (2006)

[6] V. Vetterl and J. Pokorny, *J. Electroanal. Chem.* **116**, 517 (1980)

[7] U. Retter, *J. Electroanal. Chem.* **106**, 371 (1980)

[8] A. M. O. Brett and F-M. Matysik, *J. Electroanal. Chem.* **429**, 95 (1997)

[9] S. Xu, M. Dong, E. Rauls, R. Otero, T. R. Linderoth and F. Besenbacher, *Nano Lett.* **6**, 1434 (2006)

[10] N. J. Tao, J. A. DeRose and S. M. Lindsay, *J. Phys. Chem.* **97**, 910 (1993)

[11] T. Boland and B. D. Ratner, *Langmuir* **10**, 3845 (1994)

[12] M. Furukawa, H. Fujisawa, S. Katano, H. Ogasawara, Y. Kim, T. Komeda, A. Nilsson and M. Kawai, *Surf. Sci.* **532-535**, 261 (2003)

[13] E. Koglin, J-M. Séquaris and P. Valenta, *J. Mol. Struct*, **79**, 185 (1982)

[14] T. Watanbe, O. Kawanami, H. Katoh and K. Honda, *Surf. Sci.* **158**, 341 (1985)

[15] K. Ataka and M. Osawa, *J. Electroanal. Chem.* **460**, 188 (1999)

[16] Th. Wandlowski, D. Lamper and S. M. Lindsay, *J. Electroanal. Chem.* **404**, 215 (1996)

[17] M. Östblom, B. Lindberg, L. M. Demers and C. A. Mirkin, *J. Phys. Chem. B* **109,** 15150 (2005)

[18] E. Koglin, H. H. Lewinsky and J. M. Séquaris, *Surf. Sci.* **158**, 370 (1985)

[19] K. Takamura, A. Mori and F. Watanabe, *Bioelectrochem. Bioenerg.* **8**, 125 (1981)

[20] D. J. Frankel, Q. Chen and N. V. Richardson, *J. Chem. Phys.* **124**, 204704 (2006)

[21] P. R. Callis, *Ann. Rev. Phys. Chem.* **34**, 329 (1983)

[22] M. P. Fülscher and B. O. Roos, *J. Am. Chem. Soc.* **117**, 2089 (1995)

[23] W. Hug and I. Tinoco Jnr., *J. Am. Chem. Soc.* **96**, 665 (1974)

[24] M. Preuss, W. G. Schmidt, K. Seino, J. Furthmüller and F. Bechstedt, *J. Comput. Chem.* **25**, 112 (2004)

[25] H. DeVoe and I. Tinoco, Jnr., *J. Mol. Biol.* **4**, 500 (1962)

[26] F. Žaloudek, J. S. Novros and L. B. Clark, *J. Am. Chem. Soc.* **107**, 7344 (1984)

[27] V. Mazine, Y. Borensztein, L. Cagon and P. Allongue, *Phys. Status Solidi A* **175**, 311 (1999)

[28] B. Sheridan, D. S. Martin, J. R. Power, S. D. Barrett, C. I. Smith, C. A. Lucas, R. J. Nichols and P. Weightman, *Phys. Rev. Lett.* **85,** 04618 (2000)

[29] V. Mazine and Y. Borensztein, *Phys. Rev. Lett.* **88**, 147403 (2002)

[30] P. Weightman, C. I. Smith, D. S. Martin, C. A. Lucas, R. J. Nichols and S. D. Barrett, *Phys. Rev. Lett.* **92**, 199707 (2004)

[31] C. I. Smith, N. J. Almond and P. Weightman, *J. Electrochemical Soc.* **154**, F90 (2007)

[32] C. I. Smith, A. Bowfield, N. J. Almond, C. P. Mansley, J. H. Convery and P. Weightman, *manuscript in preparation*

[33] A. Bowfield, C. I. Smith, G. J. Dolan, M. C. Cuquerella, C. P. Mansley and P. Weightman, *e-J. Surf. Sci. Nanotech.* **7**, 225 (2009)

[34] P. Weightman, D. S. Martin, R. J. Cole and T. Farrell, *Rep. Prog. Sci.* **68**, 1251 (2005)

[35] R. J. Cole and B. F. Macdonald, *Appl. Phys. Lett.* **80**, 3527 (2002)

[36] B. F. Macdonald, J. S. Law and R. J. Cole, *J. Appl. Phys.* **93**, 3320 (2002)

[37] C. P. Mansley, C. I. Smith, M. C. Cuquerella, T. Farrell, D. G. Fernig, C. Edwards and P. Weightman, *Phys. Status Solidi C* **5**, 2582 (2008)

[38] M. C. Cuquerella, C. I. Smith, D. G. Fernig, C. Edwards and P. Weightman, *Langmuir* **23**, 2078 (2007)

[39] R. LeParc, C. I. Smith, M. C. Cuquerella, R. L. Williams, D. G. Fernig, C. Edwards, D. S. Martin and P. Weightman, *Langmuir* **22**, 3413 (2006)

[40] C. I. Smith, A. Bowfield, G. J. Dolan, M. C. Cuquerella, C. P. Mansley, D. G. Fernig, C. Edwards and P. Weightman, *J. Chem. Phys.* **130**, 044702 (2009)

[41] A. Hermann, W. G. Schmidt, and F. Bechstedt, *J. Phys. Chem. B* **109**, 7928 (2005)

[42] A. Hermann, W. G. Schmidt, and F. Bechstedt, *Phys. Rev. B* **71**, 153311 (2005)

[43] P. D. Lane, G. E. Isted, D. S. Roseburgh and R. J. Cole, *Appl. Phys. Lett.* **95**, 141907 (2009)

[44] J. D. Watson and F. H. C. Crick, *Nature* **171**, 737 (1953)

[45] G. L. Zubay in Biochemistry (Wm. C. Brown Publishers, Dubuque, IA, 1998) Page 743

[46] B. G. Frederick, J. R. Power, R. J. Cole, C. C. Perry, Q. Chen, S. Haq, Th. Bertrams, N. V. Richardson and P. Weightman, *Phys. Rev. Lett.* **80**, 4490 (1998)

Chapter 5

The Detection of DNA Adsorbed at the Au(110)/Electrolyte Interface

RAS has the sensitivity necessary to observe the adsorption of $1/200^{th}$ of a monolayer onto an Au(110) substrate. With the successful studies into the behaviour of two of the nucleic bases (adenine and cytosine) and their corresponding monophosphates (AMP and CMP), this chapter takes the study one step further in the form of determining the RA spectra of ss-DNA and ds-DNA at the Au(110)/electrolyte interface.

5.1 Introduction

The applications of nucleic acid interactions have been revolutionized by the development of high-throughput techniques that exploit DNA arrays. Understanding these interactions is important for the development of more sensitive techniques for identifying unknown DNA sequences and monitoring gene expression. Optical techniques for probing nucleic acid interactions are particularly attractive since they have the potential to monitor biomolecules in a liquid environment.

DNA adsorption onto different surfaces has been extensively studied by a variety of techniques, including *in-situ* STM [1], AFM [2], SPR [3], SERS [4] and the quartz crystal microbalance (QCM) [5]. However, there have been few studies of adsorption onto Au surfaces without the use of thiolation at the 5′-position [6] as this is the preferred method of attachment for gene therapy applications. The concept of thiolation is discussed in section 5.3. RAS may provide a fast, cheap, sensitive and direct method for monitoring how biomolecules such as DNA, RNA and proteins behave on surfaces.

A previous study [7] established that both ss-DNA and ds-DNA form ordered structures at the Au(110)/electrolyte interface and that the two types of DNA were distinguishable with the use of RAS. This chapter is an extension of the work by Cuquerella *et al* [7] and reports the self assembled ordering of ss and ds calf thymus DNA at the Au(110)/liquid interface.

5.2 The Structure of DNA

Crick and Watson established the structure of DNA in 1953 [8]. They found that DNA had the form of a double helix. Subsequently it has been shown that there are three structural forms of DNA, the *A*, *B* and *Z* forms as shown in figure 5.1. All of these forms consist of phosphate sugar backbones that are hydrogen bonded internally by four types of nitrogenous base; adenine (A), thymine (T), guanine (G) and cytosine (C). The individual structure of the bases restricts the base pair bonding to A-T and C-G due to the number of available hydrogen bonding sites on each

base. A and T share two hydrogen bonds whereas C and G share three. Adenine and guanine are known as purines which are compounds made up of a five and a six membered ring. Cytosine and thymine are classed as pyrimidines and consist of a six membered ring.

The *B* form of DNA is the most common and consists of a double helix and has a major grove and a minor grove. The distance separating neighbouring base pairs in the *B* form of DNA is 3.4 Å and it takes ten base pairs to form one full turn of the helix, which equates to 34 Å [9]. The A form of DNA is wider and shorter than the *B* form and can be formed from the *B* form when in low water concentrations. The *A* form requires a smaller distance to make a complete full turn, 23 Å, but its greater width means that this consists of eleven base pairs. The final form of DNA is the *Z* form, a name chosen due to the zigzag nature of the phosphate backbone as opposed to the smoother phosphate backbones exhibited by the *A* and *B* forms. The *Z* form is left handed and its helix turns in the opposite direction to the right handed *A* and *B* forms of DNA. It takes 46 Å to complete one full turn, taking twelve base pairs to do so. The *Z* form of DNA occurs most commonly in environments of high salt concentration [9].

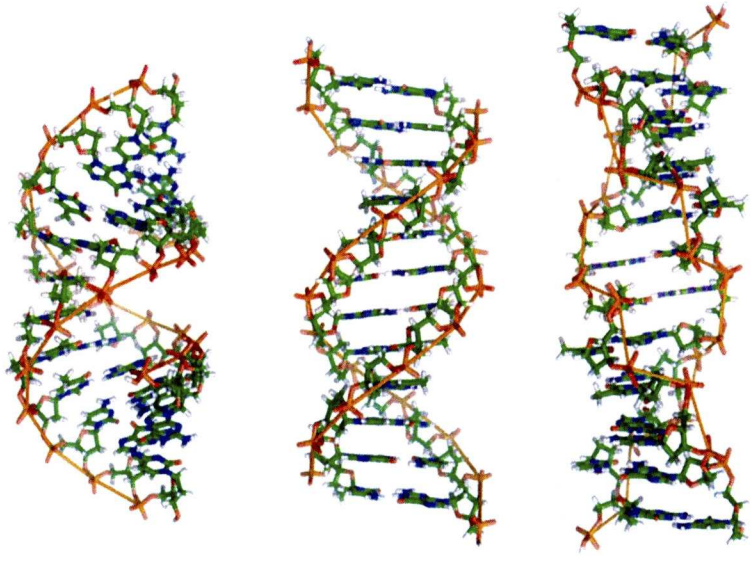

Figure 5.1: The three structural forms of DNA, *A* form (left), *B* form (centre) and the *Z* form (right). Taken from [10].

This chapter reports the adsorption of ds-DNA and ss-DNA on Au(110). The difference between the ds-DNA and the ss-DNA is as the names suggest. The ss-DNA consists of one phosphate backbone with the bases exposed to external environments; the ds-DNA has the complementary strand as well and therefore creates the double helix structure and the internal base pairing which is shielded from external environments.

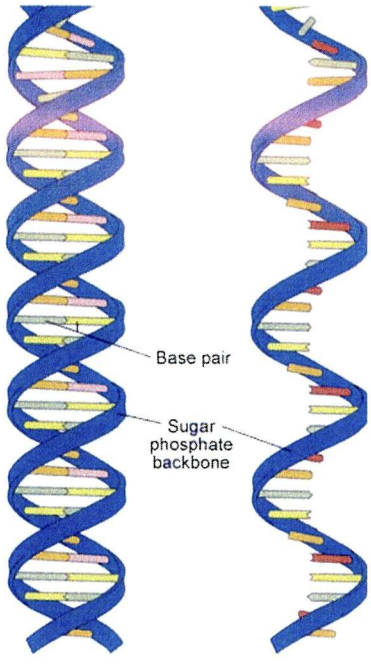

Figure 5.2: The structural differences between ds-DNA (left) and ss-DNA (right). Adapted from [11].

Ribonucleic acid (RNA) is very similar to ss-DNA but there are structural differences that need to be described for clarity. RNA is made up of the nitrogenous bases, ribose sugars and phosphate groups, but DNA is made up of nitrogenous bases, deoxyribose sugars and the phosphate groups. The deoxyribose sugar has one less oxygen in comparison to the ribose sugar. The other difference between RNA and ss-DNA is that RNA contains the nitrogenous base uracil as opposed to thymine in DNA. Uracil contains one less methyl group than thymine. The reason for using ss-DNA for the experiments reported in this thesis and not RNA is that of direct comparison. The changes in the RA response of ss-DNA and ds-DNA on the

Au(110) surface can be attributed to the structure and orientation of the molecules alone. If the RA response of ds-DNA were to be compared with that of RNA then any changes could be attributed to structure, orientation and the change in components between the two molecules.

5.3 DNA-Substrate Bonding

Many techniques used in the study of DNA require the DNA to be attached to substrates. As mentioned previously, thiolated DNA is a common method of attaching DNA to substrates. Thiolated DNA contains a sulfur atom, which readily forms a bond with an Au substrate, or a cross linking molecule [12]. 11-mercaptoundecylamine (MUAM) is a form of cross linking molecule which can be used to attach DNA to Au. One end of MUAM is thiolated (contains a sulphur group) and bonds to Au whereas the other end has an amine group (NH_2) which is free to react with other molecules [13]. Lee *et al* [14] use malemide ethyl glycol (MEG) terminated disulphide to cross link between Au coated glass slides and thiolated DNA. Lee *et al* [15] have also used 11-mercapto-1-undecanol (MCU) as a cross linking molecule between thiolated ss-DNA and Si wafers coated with Cr and then Au. Si wafers coated in Au have also been used as substrates for DNA [16-17]. Other substrates can also be used to attach DNA [18-22]. Si(100) wafers have also been used for directly attaching DNA [18] but the DNA film was found to removable under high salt concentrations. H-terminated Si could be chemically treated under UV light to produce an amine terminated Si surface that can react with thiolated DNA [19]. Amine and thiolated DNA can also be attached to aminosilane when using 1,4-phenylene diisothiocyanate (PDC) [20] and a more recent study by Smith *et al* [21] has shown that DNA hybridisation can be detected when DNA is attached to functionalised diamond surfaces.

5.4 Detection of DNA on Au(110)

The experiments reported in this chapter employed an Au(110) crystal with solutions made from NaH_2PO_4 and K_2HPO_4 (BDH, Analar grade) and calf thymus DNA (Sigma-Aldrich) without further purification in Millipore ultra-pure water (18 MΩcm) and made oxygen-free by purging with argon prior to use.

The experimental conditions of this study have one significant difference to the previous work [7] where that experiment was undertaken with an applied potential of 0.0 V vs SCE. In the work reported in this chapter there was no potential control and the Au(110) is at the open circuit potential (OCP) which is +0.1 V in this solution. This change in experimental procedure was due to the orientation of the RA spectrometer being altered. In the previous study [7], the Au(110) sample was positioned vertically in order to provide potential control, as shown in chapter 2. In this experiment the Au(110) sample was positioned horizontally with the RA spectrometer rotated through 90°. This change in orientation was to improve the ADRAS experiments of DNA on Au(110) and give a more accurate description of the orientation of DNA on Au(110). The Au(110) crystal was prepared in the usual way by flame annealing but instead of being inserted into the electrochemical cell, it was placed into a glass Petri dish that had been cleaned in an acid bath. Since these experiments, a new horizontally orientated electrochemical cell is being made so that potential controlled ADRAS experiments can be conducted.

Figure 5.3 shows the UV-visible (UV-VIS) adsorption spectrum of a 15 μg/ml solution of ds-calf thymus DNA showing the characteristic absorbance peak, λ_{max} of DNA at 260 nm (4.78 eV) [22]. The purpose of this experiment was to confirm that there was an optical transition in the DNA that could be detected in the region of the RA spectrometer.

Figure 5.4 (a) shows the RA spectra of Au(110), Au(110) + ds-DNA and ds-DNA. The latter is obtained by subtracting the RAS of the Au(110) from the RAS of the Au(110) + ds-DNA. Figure 5.4 (b) shows the RA spectra of Au(110), Au(110) + ss-DNA and ss-DNA obtained similarly to that of the ds-DNA. In the first

experiment 15 μg/ml of ds calf thymus DNA was added to the solution but only 2.16 μg/ml ss calf thymus DNA was added to the solution in the second experiment.

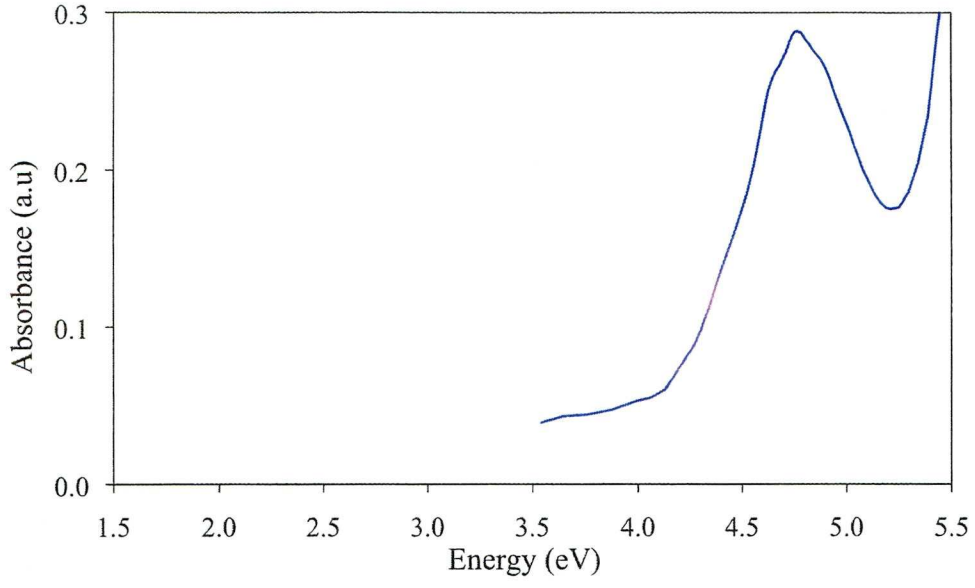

Figure 5.3: The UV-VIS spectrum of a 15 μg/ml solution of ds-calf thymus DNA in 0.1 M NaH_2PO_4/K_2HPO_4.

The RA spectra of the Au(110) surface for both experiments are similar to those published previously [23-26]. As in the previous work [7] the addition of DNA gives rise to a general increase in the RAS amplitude from about 2.5 eV onwards and the DNA transition which is expected at 4.78 eV interferes destructively with the Au spectrum in this region thereby masking the step signal. Also as previous work [7] showed, the addition of ss-DNA leads to a larger increase in the RAS than the addition of ds-DNA.

The observation of RA spectra for both the ss-DNA and ds-DNA show the presence of a monolayer upon the Au(110) surface in accordance with previous work [7] where the spectra were attributed to ss-DNA adsorbing via the bases but the ds-DNA having to attach via the phosphate backbone due to its helical structure and charge.

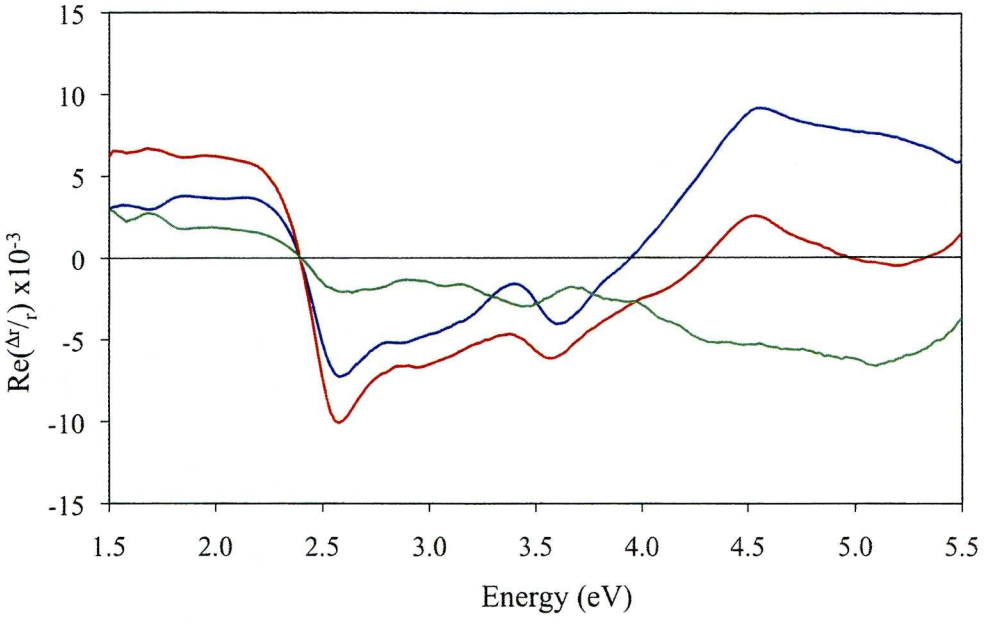

Figure 5.4 (a): RA spectra of Au(110) (blue line), Au(110) + ds-DNA (red line) and ds-DNA obtained by subtracting the RAS of Au(110) from the RAS of Au(110) + ds-DNA (green line), all in 0.1 M NaH_2PO_4/K_2HPO_4.

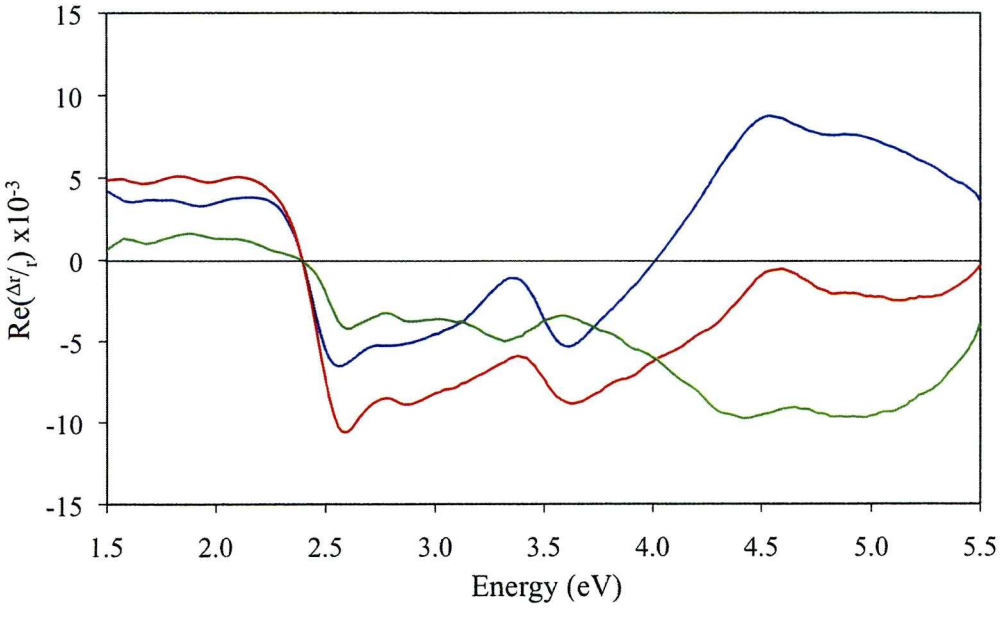

Figure 5.4 (b): RA spectra of Au(110) (blue line), Au(110) + ss-DNA (red line) and ss-DNA obtained by subtracting the RAS of Au(110) from the RAS of Au(110) + ss-DNA (green line), all in 0.1 M NaH_2PO_4/K_2HPO_4.

5.5 ADRAS of DNA on Au(110)

If the optical response of a molecule arises from a number of well-defined dipole transitions and if the orientation of these transitions with respect to the molecular axes is known then RAS can yield information on the orientation of the molecule with respect to the surface. In favourable circumstances an analysis of the RAS profile can be used to determine the three dimensional orientation of a molecule adsorbed at a surface as shown in the recent study of cytosine and cytidine 5′- monophosphate [27] adsorbed at the Au(110)/electrolyte interface.

In two separate experiments the Au(110) sample was prepared in the usual way, placed in a Petri dish and put into the RA spectrometer. The cell was then rotated through 180° with respect to the axis of the incident light and the spectra recorded at 10° intervals. Calf thymus solutions (15 μg/ml of ds calf thymus DNA and 2.16 μg/ml ss calf thymus DNA, for the first and second experiments respectively) were then added to the cell and left overnight to incubate and then the RAS was recorded at the same orientations of the cell as measured for the Au(110).

The optical axes of the Au(110) surface are along the [001] and [1 $\bar{1}$ 0] directions and the amplitude of the RAS across the whole wavelength range is expected to follow a cos 2θ dependence [27,28]. This relationship was obeyed by the RAS of the Au(110)/electrolyte interfaces obtained before the addition of the ds-DNA and ss-DNA as shown in figure 5.5 (a) and (b) respectively. Only the spectra obtained for values of θ of 0°, 45° and 90° are shown in the figures for clarity purposes. The slight deviations from zero for the RAS obtained at θ = 45° at some wavelengths is probably due to small systematic errors in determining the precise value of the origin for θ.

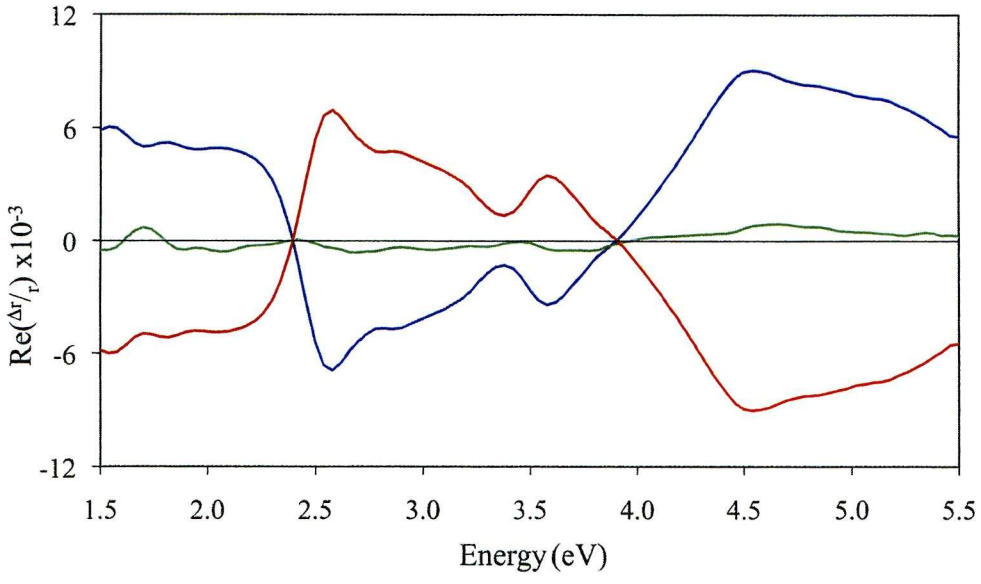

Figure 5.5 (a): The RA spectra of Au(110) in 0.1 M NaH_2PO_4/K_2HPO_4 at 0° (blue line), 45° (green line) and 90° (red line), before the addition of ds-DNA.

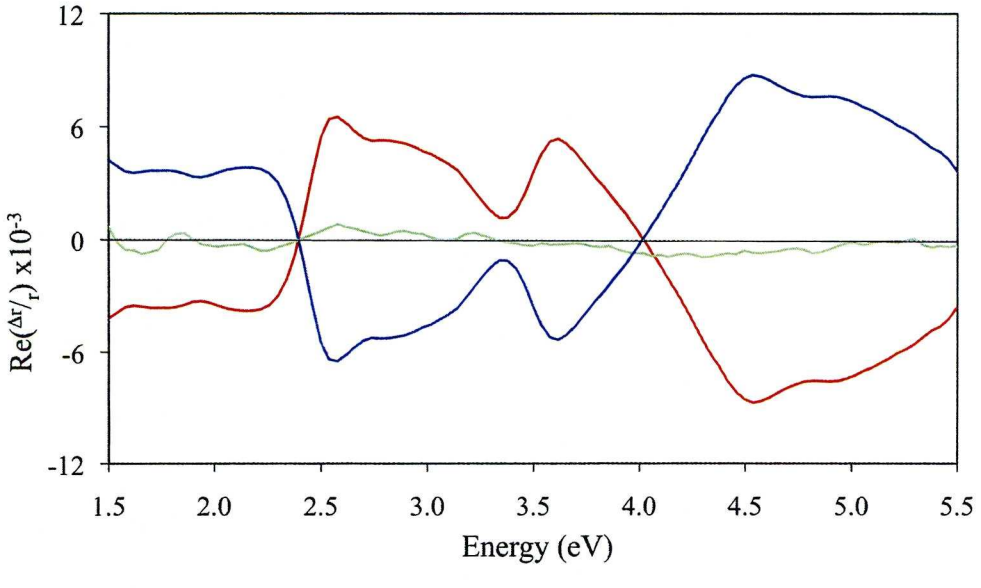

Figure 5.5 (b): The RA spectra of Au(110) in 0.1 M NaH_2PO_4/K_2HPO_4 at 0° (blue line), 45° (green line) and 90° (red line), before the addition of ss-DNA.

Figure 5.6 (a) shows the RA spectra of Au(110) + ds-DNA in 0.1 M NaH_2PO_4/K_2HPO_4 and figure 5.6 (b) shows the RA spectra of ds-DNA in 0.1 M NaH_2PO_4/K_2HPO_4 obtained from the subtraction of the RA spectra of Au(110) from the corresponding RA spectra of Au(110) + ds-DNA. The results obtained for values of θ of 0° and 90° are very similar to those obtained previously [7], showing that the adsorption of ds-DNA and ss-DNA can be distinguished as there are clear differences between the two sets of data. The RAS intensity at ~ 4.7 eV, resulting from the optical response of the DNA, is much larger from the ss-DNA (figure 5.7 (a)) in comparison to the ds-DNA (figure 5.6 (a)) The new information in figures 5.6 (a) and (b) is the observation that at $\theta = 45°$ the RAS of ds-DNA self-assembled at the Au(110)/liquid interface is essentially zero across the whole spectral range.

Figures 5.7 (a) and 5.7 (b) show the RA spectra of Au(110) + ss-DNA in 0.1 M NaH_2PO_4/K_2HPO_4 and the RA spectra of ss-DNA in 0.1 M NaH_2PO_4/K_2HPO_4 respectively. Again the results obtained for values of θ of 0° and 90° are alike to those reported in the previous study [7], with clear differences between the RA spectra of ds-DNA and the RA spectra of ss-DNA. Figures 5.7 (a) and (b) show that the RAS from ss-DNA experiment is approximately double that of the ds-DNA experiment. As with the ds-DNA, at $\theta = 45°$, the RAS of the ss-DNA self-assembled at the Au(110)/electrolyte interface is close to zero across the whole spectral range.

The observation of a strong RAS profile from a molecule adsorbed at a surface proves that the molecule adopts an ordered and anisotropic arrangement at the surface. Figures 5.6 (a) and 5.7 (a) show that at an angle of 45° for both the ss-DNA and ds-DNA adsorbed at the Au(110) surface, the RAS goes to zero across the entire spectral range. This result establishes that the optical axes of the molecules are in alignment with the optical axes of the Au(110) surface.

Figure 5.8 (a) and (b) show the angular variation of the 4.7 eV peak intensity as the sample is rotated through 180° for the Au(110) with the addition of ds-DNA and ss-DNA respectively. The angular variation of the ds-DNA (figure 5.8 (a)) and ss-DNA (figure 5.8 (b)) follow the accepted dependence on cos 2θ.

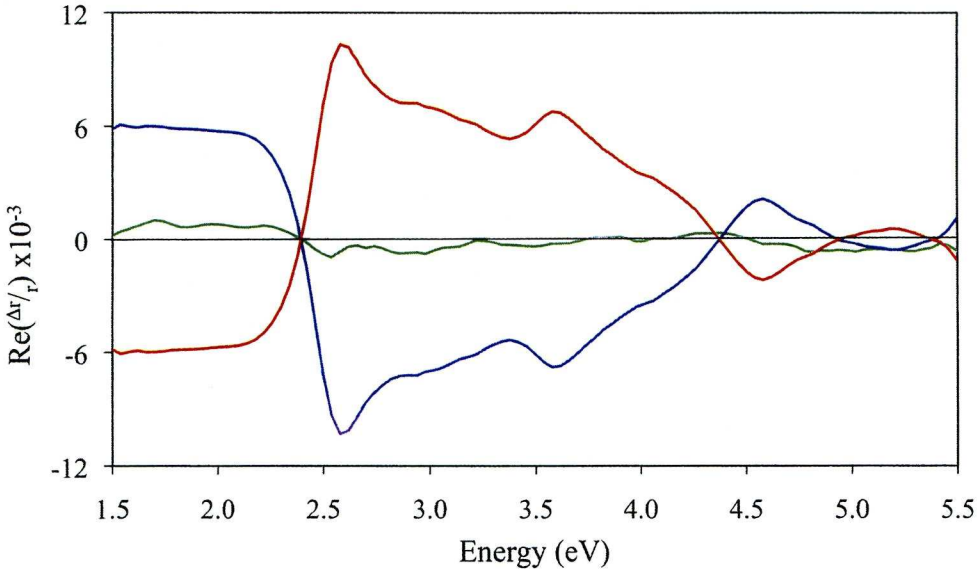

Figure 5.6 (a): The RA spectra of Au(110) + ds-DNA in 0.1 M NaH_2PO_4/K_2HPO_4 at 0° (blue line), 45° (green line) and 90° (red line).

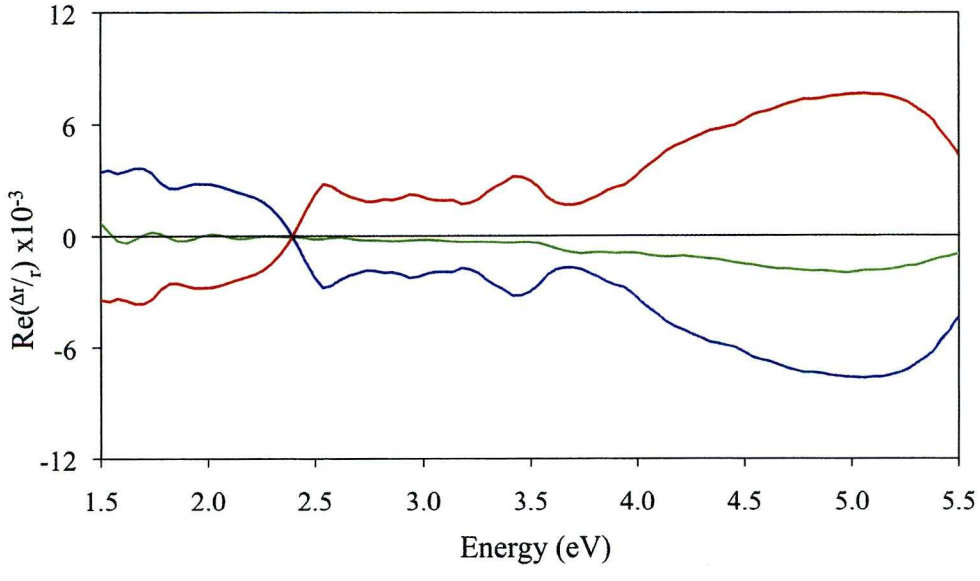

Figure 5.6 (b): The RA spectra ds-DNA in 0.1 M NaH_2PO_4/K_2HPO_4 at 0° (blue line), 45° (green line) and 90° (red line).

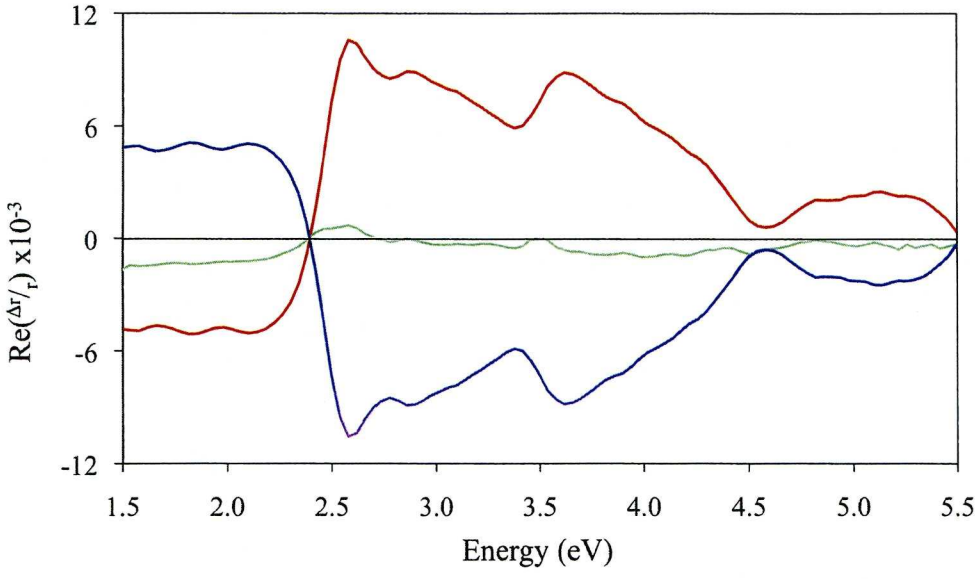

Figure 5.7 (a): The RA spectra of Au(110) + ss-DNA in 0.1 M NaH_2PO_4/K_2HPO_4 at 0° (blue line), 45° (green line) and 90° (red line).

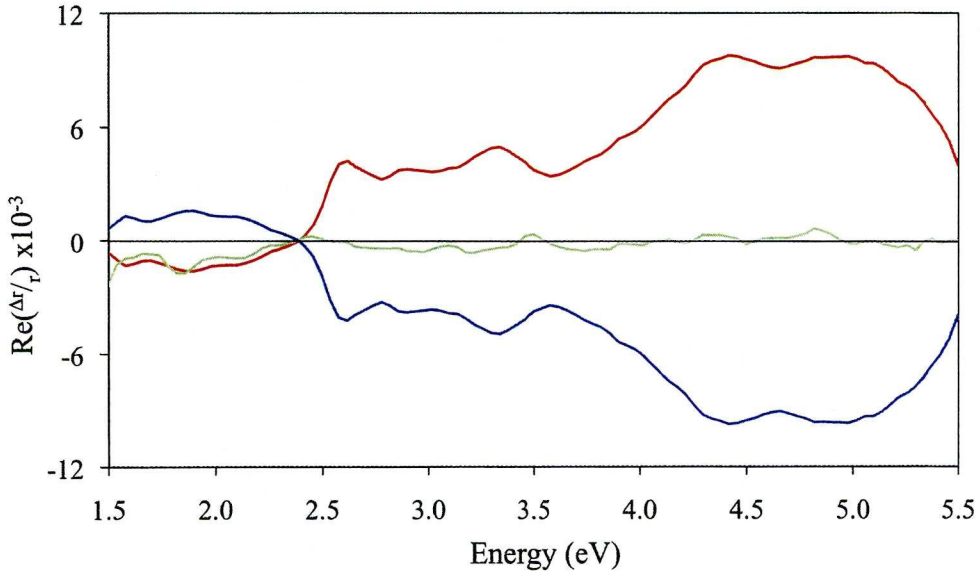

Figure 5.7 (b): The RA spectra ss-DNA in 0.1 M NaH_2PO_4/K_2HPO_4 at 0° (blue line), 45° (green line) and 90° (red line).

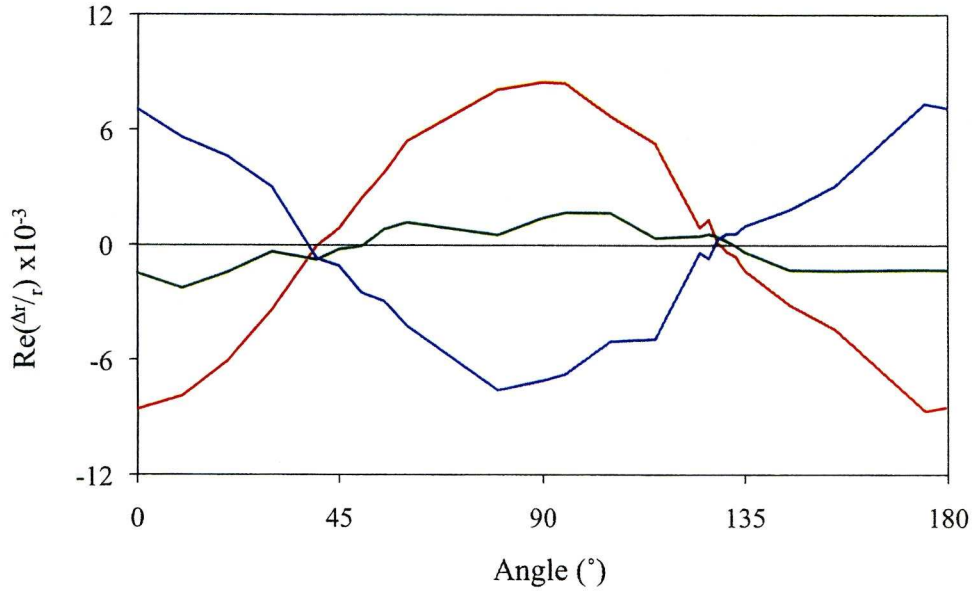

Figure 5.8 (a): The RAS peak intensity at 4.7 eV as a function of angle for Au(110) (blue line), Au(110) + ds-DNA (red line) and ds-DNA (green line), all in 0.1 M NaH_2PO_4/K_2HPO_4.

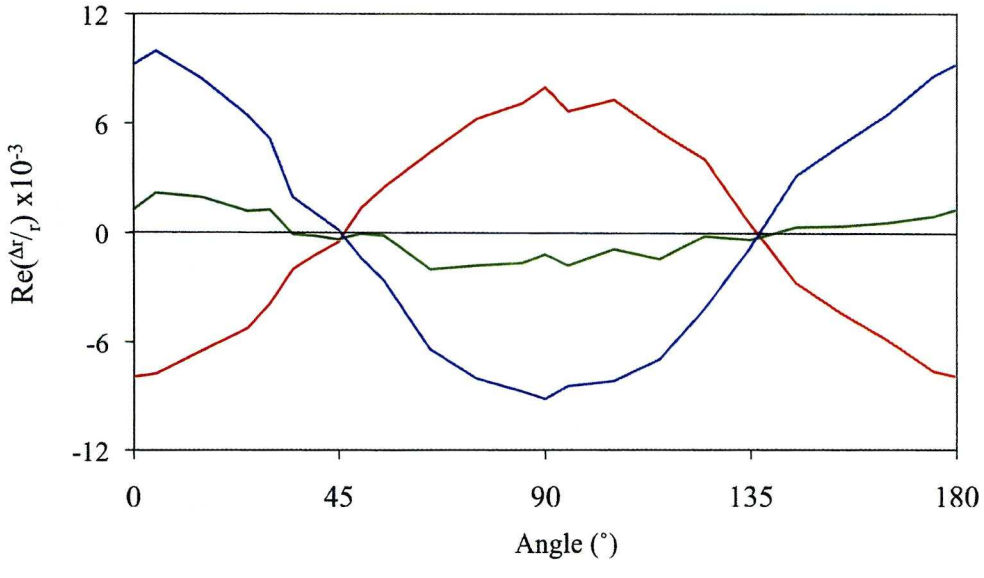

Figure 5.8 (b): The RAS peak intensity at 4.7 eV as a function of angle for Au(110) (blue line), Au(110) + ss-DNA (red line) and ss-DNA (green line), all in 0.1 M NaH_2PO_4/K_2HPO_4.

Previous work has shown that ds-DNA forms ordered structures on Au(111) [5,6]. The STM images obtained [6] of ds-DNA lying flat on a Au(111) surface show DNA molecules are packed in a parallel arrangement with no variation in the molecules orientation and have a diameter comparable to that found by Watson and Crick. Similarly an AFM study [5], showed compact, parallel "rod-like" features for ds-DNA on Au(111) which coincide with Watson and Crick's measurement of the diameter of the B form of DNA at 2 nm. Thus ds-DNA forms stable and ordered saturated layers on Au(111) [29] and furthermore the DNA electrodes are stable after long and dry storage [30], which suggests that the interactions between the phosphate backbone and the gold are strong.

As discussed in detail in [7] the conclusion from this and previous work [7] that ss-DNA forms ordered structures on Au(110) contrasts with previous studies of ss-DNA adsorbed on Au(111) [5,6] which indicate that ss-DNA did not form ordered monolayers. Investigations using electrochemical STM (EC-STM) [5] suggest that the ss-DNA is more likely to form a supercoiled structure, giving densely packed blob structures on Au(111). In addition to this, an AFM study shows little, if any ordering and the strands are "merely tangled up and piled up on the electrode surface irregularly, forming bumps and holes" [6].

5.6 DNA on Polycrystalline Au

The RA spectra discussed earlier suggest that ds-DNA and ss-DNA exhibit preferentially ordered structures on the Au(110) surface. Subsequent experiments reported in this section, were then conducted using ds-DNA and ss-DNA on a polycrystalline Au crystal. The purpose of this experiment was to determine whether the preferential ordering of the DNA was attributable to the structure of the Au(110) surface or due to interactions between strands of DNA.

A polycrystalline Au crystal was prepared in the same manner as the Au(110) crystals. This time the sample was placed into the electrochemical cell held at 0.0 V vs SCE in 0.1 M NaH_2PO_4/K_2HPO_4 in order to compare data with [7]. The sample was then rotated in the RA spectrometer at 10° intervals and spectra taken.

Figure 5.9 (a) shows the ADRAS data of the polycrystalline Au sample. The RA spectra of polycrystalline Au show a mixture of flat lines and some line shapes which bare slight resemblance to the spectral shape of an Au(110) crystal. The blend of spectral shapes is attributed to the polycrystalline Au sample having regions of Au(110) and Au(111) domains. As the polycrystalline Au had not been used in RAS before, the spectral shapes could not be normalised with regards to the polariser, this is why the RA spectra have varied positions with respect to the y-axis. A calf thymus ds-DNA solution (100 μg/ml) was then added to the cell and left overnight to incubate and then the RAS was recorded at the same orientations of the cell as measured for the bare polycrystalline Au sample. Figure 5.9 (b) shows the RA spectra of polycrystalline Au + ds-DNA in 0.1 M NaH_2PO_4/K_2HPO_4. It shows that at some angles (0° and 100°) the increase in RAS after the adsorption of ds-DNA is much greater than at some other angles (20° and 180°). It can be seen that the RA spectra which display similarities to the RA spectra of Au(110) have the changes in RAS shape after the adsorption of ds-DNA, but those which do not have the resemblance to the RAS of Au(110) are not affected. Figure 5.9 (c) shows the subtracted RA spectra.

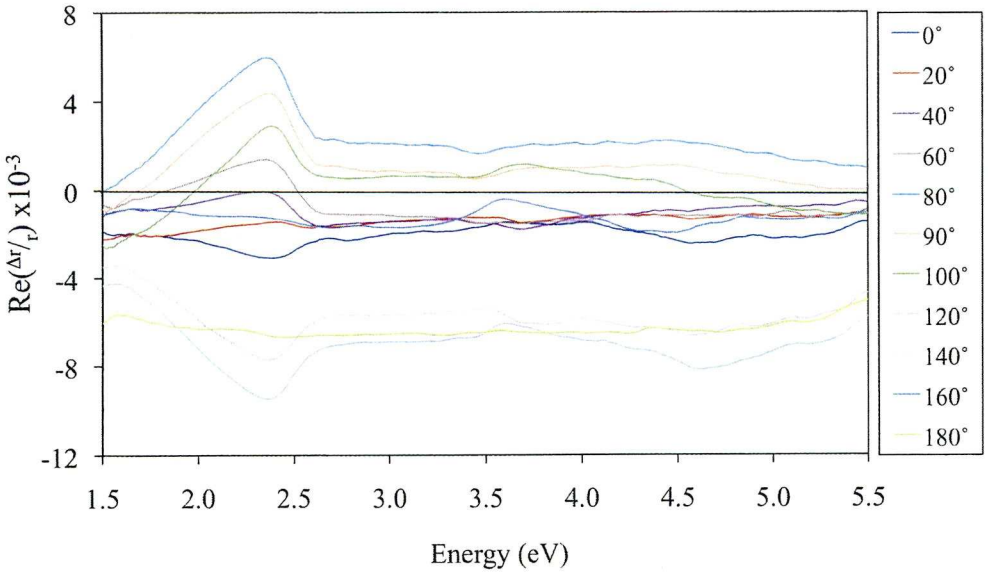

Figure 5.9 (a): The RA spectra of polycrystalline Au as a function of angular rotation, θ, from 0° to 180° at 0.0 V vs SCE in 0.1 M NaH_2PO_4/K_2HPO_4.

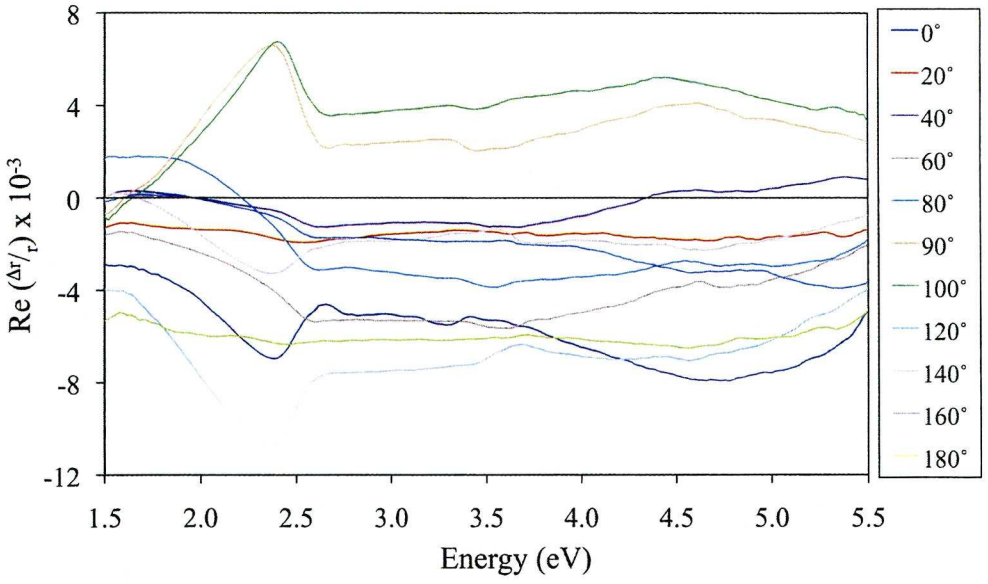

Figure 5.9 (b): The RA spectra of polycrystalline Au + ds-DNA as a function of angular rotation, θ, from 0° to 180° at 0.0 V vs SCE in 0.1 M NaH_2PO_4/K_2HPO_4.

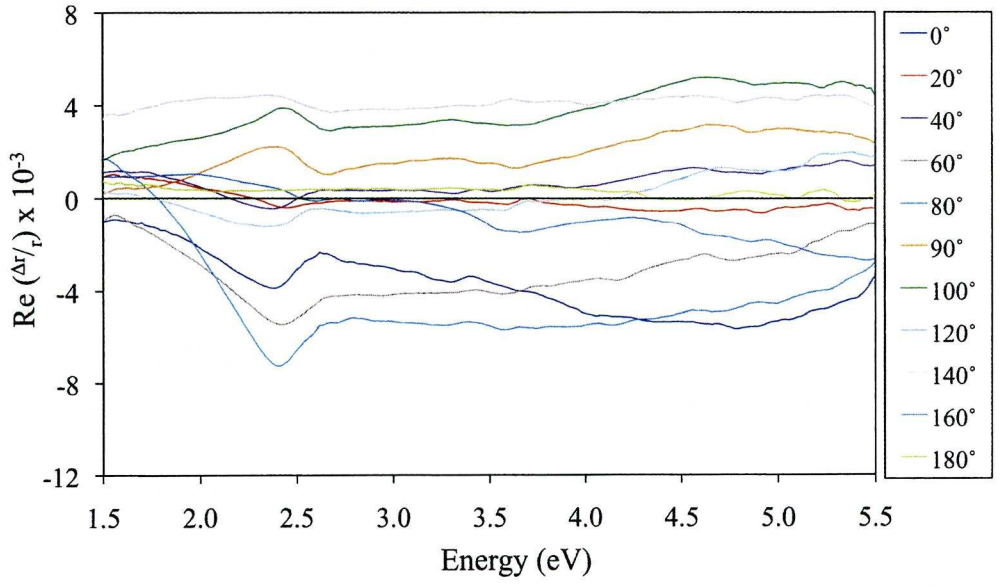

Figure 5.9 (c): The RA spectra ds-DNA as a function of angular rotation, θ, from 0° to 180° at 0.0 V vs SCE in 0.1 M NaH_2PO_4/K_2HPO_4.

It is deduced from the results that the ds-DNA does adsorb onto a polycrystalline Au sample. However the results remain inconclusive as to whether the ds-DNA adsorbs only on the Au(110) domains or if the adsorption onto the Au(111) domains in disordered and therefore not being detected by the RAS. The main difficulty with the polycrystalline sample is that the domains of each low index plane are larger than the area of the light hitting the sample from the RA spectrometer (~12 mm^2) so that when the sample is rotated, the beam will obtain data from different combinations of domains. Figure 5.10 is an image of the polycrystalline Au sample taken using a polarising microscope and it shows the size of the domains.

These inconclusive results do not answer the question as to whether the ordering of the ds-DNA and ss-DNA on the Au(110) surface arises because of their interactions with the ordered Au(110) substrate or because of interactions between different DNA molecules.

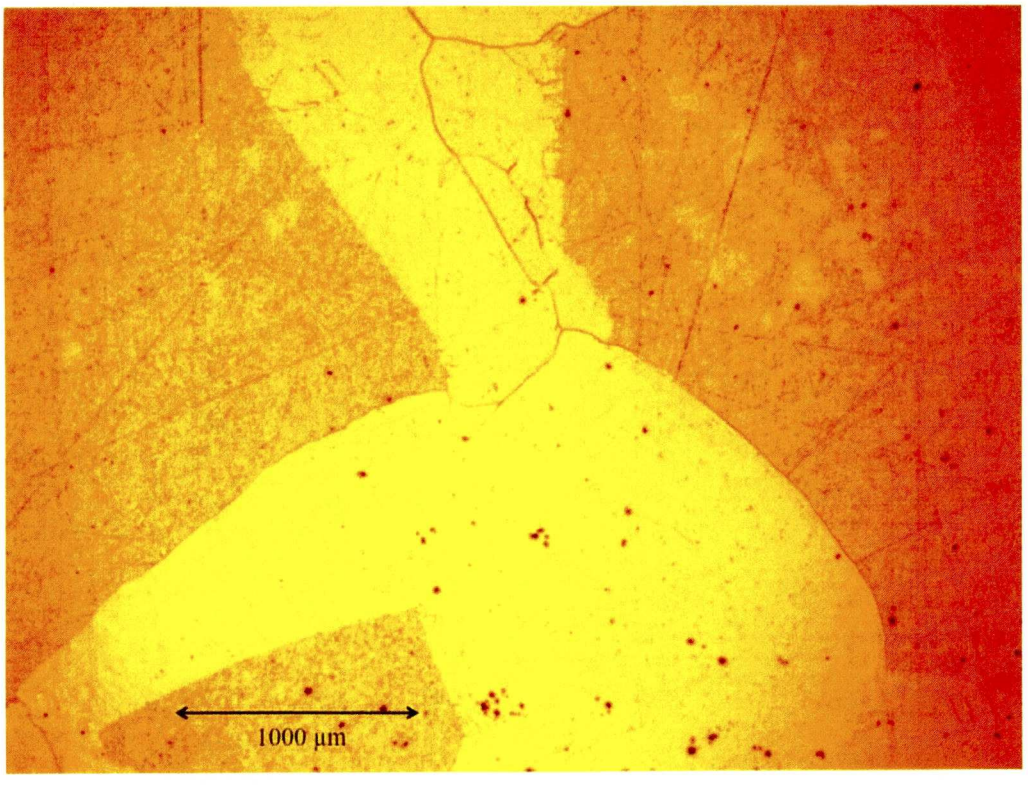

Figure 5.10: A polarising microscope image of the polycrystalline Au sample.

5.7 Conclusions

This chapter shows that long sequences of ds-DNA and ss-DNA adsorb at the Au(110)/liquid interface. The work reported in this chapter is an extension of the work of Cuquerella *et al* [7]. It shows that ss-DNA produces a greater increase in intensity over the RA spectrum of the Au(110) surface than the increase in intensity that arises from the addition of ds-DNA to an Au(110) sample. In contrast to previous work [7], which shows that ss-DNA and ds-DNA adsorb under potential control, this chapter reports that, ds-DNA and ss-DNA also adsorb via self assembly.

As a final experiment, the RAS of polycrystalline Au before and after the adsorption of ds-DNA was used to try and determine whether the preferential ordering of the ds-DNA and ss-DNA on Au(110) was attributable to interactions between the DNA and the Au(110) substrate or was due to DNA-DNA interactions. Unfortunately the results of this study were inconclusive.

5.8 References

[1] E. Shapir, H. Cohen, N. Borovok, A. B. Kotlyar and D. Porath, *J. Phys. Chem. B* **110** 4430 (2006)

[2] D. Erst, B. Polyakov, H. Olin and E. Tuite, *J. Phys. Chem. B* **107**, 3591 (2003)

[3] A. J. Thiel, A. G. Frutos, C. E. Jordan, R. M. Corn and L. M. Smith, *Anal. Chem.* **69**, 4948 (1997)

[4] E. Koglin and J. –M. Séquaris, *Topics Curr. Chem.* **134**, 1 (1986)

[5] R. Y. Zhang, D. W. Pang, Z. L. Zhang, J. W. Yan, J. L. Yao, Z. Q. Tian, B. W. Mao and S. G. Sun, *J. Phys. Chem. B* **106,** 11233 (2002)

[6] Y. D. Zhao, D. W. Pang, S. Hu, Z. L. Wang, J. K. Cheng, Y. P. Qi, H. P. Dai, B. W. Mao, Z. Q. Tian, J. Luo and Z. H. Lin, *Anal. Chim. Acta.* **388,** 93 (1999)

[7] M. C. Cuquerella, C. I. Smith, D. G. Fernig, C. Edwards and P. Weightman, *Langmuir* **23**, 2078 (2007)

[8] J. D. Watson and F. H. C. Crick, *Nature* **171**, 737 (1953)

[9] G. L. Zubay in Biochemistry (Wm. C. Brown Publishers, Dubuque, IA, 1998) Page 743

[10] www.humboldt.edu/~rap1/BiochSupp/LectSlid_Imgs/A-DNA_B-DNA_Z-DNA_8.png

[11] http://images2.clinicaltools.com/images/gene/dna_vs_rna_reversed_large.jpg

[12] E. A. Smith, M. J. Wanat, Y. Cheng, S. V. P. Barreira, A. G. Frutos, and R. M. Corn, *Anal. Chem.* **73**, 1 (2001)

[13] E. A. Smith, M. J. Wanat, Y. Cheng, S. V. P. Barreira, A. G. Frutos, and R. M. Corn, *Langmuir*, **17**, 2502 (2001)

[14] C-Y. Lee, P-C. T. Nguyen, D. W. Grainger, L. J. Gamble and D. G. Castner, *Anal. Chem.* **79**, 4390 (2007)

[15] C-Y. Lee, P. Gong, G. M. Harbers, D. W. Grainger, D. G. Castner and L. J. Gamble, *Anal. Chem.* **78**, 3316 (2006)

[16] D. Y. Petrovykh, H. Kimura-Suda, L. J. Whitman and M. J. Tarlov, *J. Am. Chem. Soc.* **125**, 5219 (2003)

[17] F. Ricci, R. Y. Lai, A. J. Heeger, K. W. Plaxco and J. J. Sumner, *Langmuir* **23**, 6827 (2007)

[18] L. A Chrisey, G. U. Lee and C. E. O'Ferrall, *Nucl. Acids Res.* **24**, 3031 (1996)

[19] Z. Lin, T. Strother, W. Cai, X. Cao, L. M. Smith and R. J. Hamers, *Langmuir* **18**, 788 (2002)

[20] P. T. Charles, G. J. Vora, J. D. Andreadis, A. J. Fortney, C. E. Meador, C. S. Dulcey and D. A. Stenger, *Langmuir* **19**, 1586 (2003)

[21] A. Bowfield, C. I. Smith, G. J. Dolan, M. C. Cuquerella, C. P. Mansley and P. Weightman, *e-J. Surf. Sci. Nanotech.* **7**, 225 (2009)

[22] V. A. Bloomfield, D. M. Crothers and I. Tinoco, Nucleic Acids Structures, Properties and Functions (University Science Books, California, 2000)

[23] V. Mazine, Y. Borensztein, L. Cagnon and P. Allongue, *Phys. Status Solidi A* **175**, 311 (1999)

[24] B. Sheridan, D. S. Martin, J. R. Power, S. D. Barrett, C. I. Smith, C. A. Lucas, R. J. Nichols and P. Weightman, *Phys. Rev. Lett.* **85**, 4618 (2000)

[25] V. Mazine, Y. Borensztein, *Phys. Rev. Lett.* **88**, 147403 (2002)

[26] P. Weightman, C. I. Smith, D. S. Martin, C. A. Lucas, R. J. Nichols and S. D. Barrett, *Phys. Rev. Lett.* **92**, 199707 (2004)

[27] P. Weightman, G. J. Dolan, C. I. Smith, M. C. Cuquerella, N. J. Almond, T. Farrell, D. G. Fernig, C. Edwards and D. S. Martin, *Phys. Rev. Lett.* **96**, 086102 (2006)

[28] P. Weightman, D. S. Martin, R. J. Cole and T. Farrell, Rep. Prog. Sci. 68, 1251 (2005)

[29] J. Wang, M. Jiang and B. Mukherjee, *Bioelectrochemistry* **52,** 111 (2000)

[30] Y. D. Zhao, D. W. Pang, Z. L. Wang, J. K. Cheng and Y. P. Qi, *J. Electroanal. Chem.* **431,** 203 (1997)

Chapter 6

The Effect of a Phosphate Solution on the RAS of DNA on Au(110)

This chapter investigates the phosphate buffer solution which surrounds the DNA and determines the effect it has on the RAS of the sample. An explanation is given as to why the changes occur and how these changes lead to a possible mechanism for the survival of these biological molecules before the existence of the ozone layer when the Earth was inundated with harmful UV radiation.

6.1 Introduction

It can be seen from previous chapters that there is an interaction between the Au(110) single crystal surface and the molecule in solution. The dipole moment of the molecule appears to interact with the dielectric function of the Au(110) surface. This chapter addresses the issue of the extent to which the solution contributes to this coupling effect.

This section reports several experiments which describe the behaviour of the RAS obtained from Au(110) after the adsorption of cytosine, CMP, a molecule known as poly-C (10 nucleotides (nts)) which is a chain of ten CMP molecules connected through the sugar phosphate backbone of DNA, ss-DNA and ds-DNA. In each case the RAS before and after the adsorption of the molecule is obtained, followed by the RAS of the Au(110) and molecule after an hour of drying and then when immersed back into the phosphate buffer solution.

6.2 Comparing the RAS of Cytosine, CMP and Poly-C on Au(110) In and Out of Solution

This section reports a comparison of the RAS of cytosine, CMP and poly-C (10nts) adsorbed on the Au(110)/electrolyte interface in three separate experiments. The aim of these experiments is to establish an understanding of the role of the solution in the coupling of the dielectric response of the Au with the biological molecule. The reason for investigating cytosine, CMP and poly-C is to progressively build upwards towards a full strand of DNA. The CMP is a cytosine base with a sugar and a phosphate group; poly-C is just ten molecules of CMP bound together as shown in figure 6.1.

In separate experiments, Au(110) crystals were prepared as described in section 2.4 and added to a Petri dish containing 0.1 M NaH_2PO_4/K_2HPO_4 buffer solution. In the first experiment 100 μM of cytosine was added to the solution and the cytosine was allowed to self assemble at the Au(110) surface. An RA spectrum was obtained from the Au(110) + cytosine, after which the buffer solution was

removed, the sample was allowed to dry for one hour and then a further RA spectrum was obtained. Fresh buffer solution was then added to the Petri dish in order to rewet the sample, left for an hour and then a final RA spectrum was obtained.

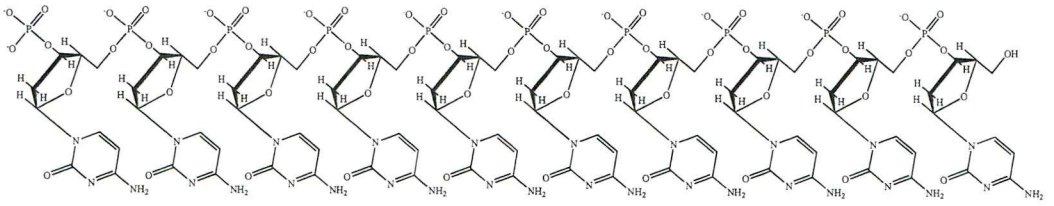

Figure 6.1: Structure of poly-C (10nts).

Figure 6.2 shows the RA spectra obtained from the Au(110), the Au(110) + cytosine, Au(110) + cytosine when dry and the Au(110) + cytosine when rewet. It can be seen from figure 6.2 that the addition of cytosine to Au(110) increases the overall intensity of the RAS obtained from clean Au(110) and produces the shoulder feature at 4.3 eV as seen in previous work [1]. The removal of the buffer solution from the cell gives rise to a decrease in RAS from 2.5 eV to 5.5 eV. Adding the clean buffer solution results in the RAS obtained from the Au(110) + cytosine when rewet to increase to an intensity just above that of the original RAS of Au(110) + cytosine in buffer solution.

In section 4.3, it was suggested that the reduction in intensity of the RAS of Au(110) + cytosine across the entire spectral range can be attributed to a reduction in the number of molecules adsorbed at the Au(110)/electrolyte interface caused by the lowering of the cytosine concentration in solution. However figure 6.2 shows that in this case, the reduction in intensity across the spectral range can not be attributed to a reduction in the number of cytosine molecules adsorbed at the Au(110) surface because when fresh buffer solution is put back into the cell, the RAS obtained from the Au(110) + cytosine increases back to an intensity similar to that obtained prior to the drying procedure.

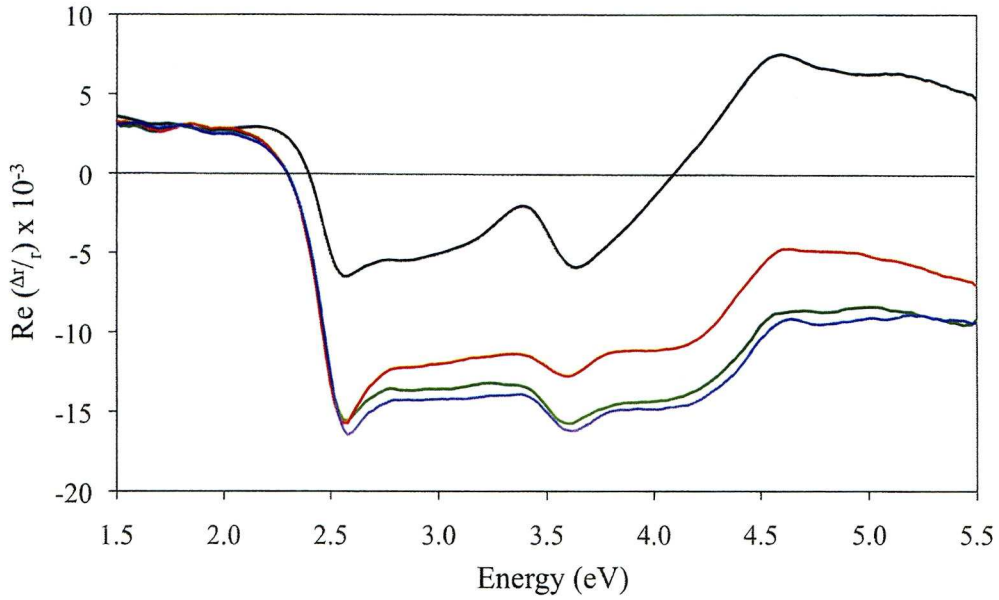

Figure 6.2: The RA spectra of Au(110) (black line), Au(110) + cytosine in solution (green line), Au(110) + cytosine after drying (red line) and Au(110) + cytosine rewet in solution (blue line).

Figure 6.3 shows the RA spectra obtained from the Au(110), and the Au(110) after the adsorption of CMP, when wet, dried and rewet in buffer solution. The behaviour of the Au(110) + CMP is similar to that of the Au(110) + cytosine as seen in figure 6.2 when wet, dry and rewet. However, the intensity of the RAS obtained from Au(110) + CMP when wet and dry is smaller than that of the corresponding RA spectra Au(110) + cytosine. Another difference is that the relative intensity of the RA spectrum obtained from the rewet Au(110) + CMP compared to its corresponding wet RA spectrum, is higher than those obtained from Au(110) + cytosine.

Figure 6.4 shows the RA spectra obtained from the experiment of poly-C adsorbed on the Au(110) surface. It shows the RA spectra of the Au(110), Au(110) + poly-C, Au(110) + poly-C when dry and Au(110) + poly-C when rewet in buffer solution. Figure 6.4 shows that the intensity of the RA spectra obtained from Au(110) + poly-C when wet and dry have a reduced intensity in comparison to the Au(110) + CMP when wet and dry. The relative intensity of the RA spectrum of Au(110) + poly-C when rewet is much larger than that of the corresponding RA spectrum of Au(110) + CMP.

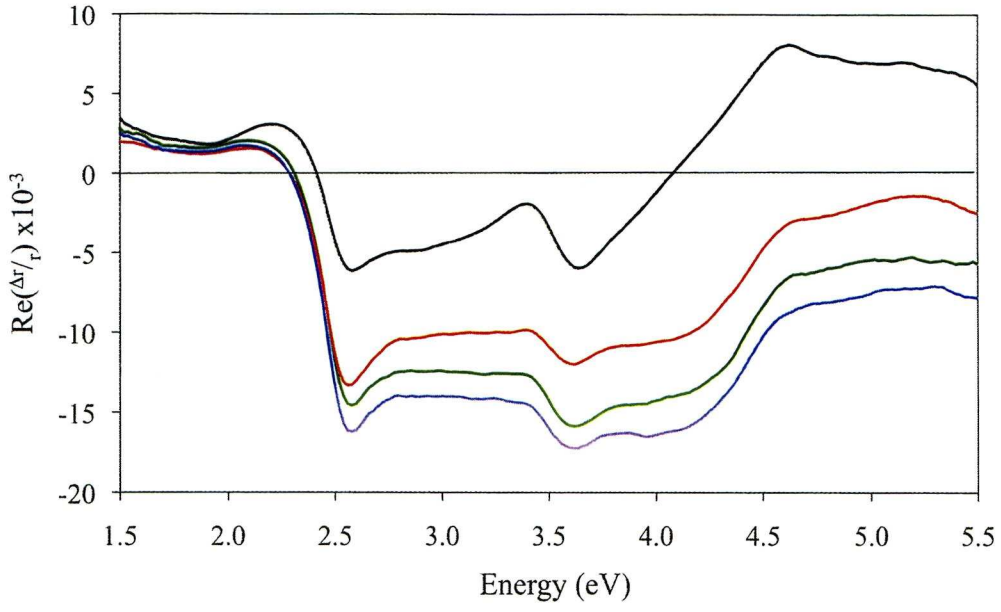

Figure 6.3: The RA spectra of Au(110) (black line), Au(110) + CMP in solution (green line), Au(110) + CMP after drying (red line) and Au(110) + CMP rewet in solution (blue line).

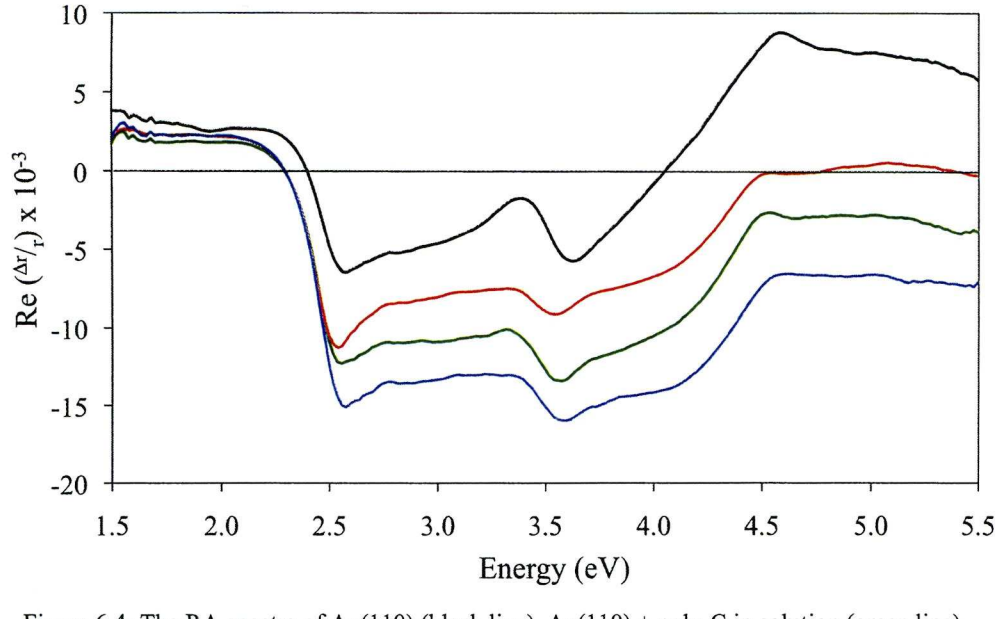

Figure 6.4: The RA spectra of Au(110) (black line), Au(110) + poly-C in solution (green line), Au(110) + poly-C after drying (red line) and Au(110) + poly-C rewet in solution (blue line).

Comparing the three experiments described in figure 6.2, 6.3 and 6.4, it can be seen that as the size of the molecule increases (i.e. in the sequence of cytosine, CMP, poly-C), the intensity of the original RA spectra obtained from the Au(110) + molecule in solution decreases.

It is known that the cytosine and the CMP molecules both adsorb at the Au(110)/electrolyte interface in alignment with the [1$\bar{1}$0] axis of the Au(110) substrate and that any variations in the RAS arising from the changes in molecule, are not attributed to the realignment of the molecules [6]. ADRAS experiments were then conducted in order to clarify that the poly-C molecules behave in a similar manner to cytosine and CMP and therefore rule out the changes in the RA spectrum observed from the Au(110) + poly-C being due to the molecule changing its orientation. Figure 6.5 shows the ADRAS obtained from Au(110) + poly-C in 0.1 M NaH_2PO_4/K_2HPO_4. It shows that the RA profile of the Au(110) + poly-C reduces to zero across the entire spectral range at 45°. This result establishes that the cytosine bases of the poly-C are also aligned with the [1$\bar{1}$0] axis of the Au(110) substrate. Furthermore, this result reinforces the idea that the changes in the total intensity of the RA spectra obtained from Au(110) after the adsorption of cytosine, CMP and poly-C respectively, are attributed to the reduction in the number of molecules adsorbing at the Au(110)/electrolyte interface.

Figures 6.6 and 6.7 show the ADRAS results obtained from the Au(110) + poly-C when dried and rewet in phosphate buffer solution respectively. Figure 6.6 shows the previously described reduction in RAS across the entire spectral range, whereas figure 6.7 shows the increase in RAS. Both figures 6.6 and 6.7 show that at 45° and 135°, the RAS across the entire spectral range goes to zero. This result indicates that the cytosine bases from the poly-C molecules align with the [1$\bar{1}$0] axis of the Au(110) substrate regardless of the phosphate buffer being present or not.

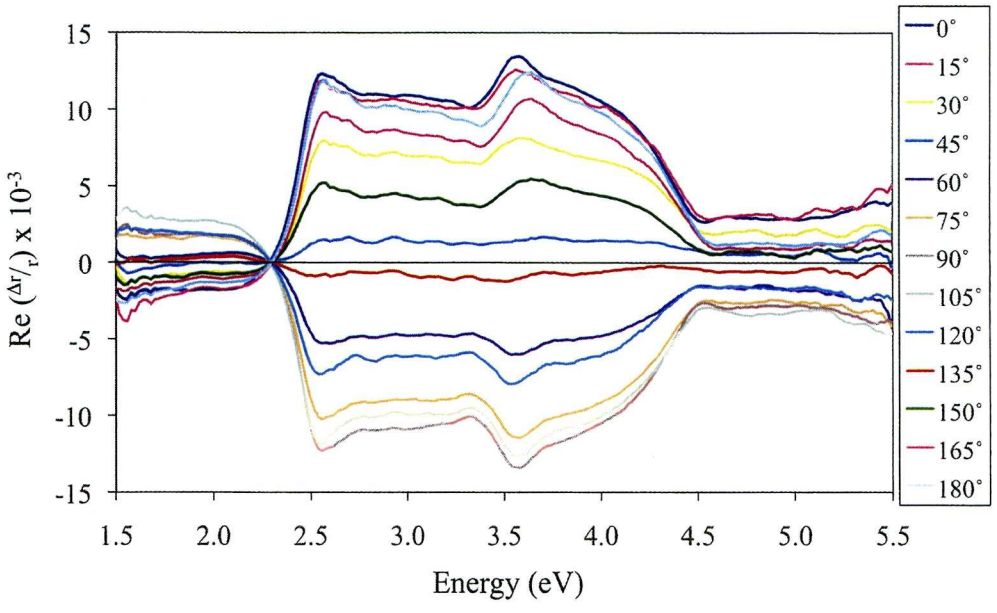

Figure 6.5: The RA spectra of Au(110) + Poly-C as a function of angular rotation, θ, from 0° to 180° in 0.1 M NaH_2PO_4/K_2HPO_4.

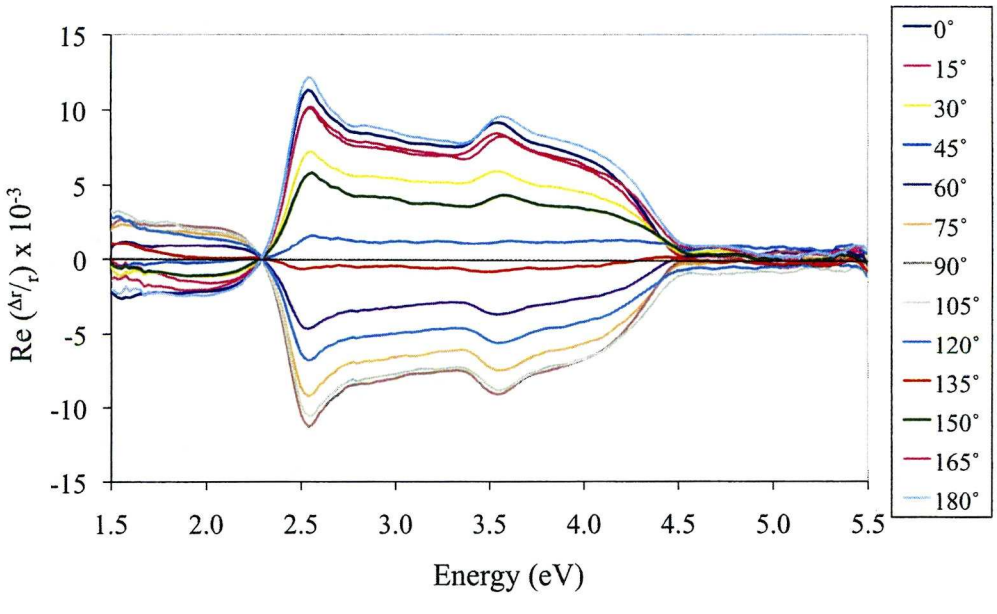

Figure 6.6: The RA spectra of Au(110) + Poly-C as a function of angular rotation, θ, from 0° to 180° dry.

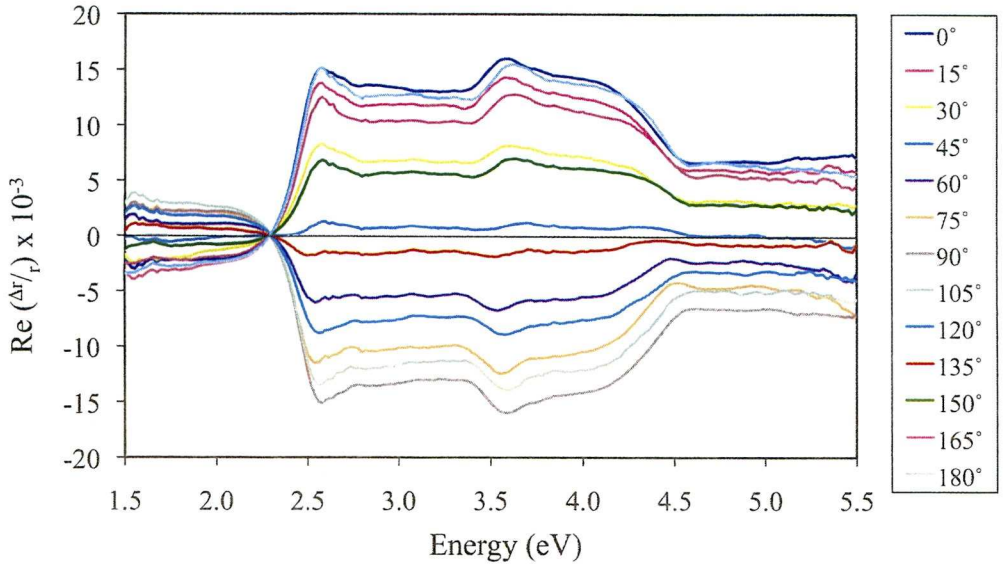

Figure 6.7: The RA spectra of Au(110) + Poly-C as a function of angular rotation, θ, from 0° to 180° in 0.1 M NaH_2PO_4/K_2HPO_4 rewet.

The comparison of the RA spectra obtained from the Au(110) after the adsorption of cytosine, CMP and poly-C after the systems have been allowed to dry, shown in figures 6.2, 6.3 and 6.4 respectively, shows that the removal of the buffer solution decreases the intensity of the optical response of the Au(110) + molecule. Figures 6.2, 6.3 and 6.4, show that the subsequent addition of fresh buffer solution to the Petri dish increases the optical response of the Au(110) + molecule beyond that obtained originally. However, adding the solution back into the Petri dish had a different effect on the RAS of the three molecules. Figure 6.2 shows that adding buffer solution back into the dish results in the RA spectrum obtained from Au(110) + cytosine to be larger than the original Au(110) + cytosine, similarly with CMP in figure 6.3 and poly-C in figure 6.4. Table 6.1 lists the RAS peak intensities at the 2.6 eV, 3.6 eV and 4.3 eV obtained from the adsorption of cytosine, CMP and poly-C. It can be seen that the rewetting of the sample gives rise to increases in RAS peak intensities on original RAS data of Au(110) + molecule and that the increase is proportional to the size of the molecule adsorbed at the Au(110) surface.

The observation that the dry samples show a reduced intensity RA spectrum that the intensity of the RAS of the wet specimen is enhanced by the surrounding hydrogen bonding network of the liquid. The way in which the cytosine base adsorbs onto the Au atoms allows water molecules to fit between adjacent cytosine molecules. It is suggested that the water couples dipole response of the molecule to the dielectric response of the Au(110) surface. When the solution is removed, the coupling effect between the optical response of the Au and the cytosine will be lost.

		RAS Intensity at		
		2.6 eV	3.6 eV	4.3 eV
Au + cytosine	Wet	-15.35	-15.75	-12.78
	Dry	-15.71	-12.70	-9.92
	Rewet	-16.33	-16.18	-13.53
Au + CMP	Wet	-14.88	-15.97	-12.53
	Dry	-13.21	-12.04	-8.38
	Rewet	-16.40	-17.40	-14.20
Au + poly-C	Wet	-12.10	-13.33	-6.82
	Dry	-10.37	-8.86	-3.48
	Rewet	-14.89	-15.98	-11.33

Table 6.1: The RAS peak intensities at 2.6 eV, 3.6 eV and 4.3 eV after the adsorption of cytosine, CMP and poly-C.

When the buffer solution is put back, coupling between the dipole response of the molecule and the dielectric response of the Au(110) surface is higher than in the initial experiment. It has been shown in this chapter and chapter 4 that the changes in RAS of Au(110) + molecule when wet and dry do not arise from the molecules desorbing from the Au(110) surface or from the molecules changing their orientation on the Au(110) surface. The ADRAS results show that the entire RAS obtained from the Au(110) + each molecule becomes featureless across the entire spectral range at angles of approximately 45° when wet, dry or rewet; a result which can be used to discard the possibility of the cytosine bases changing their orientation

or forming dimerised structures in these conditions. If the bases were to form dimerised structures then the RAS obtained from Au(110) + molecule would not give rise to featureless spectra across the whole energy range. Another possibility for the RA spectra obtained from Au(110) + molecule to change when in phosphate buffer solution, dried and then rewet in buffer solution, is the Au(110) surface reconstructing. However, as seen in section 4.6, the adsorption of cytosine at the Au(110) surface gives rise to a "freezing" of the Au(110) surface structure and therefore rules out the changes in RAS being attributed to the Au(110) surface reconstructing.

It has been established that the changes in RAS obtained from Au(110) + molecule in the different environments are not caused by the desorption of molecules from the Au(110) or changes in the molecular orientation or the Au(110) surface reconstructing. An alternative explanation for why the RA spectra of the rewet surfaces are more intense than the original wet surface might be due to the buffer solution removed from the cell containing surplus molecules of either cytosine, CMP or poly-C. The difference between the original RA spectra obtained from Au(110) + molecule in solution and the RA spectra obtained from Au(110) + molecule when rewet in fresh phosphate buffer solution can be attributed to the removal of any excess cytosine, CMP or poly-C in solution. It is suggested that these changes are due to variations in the coupling of the dipole response of the molecule to the dielectric response of the Au(110) surface. However if the excess molecules were to absorb the light whilst in the phosphate buffer solution, they would only absorb light between 4.0 eV and 5.0 eV and not give rise to the changes in RAS intensity of the Au(110) + molecule between the energies of 2.5 eV and 4.0 eV. Therefore the removal of excess molecules would increase the coverage of water surrounding the molecules at the Au(110) surface, increasing the three dimensional long range ordering of the surrounding hydrogen bonding network and thus improve its efficiency of dissipating energy from the surface.

However, as previously discussed, there is a difference observed in the rewet RA spectra of Au(110) after the adsorption of cytosine, CMP and poly-C. If the efficiency of the hydrogen bonding network is key to the coupling between the dielectric response of Au(110) and the dipole moment of the molecule, then the

relative sizes of the excess molecules removed from the buffer solution could relate to the percentage increase in efficiency of the hydrogen bonding network. A relatively large poly-C molecule would have greater interference on the hydrogen bonding network in comparison to that resulting from the presence of a much smaller cytosine molecule. This would explain why the increase in RAS obtained from Au(110) + poly-C when wet to rewet is larger than the corresponding experiments using CMP, which in turn is larger than that of cytosine.

6.3 Molecular Simulations

As the optical response of all three biological molecules, in the 1.5 eV to 5.5 eV RA spectrometer range, only arises from the two transitions of the cytosine base, any changes in the intensity of the RAS between the three molecules can be attributed to variations in the number of molecules adsorbed at the Au(110) surface; as described in chapter 4 of this thesis. One would expect that as the size of the adsorbed molecule increases, the number of available bonding sites must decrease. If a cytosine molecule occupies the length of three Au atoms along the closed packed rows, as shown in chapter 4, then the CMP might be expected to occupy more sites due to the sugar and phosphate groups preventing close packing of the bases on the Au(110) surface. Similarly, the poly-C is expected to occupy more Au sites due the steric hindrances of the phosphate backbone bonding the cytosine bases in a manner that restricts some rotations of the molecule. Results from CrystalMaker®, a molecular modeling software programme, suggest that if two cytosine molecules occupy six Au atoms along the close packed row, then it is reasonable to suppose that two CMP molecules require a minimum of seven Au atoms and that the poly-C requires eight. If this is the case, that implies that in comparison to available sites occupied by cytosine, approximately 17% of the underlying Au(110) would be "free" between CMP molecules and approximately 33% for the poly-C.

Figure 6.8 shows a schematic of how the cytosine, CMP and poly-C molecules would adsorb at the Au(110)/electrolyte interface. Note that figure 6.8 is not drawn to scale and that the poly-C only contains four cytosine bases for clarity.

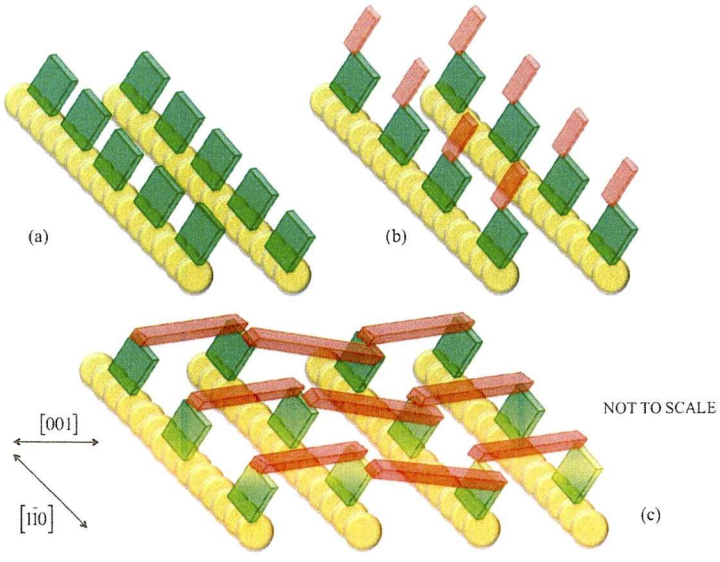

Figure 6.8: A schematic of Au(110) after the adsorption of (a) cytosine, (b) CMP and (c) poly-C.

A simple simulation supports the view that 17% and 33% of the Au(110) atoms are unoccupied following the adsorption of CMP and poly-C respectively. The simulation was a linear summation similar to that of section 4.4. It used a summation of a percentage of the RAS data obtained from Au(110) + cytosine and a percentage of the data obtained from clean Au(110) to try and estimate the percentage of clean Au after the adsorption of CMP and poly-C respectively. Figures 6.9 and 6.10 show the summations calculated and the experimental RAS data obtained from the Au(110) + CMP and Au(110) + poly-C respectively. The simulations showed that after the adsorption of CMP on Au(110) there was 18% clean Au and after the adsorption of poly-C on Au(110) there was 35% clean Au. The numbers generated by the simulations and the numbers defined by the molecular modeling software are in very close agreement with one and other. However there are slight differences between experimental and simulated RA spectra; as seen in figures 6.9 and 6.10, attributed to possible slight changes in orientation of the cytosine bases on the Au(110) surface following the adsorption of CMP and poly-C. The effect has been observed with adenine in previous work [2] but is much weaker for cytosine which "freezes" the Au(110) surface.

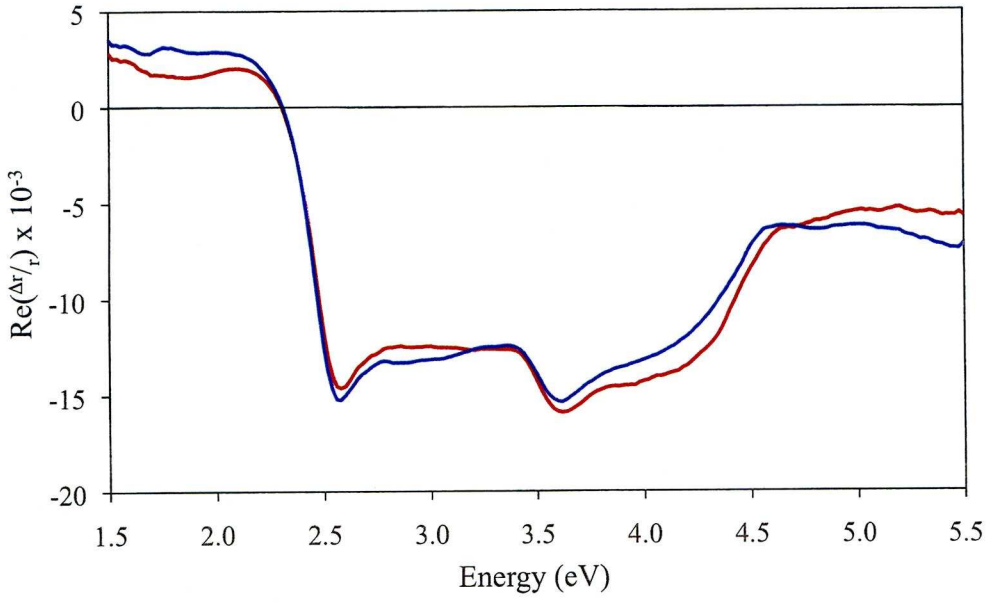

Figure 6.9: The simulated RA spectrum of 82% Au(110) + cytosine and 18% Au(110) (blue line) and the RA spectrum of Au(110) + CMP in 0.1 M NaH_2PO_4/K_2HPO_4 (red line).

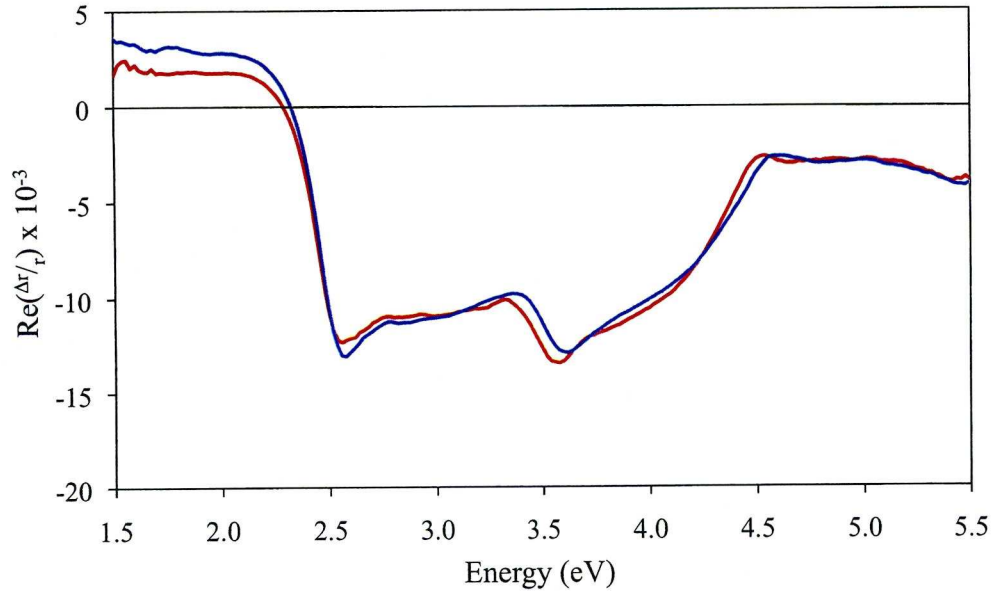

Figure 6.10: The simulated RA spectrum of 65% Au(110) + cytosine and 35% Au(110) (blue line) and the RA spectrum of Au(110) + poly-C in 0.1 M NaH_2PO_4/K_2HPO_4 (red line).

6.4 The Theoretical Modeling of Au(110) + Cytosine

In a similar analysis to that described in section 4.8, the RA spectra obtained from Au(110) and Au(110) + cytosine were simulated using the Lorentzian Transition Model, as were the RA spectra obtained from Au(110) + cytosine when dry and Au(110) + cytosine when rewet in phosphate buffer solution.

The experimental results reported in section 6.2 show that there are clear differences between the RA spectra obtained from the Au(110) and Au(110) + cytosine when wet, dry and rewet in phosphate buffer solution. Each of these experimental RA spectra are now compared with simulated RA spectra that were generated using the Lorentzian Transition Model. Table 6.2 lists the parameters used to simulate the RAS data and the simulations are compared with the experimental results in figures 6.11 (a) to (d).

Figure 6.11 (a) shows the experimental RA spectrum obtained from Au(110) in 0.1 M NaH_2PO_4/K_2HPO_4 and the simulated RA spectrum. There are regions where the simulated RA spectrum does not quite match the experimental RA spectrum but the simulation is deemed to be a close enough representation for what follows. When comparing the parameters used to generate this RAS simulation (from table 6.2) to the simulation of the RAS of Au(110) in section 4.8 (from table 4.2), it can be seen that the parameters used in the two simulations are very similar and lie within quite small error boundaries.

Figure 6.11(b) shows the RA spectrum from Au(110) after the adsorption of cytosine and the corresponding simulated RA spectrum. The simulation provides a very accurate representation of the experimental RA spectrum and a comparison of the parameters from table 4.2 with table 6.2 shows that the numbers used to generate each RA spectra are similar. One noticeable difference however is that the seventh transition used for the simulation shown in figure 6.11(b) is a much broader transition than its counterpart in section 4.8, figure 4.13 (d), this difference is attributed to the apparatus undergoing improvements to its sensitivity in the 5.0 eV to 5.5 eV region of the spectrum between the two experiments.

Figures 6.11 (c) and 6.11 (d) show comparisons of the simulated RA spectra of Au(110) + cytosine when the phosphate buffer solution is removed and Au(110) + cytosine when the buffer is replaced, respectively, with the corresponding experimental RA spectra.

Figure 6.11 (c) shows that the drop in the intensity of the RAS which arises from the removal of the buffer solution can also be generated using the simulation. Interestingly, the parameters required to model this effect in (table 6.2) the simulated RA spectrum show only a need for a large alteration in the energy of the first optical transition from 1.50 eV to 1.68 eV. However there are changes to the intensities of the third, fourth and seventh transitions, showing that the intensities for the simulation of the dry specimen are much larger than those of the original simulation of the wet specimen. The comparison shown in figure 6.11 (d) and the parameters used in the simulation listed in table 6.2, show that when the fresh buffer solution is replaced in the cell, the parameters required in the simulation return to very similar numbers to those used to simulate the RA spectrum of Au(110) + cytosine prior to the drying procedure. This result is another indication of the importance of the liquid environment for the optical response of biological molecules adsorbed at the Au(110) surface.

The first optical transition simulated in the Lorentzian Transition Model is a very strong transition which has an effect across the entire RA spectral range. The fact that the transition is shifted to a higher energy and becomes much narrower in the dry environment gives rise to the reduction in intensity across the whole spectral range. This supports the view that the phosphate buffer solution and its hydrogen bonding network play a key role in enhancing the optical response of the Au(110) surface and coupling the dielectric function of the Au(110) to the dipole moments of the adsorbed cytosine molecules.

Table 6.2: The parameters for the simulated RA spectra of Au, Au + cytosine, Au + cytosine (dry), Au + cytosine (rewet).

	Transition	1	2	3	4	5	6	7
	Direction	[001]	[001]	[1 $\bar{1}$ 0]	[001]	[001]	[1 $\bar{1}$ 0]	[1 $\bar{1}$ 0]
Au	ωt/eV	1.50 ± 0.09	3.50 ± 0.06	3.93 ± 0.07	4.60 ± 0.05	5.56 ± 0.15	.	.
	Γ/eV	1.10 ± 0.20	0.62 ± 0.09	1.92 ± 0.15	2.00 ± 0.15	0.05 ± 0.09	.	.
	S[a]	1.00 ± 0.08	0.19 ± 0.02	1.13 ± 0.10	1.03 ± 0.11	0.16 ± 0.02	.	.
Au/C - WET	ω_t/eV	1.50 ± 0.09	3.50 ± 0.06	3.90 ± 0.07	4.65 ± 0.05	5.60 ± 0.15	4.38 ± 0.04	5.45 ± 0.10
	Γ/eV	1.10 ± 0.20	0.36 ± 0.09	2.10 ± 0.15	2.30 ± 0.15	1.10 ± 0.09	0.57 ± 0.07	3.00 ± 0.10
	S[b]	1.00 ± 0.08	0.06 ± 0.02	0.73 ± 0.10	0.53 ± 0.11	0.01 ± 0.02	0.10 ± 0.04	1.07 ± 0.04
Au/C - DRY	ω_t/eV	1.68 ± 0.15	3.50 ± 0.10	3.90 ± 0.20	4.65 ± 1.00	5.60 ± 1.00	4.38 ± 0.04	5.45 ± 0.10
	Γ/eV	0.70 ± 0.30	0.32 ± 0.15	2.10 ± 0.40	2.30 ± 0.40	1.10 ± 0.40	0.57 ± 0.07	3.00 ± 0.10
	S[c]	1.00 ± 0.11	0.05 ± 0.01	1.15 ± 0.09	1.00 ± 0.01	0.02 ± 0.05	0.15 ± 0.04	1.58 ± 0.04
Au/C - REWET	ωt/eV	1.50 ± 0.15	3.50 ± 0.10	3.90 ± 0.20	4.65 ± 1.00	5.60 ± 1.00	4.38 ± 0.04	5.45 ± 0.10
	Γ/eV	1.10 ± 0.30	0.36 ± 0.15	2.10 ± 0.40	2.30 ± 0.40	1.10 ± 0.40	0.57 ± 0.07	3.00 ± 0.10
	S[d]	1.00 ± 0.11	0.05 ± 0.01	0.65 ± 0.09	0.48 ± 0.01	0.01 ± 0.05	0.09 ± 0.04	0.97 ± 0.04

[a,b,c,d]Relative intensities. Absolute intensities of transition 1 are 8000 (Au), 8900 (Au/C), 6000 (Au/C – dry), 9800 (Au/C – rewet).

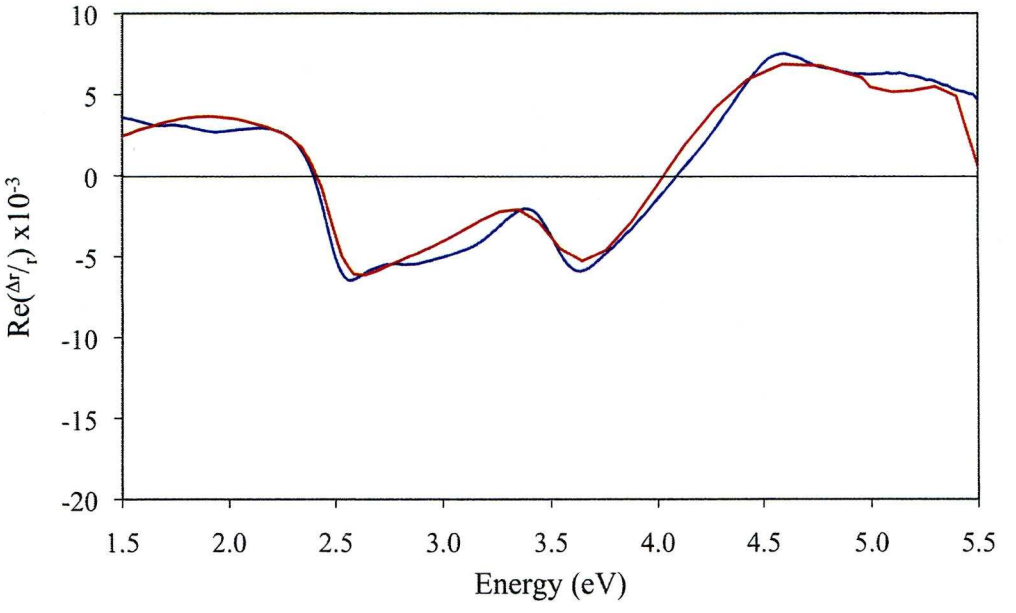

Figure 6.11 (a): The RA spectra of Au(110) in 0.1 M NaH_2PO_4/K_2HPO_4 (blue line) and the corresponding simulated RA spectrum (red line).

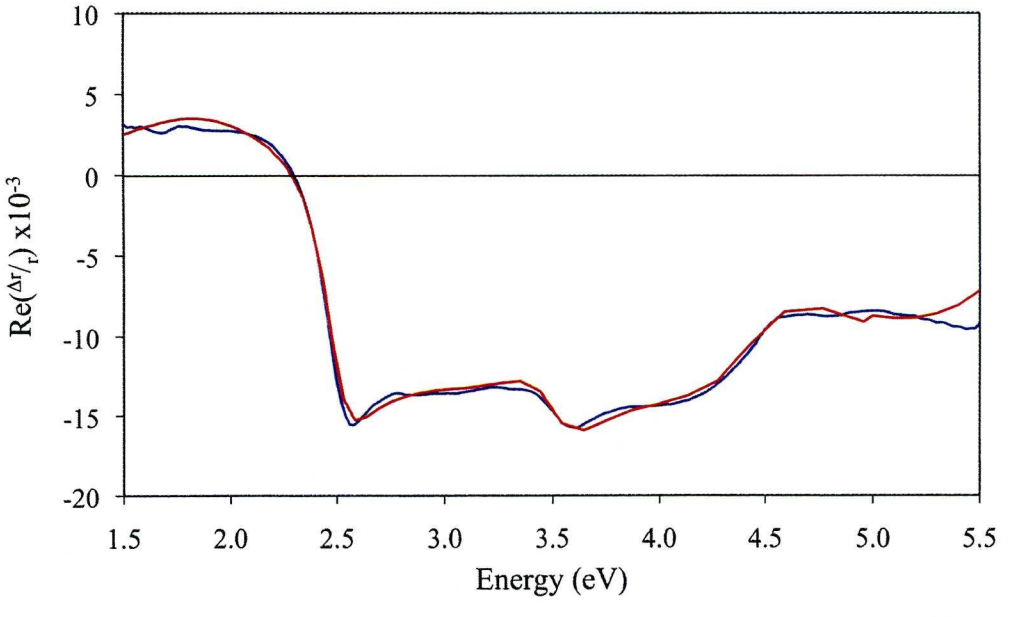

Figure 6.11 (b): The RA spectra of Au(110) + 100 μM of cytosine in 0.1 M NaH_2PO_4/K_2HPO_4 (blue line) and the corresponding simulated RA spectrum (red line).

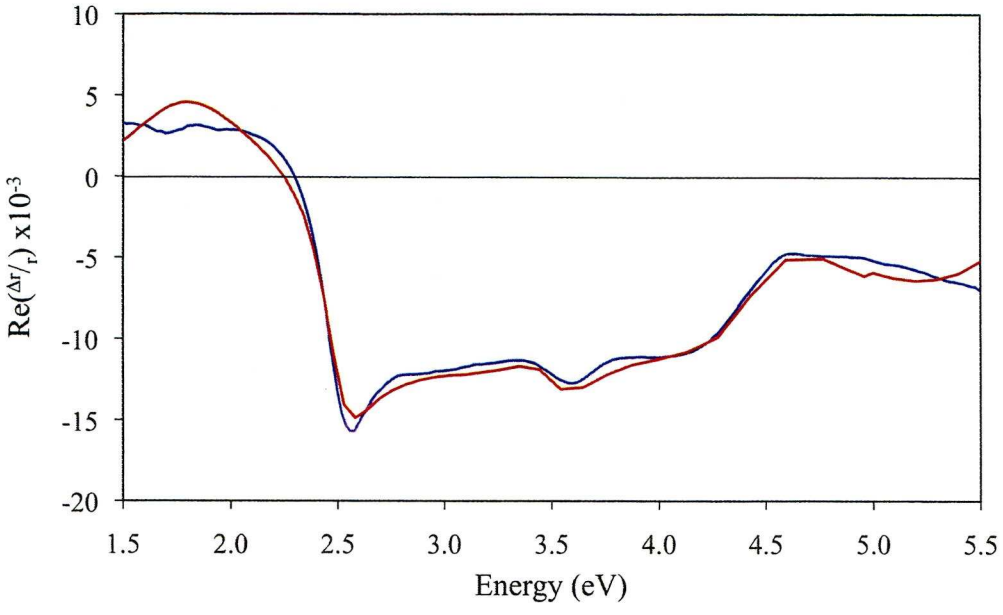

Figure 6.11 (c): The RA spectra of Au(110) + 100 μM of cytosine no longer in 0.1 M NaH_2PO_4/K_2HPO_4 (blue line) and the corresponding simulated RA spectrum (red line).

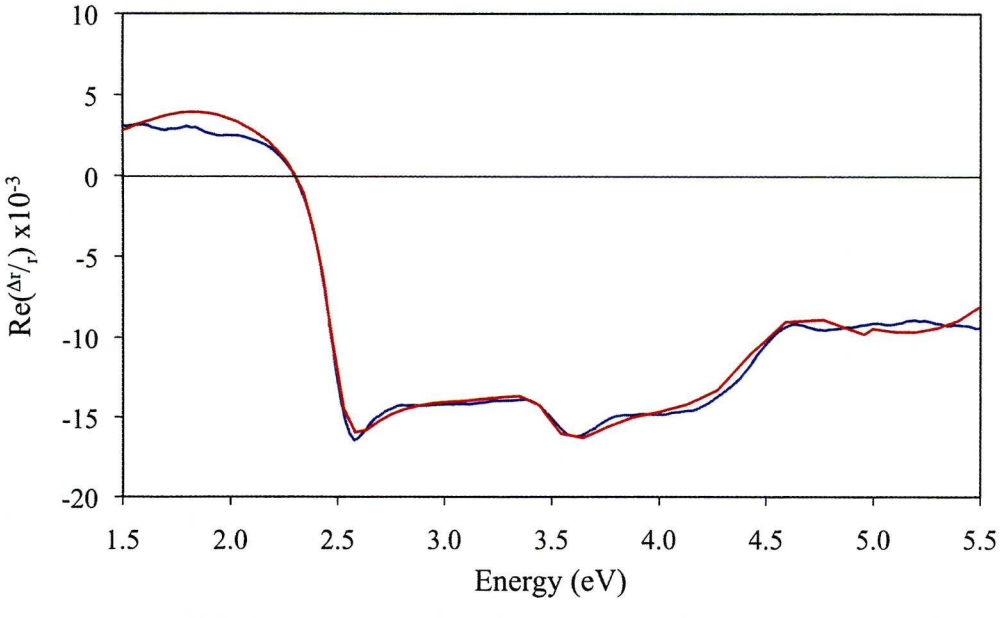

Figure 6.11 (d): The RA spectra of Au(110) + 100 μM of cytosine back in 0.1 M NaH_2PO_4/K_2HPO_4 (blue line) and the corresponding simulated RA spectrum (red line).

6.5 Comparing The RAS of Au(110) + DNA In and Out of Solution

The results described so far in this chapter have been used to suggest that the phosphate buffer solution, and in particular the hydrogen bonding network within the solution, enhance the RAS of an Au(110) surface after the adsorption of the biological molecules cytosine, CMP and poly-C. Having observed in chapter 5 the adsorption of calf thymus ss-DNA and ds-DNA on the Au(110) surface, it was only natural to investigate the effect of the buffer solution on the ss-DNA and the ds-DNA at the Au(110) surface. Consequently, as in to the experiments involving cytosine, CMP and poly-C, the ss-DNA and ds-DNA were left to self assemble on the Au(110) surface in 0.1 M NaH_2PO_4/K_2HPO_4. In each case an RA spectrum was obtained before the adsorption of the DNA, after the adsorption, after the buffer solution was removed and the sample allowed to dry, and finally a spectrum was taken after fresh buffer solution was put back into the cell. For these experiments investigating the two types of DNA on the Au(110) surface, the newly developed UV RA spectrometer was employed in addition to the normal range RA spectrometer. The sample was probed using both sets of apparatus at strategic times in the experiments, i.e. before the adsorption of DNA, after adsorption, whilst dry and finally when rewet in solution. The data from each RA spectrometer were then matched together in the same fashion as that described in section 2.5, with the intention of providing more accurate RA spectra over a wider spectral range.

Figure 6.12 shows the extended RA spectra obtained from Au(110), Au(110) + ds-DNA in buffer, Au(110) + ds-DNA with the buffer removed and Au(110) + ds-DNA with the buffer put back into the cell. This figure shows that the adsorption of ds-DNA increases the overall RAS of the Au(110) surface and gives rise to a very broad peak between 4.5 eV and 6.5 eV. This is a similar result to that described in section 5.4 of this thesis. It can also be seen that the drying process gives rise to a decrease in the RAS between 2.5 eV and 4.5 eV, but between 4.5 eV and 6.8 eV the RAS is unchanged, a result which differs to that seen with cytosine, CMP and poly-C in the range 4.5 eV to 5.5 eV. The RA spectrum obtained from the dry

sample has approximately the same RAS intensity as the RA spectrum obtained from the clean Au(110) sample between 2.5 eV and 3.5 eV. However the rewetting of the sample results in an overall increase in RAS, this result is similar to that observed with cytosine, CMP and Poly-C.

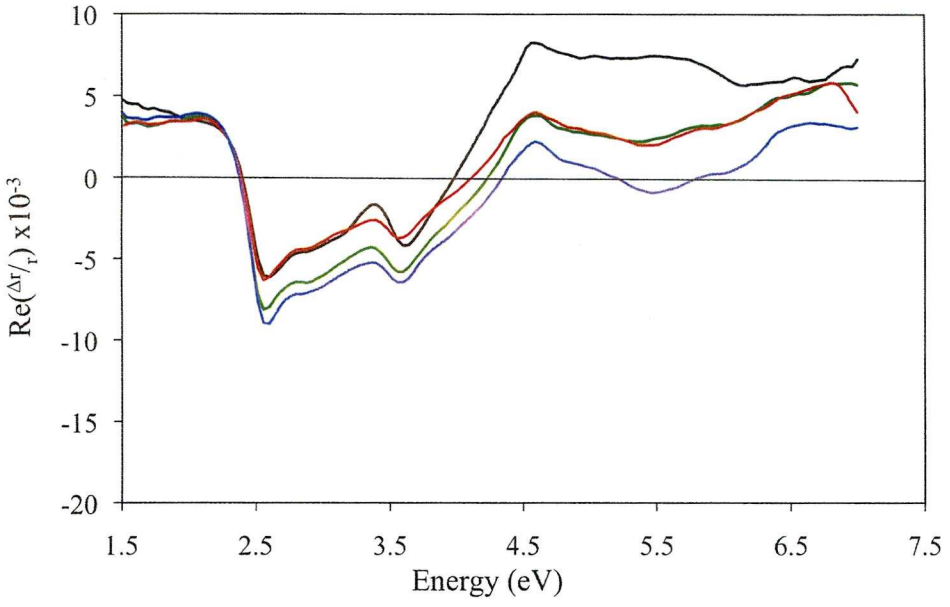

Figure 6.12: The RA spectra of Au(110) (black line), Au(110) + ds-DNA in 0.1 M NaH_2PO_4/K_2HPO_4 (green line), Au(110) + ds-DNA dry (red line) and Au(110) + ds-DNA rewet in 0.1 M NaH_2PO_4/K_2HPO_4 (blue line).

Figure 6.13 shows the spectra obtained at the same experimental intervals as those shown in figure 6.12 but this time it is with the adsorption of ss-DNA instead of ds-DNA. The RA spectra obtained from the Au(110) sample is very similar for both figures 6.12 and 6.13, but as seen in previous work [3] and in chapter 5 of this thesis, there is a distinct difference of between the RA spectrum of Au(110) + ds-DNA and the RA spectrum of Au(110) + ss-DNA. The RA spectrum of Au(110) + ss-DNA has a greater overall intensity than its ds-DNA equivalent.

Figure 6.13 also shows that the removal of the phosphate buffer solution from the sample results in the RAS obtained from the Au(110) + ss-DNA to decrease across the entire spectral range. This is a result which is also observed with cytosine, CMP, and Poly-C and to a lesser extent with the ds-DNA. This result is

further evidence that there is a coupling between the dielectric function of the Au(110) and the dipole moments in the biological molecules adsorbed at the Au(110)/electrolyte interface.

The rewetting of the Au(110) + ss-DNA sample gives rise to an interesting result. Unlike the adsorption of cytosine, CMP, poly-C and ds-DNA, the RAS obtained from Au(110) + ss-DNA when rewet in phosphate buffer solution does not result in an overall increase in intensity which is greater than that of the original RA spectrum of Au(110) + ss-DNA in phosphate buffer solution.

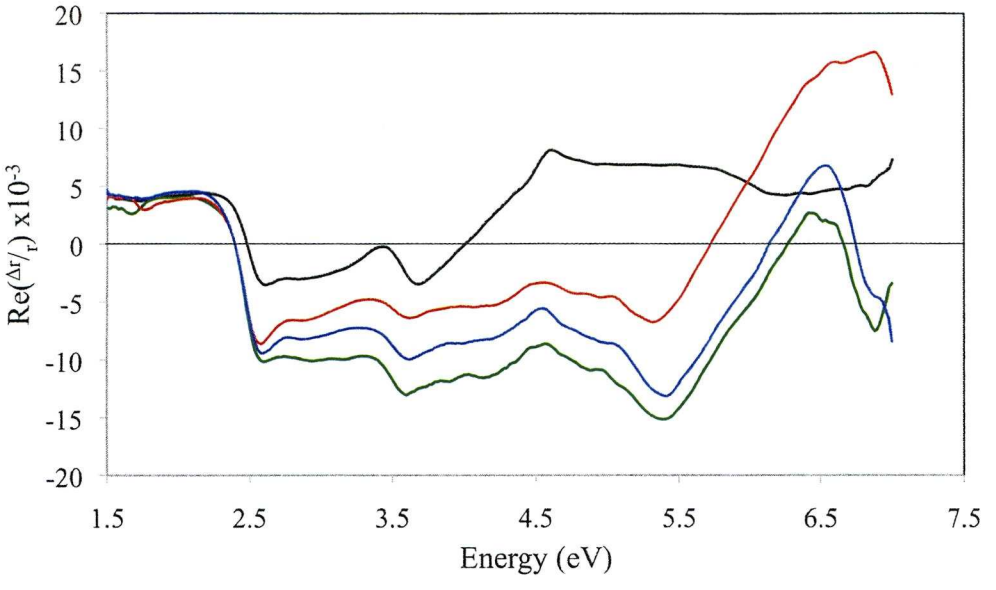

Figure 6.13: The RA spectra of Au(110) (black line), Au(110) + ss-DNA in 0.1 M NaH_2PO_4/K_2HPO_4 (green line), Au(110) + ss-DNA dry (red line) and Au(110) + ss-DNA rewet in 0.1 M NaH_2PO_4/K_2HPO_4 (blue line).

The results described above do not show a simple trend in which the environmental dependence of the RAS results vary smoothly with the increasing size of the biological molecules (cytosine, CMP, poly-C, ds-DNA and ss-DNA). In section 6.2, which compared the results for cytosine, CMP and poly-C, there are two clear trends, firstly that the larger the molecule the smaller the RAS response which was interpreted in terms of the reduced number of available bonding sites to the Au(110) surface. Secondly, that the intensity of 'rewet' RA spectra in comparison to

the corresponding original 'wet' RA spectra, increased as the size of the adsorbed molecule increased. The latter effect was attributed to the removal of excess molecules when the first phosphate buffer solution was removed and replaced by a fresh buffer solution thus improving the long range ordering of the surrounding hydrogen bonding network and improving its efficiency at dissipating radiation from the adsorbed biological molecules.

This hypothesis breaks down when applied to the RAS results obtained from Au(110) + ds-DNA and Au(110) + ss-DNA. There are two possible reasons as to why the theory breaks down, the first being that the bases adenine, thymine and guanine and their corresponding monophosphates and oligonucleotides, behave differently to cytosine, CMP and poly-C. As the three other bases are present in the ss-DNA and ds-DNA but in unknown quantities, their behaviour may be effecting the RAS studies to an extent which, as of yet, are too complex to understand fully. The second possibility could be that the thirty minute exposure of the ds-DNA and ss-DNA on the Au(110) sample whilst dry to the UV lamp in the UV RA spectrometer resulted in the DNA being denatured and therefore giving distorted results. However if such denaturing does occur it does affect the RA spectrum and hence the orientation of the molecules on the Au(110) surface. Greater changes in intensity of the RAS occur after the UV exposure to the adsorbed ss-DNA on the Au(110) surface as opposed to the adsorbed ds-DNA. This result can be attributed to the ds-DNA being more protected against the UV radiation due to internal hydrogen bonding across the bases, a mechanism which is does not occur in the ss-DNA.

6.6 Conclusions

This chapter shows that the adsorption of the cytosine occurs at the Au(110)/electrolyte interface by self assembly. It also shows that as the cytosine base is replaced by CMP (a cytosine base with a sugar and a phosphate group attached), the intensity of the RAS obtained is reduced. When the CMP is replaced by poly-C (10nts) (ten CMP molecules connected via their phosphate groups), the RAS obtained is reduced further. The reduction in the RAS intensity is attributed to

the increasing size of the molecules reducing the number of available bonding sites on the Au(110) surface.

In addition to this effect, the drying of the Au(110) crystals after the adsorption of cytosine, CMP and poly-C results in the RAS obtained from each sample being reduced in comparison to their complimentary wetted RA spectra. This result is attributed to the removal of the coupling between the dielectric function of the Au(110) and the dipole moments of the biological molecules via the hydrogen bonding network of the buffer solution. Rewetting the samples in clean buffer solution resulted in the RA spectra obtained from the Au(110) + molecules increasing in intensity across the entire spectral range to higher values than previously due to the restoring of the hydrogen bonding network.

The adsorption of ds-DNA and ss-DNA separately on the Au(110) samples did not give rise to the same effect as that of the cytosine, CMP and poly-C on the RAS. The RAS obtained from the Au(110) + ds-DNA showed only a small difference between the wet and dry samples, but the rewet sample resulted in an overall increase in RAS to a higher value than observed initially. The ss-DNA behaved differently: the RAS obtained from the Au(110) + ss-DNA dry sample giving rise to a reduced intensity across the entire spectral range, but unlike the experiments involving cytosine, CMP, poly-C and ds-DNA, the RA spectrum of the rewet sample did not have a greater intensity compared to that of its original wet RA spectrum. These differences between DNA and the three cytosine based molecules might be explained by the effect of the three other bases adenine, thymine and guanine present in the ds-DNA and ss-DNA. Alternatively the UV radiation from UV RA spectrometer might have denatured both forms of the DNA during their time in the spectrometer.

6.7 The Wider Context

The atmosphere of the early earth did not have an ozone layer to shield molecules from the damaging effects of UV radiation [4]. It is known that DNA is damaged by UV radiation and the question arises as to how DNA was able to evolve in the

environment of the early earth. A key observation is that the four bases in DNA all have very low fluorescence yields indicating that they have a "protection" mechanism which dissipates the energy adsorbed from UV photons without damaging the molecule [5]. These dissipative mechanisms, which are usually attributed to efficient radiationless electronic relaxation processes, vary with the structure of DNA [6,7]. However while the liquid environment of DNA is known to have a major influence on its properties and functional behaviour [8-11] the role of a liquid environment in these dissipative mechanisms is unclear [5,12,13]. The results reported in this chapter show that a liquid environment has a major influence on the dissipation of the energy absorbed from the UV radiation by both ds-DNA and ss-DNA as well as the DNA base cytosine, its monophophate, CMP, and an oligonucleotide comprising of ten CMP molecules connected through a phosphate backbone (poly-C (10nts)). This mechanism involving the liquid environment would therefore have facilitated the evolution of DNA.

This study is made possible by the observation that the optical response of cytosine [1], adenine [14] ss-DNA and ds-DNA [3] adsorbed at Au(110)/electrolyte interfaces involves a strong coupling to the dielectric response of the Au(110) substrate. Furthermore the strength of this coupling in ss-DNA depends on whether the ss-DNA adsorbs on the Au(110) through the phosphate backbone or through the bases indicating [3] that the coupling between the optical dipole of the bases and the Au depends on the detail of the local molecular environment. The coupling of the optical response of these adsorbed molecules to the optical response of the Au(110) substrate varies dramatically when the liquid environment is removed.

6.8 References

[1] P. Weightman, G. J. Dolan, C. I. Smith, M. C. Cuquerella, N. J. Almond, T. Farrell, D. G. Fernig, C. Edwards and D. S. Martin, *Phys. Rev. Lett.* **96**, 086102 (2006)

[2] A. Bowfield, C. I. Smith, G. J. Dolan, M. C. Cuquerella, C. P. Mansley and P. Weightman, *e-J. Surf. Sci. Nanotech.* **7**, 225 (2009)

[3] M. C. Cuquerella, C. I. Smith, D. G. Fernig, C. Edwards and P. Weightman, *Langmuir* **23**, 2078 (2007)

[4] A. L. Sobolewski and W. Domcke, *Europhys. News* **37**, 20 (2006)

[5] C. E. Crespo-Hernández, B. Cohen, P. M. Hare and B. Kohler, *Chem. Rev.* **104,** 1977 (2004)

[6] N. K. Schwalb and F. Temps, *Science* **322,** 243 (2008)

[7] T. Takaya, C. Su, K. de La Harpe, C. E. Crespo-Hernández and B. Kohler, *P. Natl. Acad. Sci.* **105,** 10285 (2008)

[8] J. Berashevich and T. Chakraborty, *J. Phys. Chem B* **112,** 14083 (2008)

[9] D. H. Ha, H. Nham, K-H Yoo, H-M. So, H-Y. Lee and T. Kawai, *Chem. Phys. Lett.* 355, 405 (2002).

[10] S. Tuukkanen, A. Kuzyk, J. J. Toppari, V. P. Hytönen, T. Ihalainen and P. Törmä, *Appl. Phys. Lett.* **87**, 183102 (2005)

[11] T. Kleine-Ostmann, C. Jördens, K. Baaske, T. Weimann, M. Hrabe de Angelis, M. Koch, *Appl. Phys. Lett.* **88**, 102102 (2006)

[12] K.E. Furse and S.A. Corcelli, *J. Am. Chem. Soc.* **130,** 13103 (2008)

[13] S. Pal, P. K. Maiti, B. Bagchi and J. T. Hynes, *J. Phys. Chem. B* **110**, 26396 (2006)

[14] C. I. Smith, A. Bowfield, G. J. Dolan, M. C. Cuquerella, C. P. Mansley, D. G. Fernig, C. Edwards and P. Weightman, *J. Chem. Phys.* **130**, 044702 (2009)

Chapter 7

Conclusions

This chapter brings together all the findings that have arisen from this thesis and provides an indication as to how this research can be taken forward.

7.1 Introduction

The results that have arisen from the work reported in this thesis are summarised in the following sub-sections.

7.1.1 The RAS of Au(110)

The characteristic RA profiles of the Au(110)–(1×1) surface structure as well as the (1×2) and (1×3) surface reconstructions in varied environments of pH, electrolyte anion and applied electrode potential, were summarised from studies reported by previous research students in order to describe the behaviour of the Au(110) surface that has been used extensively throughout this study. In an extension to previous Au(110) studies, the Au(110) surfaces which consist of mixed regions of the (1×1) and (1×2) surface structures or the (1×2) and (1×3) surface reconstructions, have been simulated using the experimental data obtained by the RAS of the (1×1) surface structure and the (1×2) and (1×3) surface reconstructions.

The development of a second RA spectrometer, which can probe into the UV spectral range (4.0 eV to 6.8 eV), facilitated the study of the optical response of the Au(110) crystal under a liquid environment for the first time using RAS in this spectral range. The use of the new RA spectrometer in conjunction with the normal RA spectrometer (1.5 eV to 5.5 eV) enabled extended RA spectra to be obtained via a series of data matching procedures. Theoretical modeling of the extended RA spectra of the Au(110) surface was used to show that a sixth transition (at 6.43 ± 0.01 eV) is required in order to simulate the optical transitions of the Au(110) crystal surface. The modeling of the extended RA spectra also showed that the fifth transition observed in the normal RA spectrometer (at ~5.0 eV) is actually a much broader and more intense transition (at ~5.5 eV) when probed by the new UV range RA spectrometer. The discrepancy is attributed to the optical components in the normal RA spectrometer being less sensitive than the new UV RA spectrometer in the spectral region above 5.0 eV.

7.1.2 The RAS of Au(110) + Cytosine

The adsorption of cytosine at the Au(110)/electrolyte interface under various conditions has produced several interesting RA spectra. The RAS of Au(110) after the adsorption of four different concentrations of cytosine, were used to show that as the concentration of cytosine was increased, the optical response of the Au(110) increased as well as the cytosine peak at 4.3 eV.

Theoretical simulations of the RAS obtained from the sub-monolayer coverage of cytosine at the Au(110)/electrolyte interface can be reproduced by the linear summation of various percentages of the RAS data obtained from a clean Au(110) surface and RAS data obtained from a cytosine saturated Au(110) surface.

Further experiments showed that an applied potential of -0.6 V was sufficiently negative to drive all the cytosine molecules from the surface of the Au(110) sample. At a potential of -0.4 V, a reduced RA response from the cytosine adsorbed on the Au(110) surface leads to the suggestion that at this voltage, the cytosine has started to be driven from the Au(110). The RAS obtained from Au(110) + cytosine at potentials of -0.2 V to +0.6 V are almost identical. This lack of variation suggests that the surface structure and orientation of the cytosine molecules do not change and thus indicates that the cytosine molecules, when adsorbed at 0.0 V, are freezing the surface reconstruction. Further simulations also show this freezing effect.

The application of ADRAS determines that the cytosine molecules adsorb vertically at the Au(110)/electrolyte interface regardless of whether there is a monolayer coverage of cytosine molecules or sub-monolayer coverage. The application of theoretical modeling of the ADRAS results obtained from Au(110) + cytosine, indicate that the transitions in the cytosine molecules are polarised in the $[1\,\bar{1}\,0]$ direction of the Au(110) crystal. These results alongside computer software modeling specify that the cytosine adsorbs to the Au(110) via three bonding sites on the molecule, the NH_2 group and the N(3) and O atoms.

The final experiment observed the behaviour of the cytosine adsorption at the Au(110)/electrolyte interface at variable pH. The RAS data shows that the

cytosine adsorbs at 0.0 V under neutral (pH 7.1) and alkali (pH 12.8) conditions but that the cytosine does not adsorb under acidic (pH 1.2) conditions. However, cytosine has been observed to adsorb under acidic conditions and form random dimerised structures therefore leaving open the argument the cytosine is adsorbed at the Au(110)/electrolyte interface but in a random manner and thus undetectable by RAS studies.

7.1.3 The RAS of Au(110) + DNA After Self Assembly

The changes in the RA spectra of Au(110) before and after the self assembled adsorption of ss-DNA and ds-DNA are an indication that both the long chained biological molecules adsorb at the Au(110)/electrolyte interface in a manner which has a preferential ordering across the Au(110) surface. However the adsorption of the ss-DNA on the Au(110) surface resulted in a larger increase in the RAS of the Au(110) than that produced by the adsorption of the ds-DNA. The amount of ss-DNA dissolved in solution was much smaller than the amount of ds-DNA dissolved. The smaller concentration of ss-DNA resulted in a much larger optical response and a greater coupling between the dielectric functions of the ss-DNA and the Au(110) surface when compared to the optical response of the ds-DNA at the Au(110) surface. This greater optical response from a lower concentration of the ss-DNA is attributed to the DNA bases, which are exposed in ss-DNA, bonding to the Au(110) surface, a result which can not occur with the ds-DNA due to the bases being protected by the phosphate backbone.

The RAS obtained by the DNA adsorbing in an ordered manner at the Au(110)/electrolyte interface can not be attributed to either the Au(110) surface driving the ordered monolayer or the interactions which occur between the long DNA chains themselves. The RAS obtained from ds-DNA adsorbed at the polycrystalline Au/electrolyte interface unfortunately produced inconclusive results and could not help determine the mechanism by which the DNA orders on the Au(110) surface.

7.1.4 The Effect of Solution on the RAS of Au(110) + DNA

The role of an aqueous solution surrounding biological molecules is one of great importance, with suggestions being made that a water environment aided the "self protection" mechanism of DNA bases when early Earth was bathed in harmful UV radiation, and thus allowing the evolution of DNA and life.

The RAS studies described in chapter six show that the phosphate buffer solution enhances the optical response of the adsorbed biological molecules on the Au(110) surface. The results give rise to the suggestion that the hydrogen bonding network in the phosphate buffer solution mediates the coupling between the dielectric function of the Au(110) surface and the dipole moments in the biological molecules.

Removing the liquid from the Petri dishes lead to the reduction in RAS across the entire spectral range of investigation, a result which was observed for four of the five molecules (cytosine, CMP, poly-C and ss-DNA) adsorbed at the Au(110) surface. The dry sample of Au(110) + ds-DNA resulted was different to those of the other four molecules, this being that the intensity of the RAS between 4.5 eV and 7.0 eV did not change when wet or dry.

Rewetting the samples in clean phosphate buffer solution gave rise to a greater intensity than the original wet RA spectra across the spectral range for the RAS experiments of Au(110) after the adsorption of cytosine, CMP, poly-C and ds-DNA. The RAS experiment of Au(110) + ss-DNA did not show this effect, with the RA spectrum obtained from the Au(110) + ss-DNA when rewet not having a greater overall intensity than the RA spectrum obtained from Au(110) + ss-DNA before the sample was allowed to dry. This result is not fully understood but it is suggested that the effect of the other bases; adenine, thymine and guanine, may behave differently to cytosine which had been studied. In addition to this, the exposure of the ss-DNA and ds-DNA to the intense UV radiation from the UV RA spectrometer may have caused a denaturing of the DNA. Any damage to the DNA would reduce its optical response and, furthermore, its RAS.

7.2 Future Work

The experiments reported in this thesis were undertaken with the intention to methodically develop an understanding of the behaviour of DNA at the Au(110)/electrolyte interface. The understanding is built up from probing the smaller parts of DNA: the bases, through to the ds-DNA itself.

The implementation of RAS to probe biological molecules at the Au(110)/electrolyte interface can lead to a deeper understanding of the behaviour of one of the most important biological molecules. The preliminary results reported in this thesis can aid in progressing studies into bio-electronic devices. However, more investigations need to be undertaken. So far there have been investigations into the RAS of adenine and cytosine on Au(110), therefore the most logical path of future studies would be to probe the adsorption of the two remaining DNA bases; thymine and guanine, at the Au(110)/electrolyte interface using RAS. A greater understanding into the kinetics of these final two DNA bases may aid in the understanding of full chain DNA strands adsorbed on Au(110).

With regards to experimental equipment there are two additions which would greatly benefit the research of DNA at the Au(110)/electrolyte interface, one of which is an upgrade to existing equipment in the laboratory and the other is a purchase that would complement RAS as a probe.

The upgrade is to change the existing dish which holds the Au(110) crystals in place for RAS investigations performed with the Au(110) crystal placed horizontally. The existing dish cannot accommodate electrochemical studies. ADRAS investigations with a new electrochemical cell which holds the Au(110) crystal horizontally, would lead to more accurate angular variation experiments whereby the experiments are under potential control instead of self assembly. This new horizontal electrochemical cell would be required to fix the Au(110) crystals in place and have a window which can trap a thin layer of the electrolyte above the crystal surface. Reducing the amount of electrolyte to a minimum would reduce the amount of light scattering and UV light being absorbed in the new UV RA spectrometer by the electrolyte, thus potentially increasing the range of the new UV

RA spectrometer to 7.0 eV or beyond. Increasing the range of investigation for Au(110) + DNA could lead to very important results.

The second avenue of future study would be to invest in an EC-STM. The application of an EC-STM would give rise to results that would without doubt strengthen or shatter the analysis of the RAS studies reported in this thesis.

At present the horizontal electrochemical cell is in a prototype form and the finances are being put in place to purchase an EC-STM to the University of Liverpool RAS research group.

Publications

Chapter 3

A New UV Reflection Anisotropy Spectrometer and its Application to the Au(110)/Electrolyte Surface.
C. P. Mansley, T. Farrell, C. I. Smith, P. Harrison, A. Bowfield and P. Weightman.
J. Phys. D: Appl. Phys. **42**, 115303 (2009)

Spectral Signatures of the Different Reconstructions of Au(110).
C. I. Smith, A. Bowfield, N. J. Almond, C. P. Mansley, J. H. Convery and P. Weightman.
Submitted for Publication

Chapter 4

Prevention of Surface Reconstruction at the Au(110)/Electrolyte Interface by the Adsorption of Cytosine.
C. P. Mansley, C. I. Smith, A. Bowfield, D. G. Fernig, C. Edwards and P. Weightman.
J. Chem. Phys. **132**, 214708 (2010)

Chapter 5

Ordered Structures of DNA on Au(110)
C. P. Mansley, C. I. Smith, M. C. Cuquerella, T. Farrell, D. G. Fernig, C. Edwards, P. Weightman. *Phys. Status Solidi C* **5**, 2582 (2008)

Chapter 6

The Importance of Water in the Origin of Life.
C. P. Mansley, C. I. Smith, T. Farrell and P. Weightman.
Manuscript in Preparation

Other Publications

Determination of the Structure of Adenine Monolayers Adsorbed at Au(110)/Electrolyte Interfaces Using Reflection Anisotropy Spectroscopy.
C. I. Smith, A. Bowfield, G. J. Dolan, M. C. Cuquerella, C. P. Mansley, D. G. Fernig, C. Edwards, P. Weightman.
J. Chem. Phys. **130**, 044702 (2009)

Detection of DNA Hybridisation on a Functionalised Diamond Surface Using Reflection Anisotropy Spectroscopy.
C. I. Smith, A. Bowfield, M. C. Cuquerella, C. P. Mansley, T. Farrell, P. Harrison, D. S. Martin, D. G. Fernig, C. Edwards, J. E. Butler, R. J. Hamers, B. Sun, X. Wang, Weightman, P.
Euro Phys. Lett. **85**, 18006 (2009)

The Structure of Adenine Adsorbed at Sub-Saturation Coverage at Au(110)/Electrolyte Interfaces.
A. Bowfield, C. I. Smith, G. J. Dolan, M. C. Cuquerella, C. P. Mansley and P. Weightman,
e-J. Surf. Sci. Nanotech. **7**, 225 (2009)